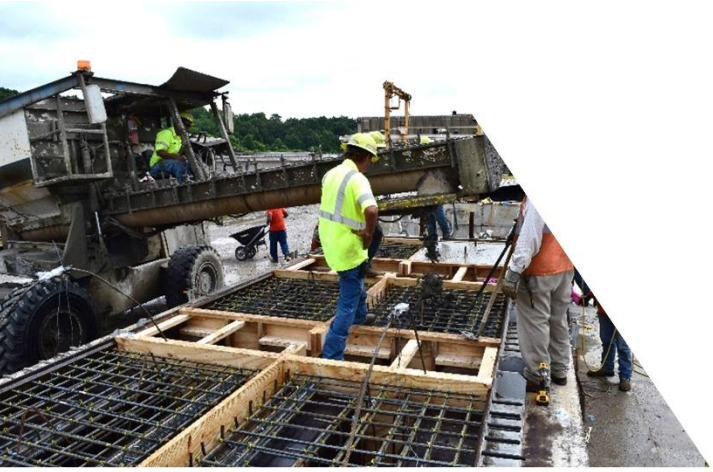

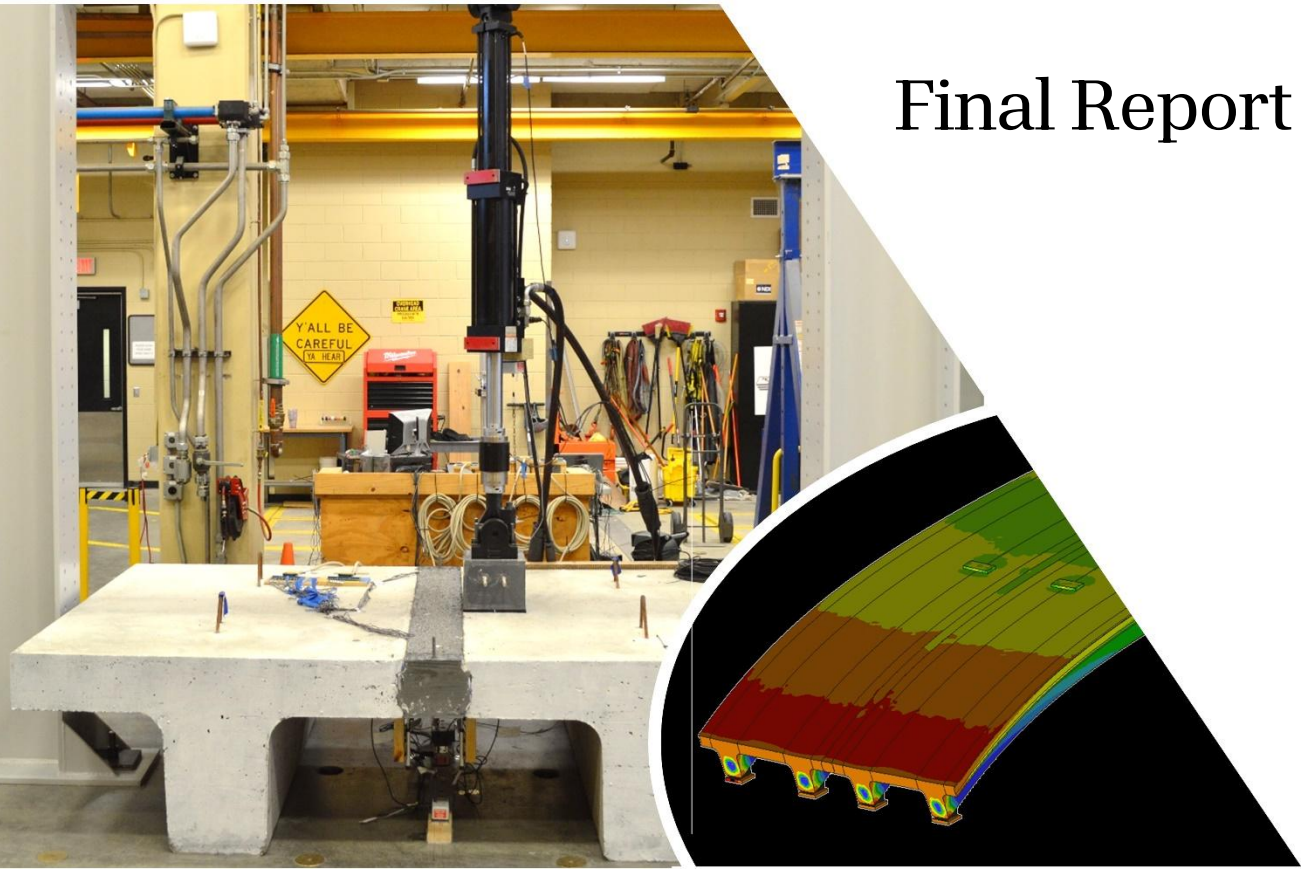

Final Report

Performance Characterization of an Ultra-High Performance Concrete Deck Connection for Alabama Bridges

Sponsored by
Alabama Department of Transportation (Project No. 931-047)

Performance Characterization of an Ultra-High Performance Concrete Deck Connection for Alabama Bridges

Final Report

Principal Investigators

Sriram Aaleti and Michael E. Kreger
Department of Civil, Construction, and Environmental Engineering
The University of Alabama

Graduate Assistant

Daniel Bridi Valentim, PhD student

Authors

Daniel Bridi Valentim, Sriram Aaleti, and Michael E. Kreger

Sponsored by
Alabama Department of Transportation
(Project No. 931-047)

Preparation of this report was supported by
Alabama Department of Transportation

A Report from
Department of Civil, Construction, and Environmental Engineering
The University of Alabama
3043 H.M. Comer
245 7th Avenue
Tuscaloosa, AL 35487
https://cce.eng.ua.edu

TABLE OF CONTENTS

1 INTRODUCTION 1
1.1 Background 1
1.2 Scope of Research 4
1.3 Research Approach and Report Layout 4
2 LITERATURE REVIEW 5
2.1 Deck panel-to-Deck panel connections with non-UHPC joint materials 5
2.2 Connections used in adjacent butted beam systems 8
2.3 UHPC Joints 15
3 UHPC Material Characterization 17
3.1 Standard specimen geometry and fabrication 17
3.1.1 Casting and curing 18
3.1.2 Compressive strength and Elastic Modulus 20
3.1.3 UHPC Tension Behavior 22
3.1.3.1 Direct Tension Test 22
3.1.3.2 Four-point Bending Test 24
3.1.4 Shrinkage Behavior 26
3.1.5 UHPC-NC Bond Behavior under Tension 28
4 EXPERIMENTAL TESTING OF SLAB AND DOUBLE-TEE SPECIMENS 30
4.1 Specimen dimensions and Joint details 31
4.2 Test Specimen Fabrication and Material Properties 33
4.3 Test matrix and Load Protocols 36
4.4 Test setup and Instrumentation 38
4.5 Observations and Results from the Slab Specimen Tests 43
4.5.1 Test S1 – Fatigue Tests for 1,000,000 cycles 44
4.5.2 Test S2 – Stiffness Measurement Test 49
4.5.3 Test S3 – Overload test 52
4.5.4 Test S4 – Failure test 54
4.6 Observations and Results from the Double-tee Specimen Tests 60
4.6.1 Test D1 – fatigue, 1,000,000 cycles 60
4.6.2 Test D2 – Stiffness Measurement Test 63
4.6.3 Test D3 – Overload Test 65
4.6.4 Test D4 – Overload Cyclic Test 66

4.6.5 Test D5 – Final Overload Test 69
5 FINITE ELEMENT MODELING 73
5.1 Structure geometry, reinforcement, boundary conditions, and loading 73
5.1.1 Slab and double-tee models 73
5.1.2 Bridge model 74
5.2 Calibration of FEA models 74
5.2.1 Slab and double-tee models 74
5.2.2 Bridge Model 77
5.3 Finite Element Analysis Results 78
5.3.1 Comparison of Experimental and FEA results 78
5.3.2 Comparison of DTee-SL and DTee-DL FEA models to DTee-Headed FEA model 83
5.3.3 Bridge model 84
6 CONCLUSIONS AND RECOMMENDATIONS 86
7 REFERENCES 89

LIST OF FIGURES

Figure 1. Precast bridge elements used in accelerated bridge construction 1
Figure 2. Standard cross-section details of typical NEXT beams 2
Figure 3. Deck-to-deck connection detail with post-tensioning first used in 1990 6
Figure 4. Deck-to-deck connection detail with post-tensioning, first used in 1997. 6
Figure 5. Deck-to-deck connection detail without post-tensioning used in Seymour, CT, in 2001. 7
Figure 6. Deck-to-deck connection detail developed in NCHRP 584 (Badie and Tadros 2008) and used in Texas in 2008. 7
Figure 7. NCHRP 10-71 longitudinal panel-to-panel connection (French et al. 2011) 8
Figure 8. Typical span ranges for different butted beam systems according to the FHWA. 9
Figure 9. Double-tee section used by the Florida DOT 9
Figure 10. Double-tee section used by the Texas DOT. 9
Figure 11. Deck bulb tee section provided by the PCI Bridge Design Manual 10
Figure 12 Deck bulb tee section designed by PCINE 10
Figure 14. Welded tie connection detail for double-tee beams used by the Texas DOT. 11
Figure 15. Welded tie connection for double-tee beams, spaced every 5 ft. 12
Figure 16. Welded tie connection detail for bulb tee beams used in Washington State, spaced at a maximum of 5 ft. 13
Figure 17. Welded tie connection detail for bulb tee beams used by the Wyoming DOT over Fork Crazy Woman Creek, spaced approximately every 6 ft. 14
Figure 18: Common panel-to-panel UHPC connection details: (a) waffle deck panel-to-panel connection detail, (b) panel-to-panel headed connection detail, (c) panel-to-panel straight connection detail, and (d) panel-to-panel hairpin reinforcement [Aaleti and Sritharan, 2014]. ..15
Figure 19: UHPC joint concept and shear key details developed for adjacent box beam connections, Yuan et al., 2018). 16
Figure 20. Formwork construction and assemble for material characterization specimens 18
Figure 21. Specimen geometries of different test specimens used for UHPC material characterization 18
Figure 22. UHPC materials and cylinders, shear horizontal mixer, and flow direction of UHPC 19
Figure 23. Concrete cylinder strain gauges and test setup for elastic modulus testing. 21
Figure 24. Compressive strength behavior of the different used UHPC types. 21
Figure 25. DT and 4PB instrumentation and test setup 22
Figure 26. Measured Tensile stress-strain behavior of UHPC using DT method 23
Figure 27. Stress and strain assumptions for inverse analysis procedure 25
Figure 28. Typical observed failure in 4PB specimens and calculated inverse analysis results 25
Figure 29. Instrumentation used to monitor shrinkage of shrinkage beams and UHPC joint. 27
Figure 30. Measured shrinkage strains in the three UHPC mixes 27
Figure 31. Test setup and details of bond specimens and rebars 28
Figure 32. UHPC-NC bond specimen response in tension and observed failure locations. 29
Figure 33: Schematics of NEXT D beams used in bridge projects 30
Figure 34. Phase-I slab specimen dimensions and joint details 31
Figure 35. Double-tee specimen dimensions and joint details 32
Figure 36. Formwork used for slab and double-tee specimens 34
Figure 37. Details of mild steel reinforcement placed in double-tee formwork 35
Figure 38. Casting and curing of normal concrete slab and double-tee components and UHPC joints. 35

Figure 39. Instrumentation details used in all four slab specimens during Tests S1, S2, and S3 39
Figure 40. Test setup used for the slab specimens tests S1, S2, and S3 40
Figure 41. Test setup used for Test S4 for all the slab test specimens. 41
Figure 42. Strain gauges applied in the joint of double-tee specimens 42
Figure 43. Location of string potentiometers and LVDTs during all double-tee tests 42
Figure 44. Test setup used for double-tee specimens Tests D1, D2, D3, and D4.....43
Figure 45. Test setup used for Test D5 of all the double-tee specimens. 43
Figure 45. Initial boundary condition configuration used for specimen Slab-SL-UH1.....44
Figure 46. Difference in deflections of Slab-SL specimens 45
Figure 47. Difference in deflections of Slab-DL specimens.....45
Figure 48. Schematics of strain gauges applied on slab specimens.....46
Figure 49. Strain responses of specimen Slab-SL-UH1 during fatigue test S1.....47
Figure 50. Strain responses of specimen Slab-SL-UH2 during fatigue test S1.....47
Figure 51. Strain responses of specimen Slab-DL-UH1 during fatigue test S1 48
Figure 52. Strain responses of specimen Slab-DL-UH2 during fatigue test S1 48
Figure 53. Difference in joint opening of Slab-SL specimens 49
Figure 54. Difference in joint opening of Slab-DL specimens 49
Figure 55. String potentiometer responses during tests S2.....50
Figure 56. Strain responses during tests S2 51
Figure 57. Average joint opening responses during tests S2.....52
Figure 58. Slab specimens response during test S3 53
Figure 59. Typical cracking in Slab-DL specimens during test S3 54
Figure 60. Measured string potentiometer deflections in all slab specimens during tests S4 55
Figure 61. Measured strain gauge responses of Slab-SL specimens during tests S4.....55
Figure 62. Measured strain gauge responses of Slab-DL specimens during tests S4.....56
Figure 63. Measured Joint opening in slab specimens using LVDTs during tests S4 57
Figure 64. Measured LED joint opening and joint cracking of specimen Slab-SL-UH1.....57
Figure 65. Measured LED joint opening and joint cracking of specimen Slab-SL-UH2.....58
Figure 66. Measured LED joint opening and joint cracking of specimen Slab-DL-UH1 58
Figure 67. LED joint opening and joint cracking of specimen Slab-SL-UH2.....59
Figure 68. The observed crack patterns in all the slab specimens after Test S4 59
Figure 69. Measured deflections in double-tee specimens during tests D1.....60
Figure 70. Schematic of strain gauges in double-tee specimens 61
Figure 71. Strain gauge responses in DTee-SL specimens during tests D1 62
Figure 72. Measured strain gauge responses in DTee-DL specimens during tests D1 62
Figure 73. Measured interface opening using LVDT during tests D1 63
Figure 74. Selected string potentiometer response during tests D2 64
Figure 75. Measured response of steel strain gauge A6 during tests D2 64
Figure 76. Response of selected LVDT during tests D2.....65
Figure 77. Double-tee specimen responses during tests D3.....66
Figure 78. Measured String potentiometer deflections during tests D4 67
Figure 79. Measured strain gauge responses in DTee-SL specimens during tests D4.....67
Figure 80. Measured strain gauge responses in DTee-DL specimens during tests D4 68
Figure 81. Measured joint opening responses using LVDTs during tests D4.....68
Figure 82. Measured deflection response of double-tee specimens during Test D5 69
Figure 83. Measured strain gauge responses for specimens DTee-SL during tests D5 70
Figure 84. Measured Strain gauge responses for specimens DTee-DL during tests D5.....70
Figure 85. Measured joint interface opening in double-tee specimens with LVDT during tests D5 ..71

Figure 86. Cracking observed in specimens DTee-SL-UH1, DTee-DL-UH1, and DTee-DL-UH3 during tests D5 72
Figure 87. Geometry, reinforcement, boundary conditions, and applied loading of slab and double-tee models 73
Figure 88. Geometry, reinforcement, boundary conditions, and applied loading of bridge model. 74
Figure 89. Normal stiffness behavior used in FEA. 75
Figure 90. Mesh study performed on Slab-SL specimens 76
Figure 91. Response of each mesh configuration for slab mesh study 77
Figure 92. Mesh configuration used in slab and double-tee specimens 77
Figure 93. Comparison of FEA results from slab and double-tee models with measured response 78
Figure 94. FEA and experimental strain gauge responses in Slab-SL specimens 79
Figure 95. FEA and experimental strain gauge responses in Slab-DL specimens 80
Figure 96. FEA and experimental strain gauge responses in DTee-SL specimens 80
Figure 97. FEA and experimental strain gauge responses in DTee-DL specimens 81
Figure 98. Strain gauge responses in DTee-SL specimens for load distribution study 82
Figure 99. Strain gauge responses in DTee-DL specimens for load distribution study 82
Figure 100. Comparison of DTee-SL and DTee-DL FEA models to DTee-Headed FEA model 83
Figure 101. Mesh study developed for bridge models 84
Figure 102. Bridge FEA model results under single wheel load. 85

LIST OF TABLES

Table 1. Geometric properties of deck bulb tee sections provided by the PCI Bridge Design Manual 10
Table 2. Geometric properties for deck bulb tee sections designed by PCINE 10
Table 3. Mix proportions of three commercially available UHPCs 19
Table 4. Test matrix containing number of tested UHPC and joint interface specimens 19
Table 5. Concrete compressive strengths at the time of testing 21
Table 6. Peak tensile strengths of UHPC Mixes 23
Table 7. 4PB specimens peak loads and tensile strengths 26
Table 8. Bond specimen macrotexture depth test results 29
Table 9. Test matrix for slab and double-tee specimens 36
Table 10. Naming Scheme used for test specimens 36
Table 11. Details of Test matrix and load protocols used for slab specimens 37
Table 12. Details of Test matrix and load protocols used for double-tee specimens 37
Table 13. S1 cycle number in which test S2 was performed 38
Table 14. D1 cycle number in which test D2 was performed 38
Table 15. Material parameters used for slab and double-tee specimens 75
Table 16. Parameters used for the interface behavior between NC and UHPC 76
Table 17. Mesh study performed on Slab-SL specimens 77
Table 18. Elastic modulus of materials used in the bridge model 78

1 INTRODUCTION

1.1 Background

Cast-in-place bridges using normal concrete have been commonly used in the state of Alabama for short-span bridges. Even though their performance is satisfactory after construction and opening to traffic, this construction method requires a significant amount of construction time and on-site labor compared to the use of precast systems. The Accelerated Bridge Construction (ABC) method is a technique that is becoming increasingly common in the United States. It involves the use of large prefabricated bridge elements and systems (PBES) in bridge construction, providing improvements in safety, quality, durability, social costs, and environmental impacts.[1] PBES comprises a deck, beam, column, pier, abutment, wall, and other miscellaneous elements that are prefabricated in factory settings, transported and assembled onsite, becoming part of the constructed bridge. Figure 1 shows typical PBES members used in ABC technology being installed onsite.

(a) Precast deck panel installation on top of precast girders in a bridge in Utah

(b) Full depth precast concrete deck panel installed in a bridge in New Hampshire

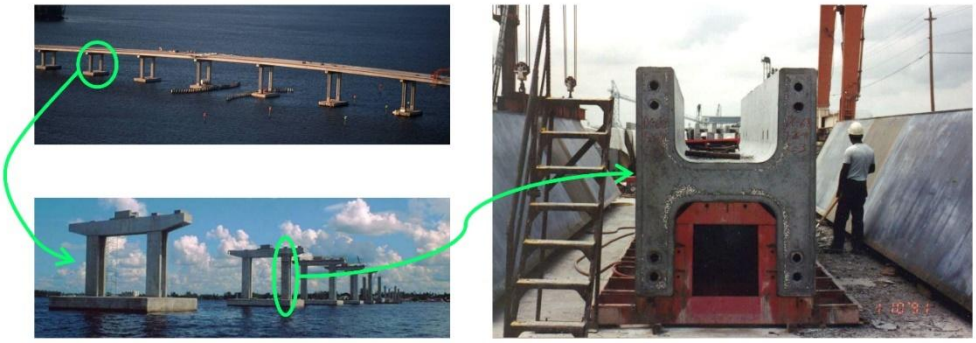

(c) Edison Bridge, FL, with precast concrete pier caps and H-shaped columns

Figure 1. Precast bridge elements used in accelerated bridge construction

In 2009, a relatively new type of beam, the Northeast Extreme Tee (NEXT) beam, was first introduced with the development of the NEXT Beam Guide Details. This beam, which falls under the ABC umbrella, had its details combined into one document in 2015.[2] The NEXT Beam Guide Details were prepared by the PCI Northeast Bridge Technical Committee, which includes committee members from the Connecticut, Maine, Massachusetts, New Hampshire, New York, and Rhode Island DOTs. There are currently three types of NEXT beams: NEXT D, NEXT E, and NEXT F beams. Although each NEXT beam type has its own advantages and disadvantages, the NEXT D beams are the most suitable for ABC, according to the NEXT Beam Guide Details (see Figure 2).[10] While the NEXT E and NEXT F beams require a cast-in-place concrete deck, the precast deck of a NEXT D beam

is sufficient for structural purposes. Moreover, there is minimal potential for flange cracking in the NEXT D beam during handling since its section is very stout compared to the other NEXT beams. All NEXT beam types contain prestressing strands in their webs and mild steel reinforcement elsewhere. During fabrication, the absence of draped strands provides it a significant advantage. The elimination of deck formation in the field saves significant time during construction while also providing an instant work platform, resulting in a significantly safer project. Bridges using NEXT beams are cost-effective structures that have reduced the overall cost of bridge construction in the Northeast.[3]

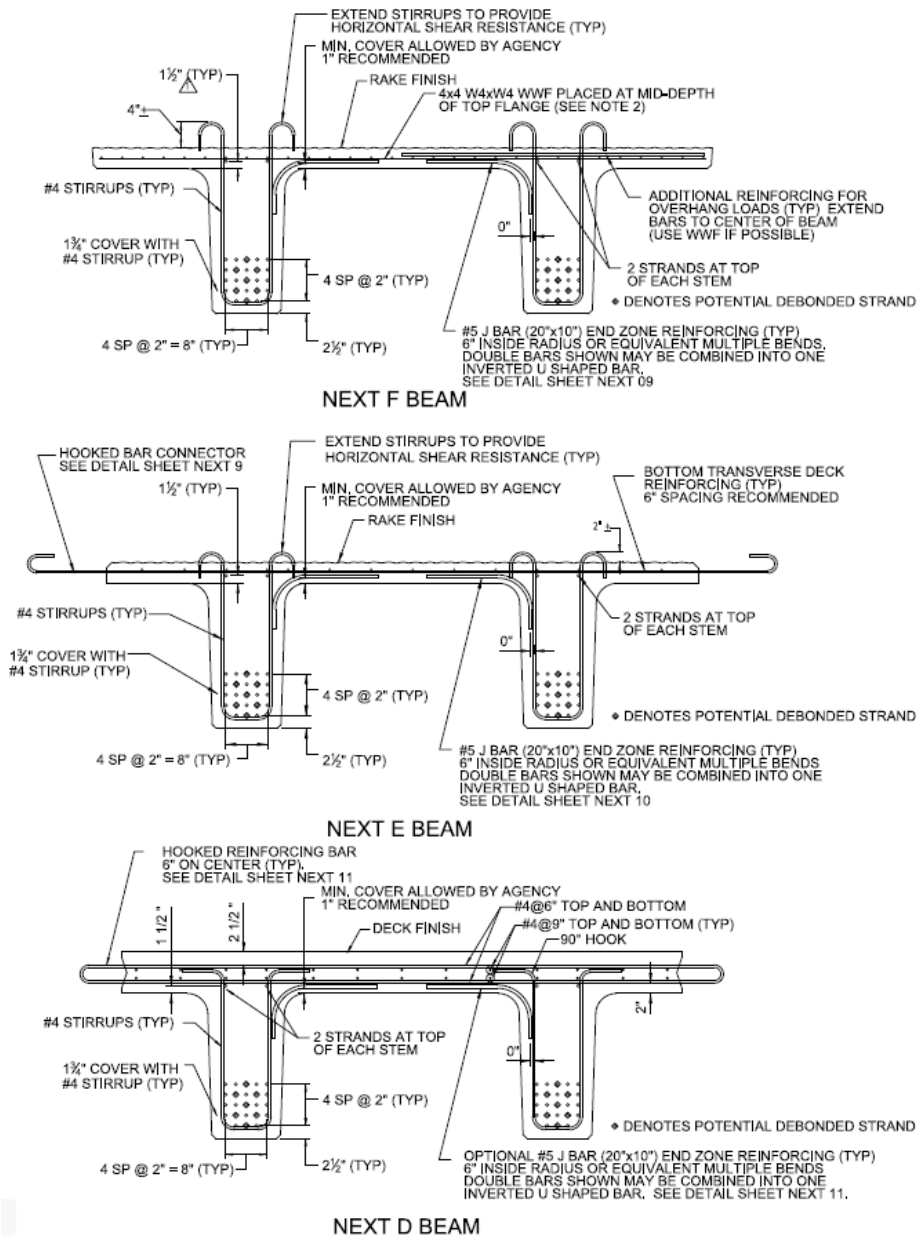

Figure 2. Standard cross-section details of typical NEXT beams.

A bridge constructed using NEXT beams is formed with several NEXT beams placed side by side. The beams are connected by lap splicing their reinforcement that protrudes from the sides of their

flanges, and by subsequently pouring a cementitious material connecting the beams and forming a cast-in-place joint. The original design suggests the use of grout to fill the joint between NEXT beams. Even though the NEXT D beam is potentially one of the best butted beam systems for ABC, the conventional grout or concrete connecting two adjacent beams has resulted in issues with shear key cracking reported by the FHWA [12]. The structural integrity of concrete shear keys is challenged by loads induced from vehicular movement as well as those induced by volumetric changes in concrete due to changes in ambient environmental conditions such as diurnal and seasonal variations in temperature and relative humidity [13]. It is vital for the integrity of the connection that a tight seal is maintained between the joint material and the surrounding concrete in order to prevent fluid and chloride ion intrusion into the concrete. This could potentially initiate and accelerate corrosion of the mild steel reinforcement and result in concrete cracking.

Ultra-high performance concrete (UHPC) is a reactive powder concrete mixture and a relatively new class of cementitious material that exhibits superior properties such as compressive strength, durability, and long-term stability when compared to conventional grout or high-performance concrete.[14] This cementitious material is composed of an optimized gradation of granular constituents, a water-to-cementitious material ratio less than 0.25, and a high percentage of discontinuous internal fiber reinforcement.[15] The discrete steel fibers give the UHPC material a characteristic sustained post-cracking tensile strength.[16, 17] Even though UHPC's mechanical properties vary based on the mix design and steel fiber content, the FHWA defines the minimum compressive strength of UHPC as 17.4 ksi and its minimum pre- and post-cracking tensile strengths as 0.72 ksi.[16] The use of a structurally superior material as opposed to conventional reinforced concrete or grout, such as UHPC, is appealing to address the presented concern above related to the traditional ABC connections with traditional materials. Besides having a higher compressive strength, tensile strength, durability, long-term stability, and shorter development lengths compared to conventional cementitious mixtures, UHPC has a higher bond strength when in contact with reinforcement bars, prestressing strength, and normal concrete (NC). The higher bond strength between UHPC and NC is essential for ABC connections due to the fact that it could prevent fluid and chloride ion intrusion into the concrete, thus preventing accelerated corrosion of the reinforcement resulting in concrete cracking.

The Alabama Department of Transportation (ALDOT) has recently designed, for the first time, a bridge for the city of Mobile, AL, using NEXT28D beams (28-in. deep NEXT type D beams). The NEXT type D beam is a beam with an integral full-depth flange that acts as the structural bridge deck. This allows the bridge to be ready for traffic soon after the beams are erected.[4] The constructed bridge in Mobile is 60-ft. (1,524 mm) long and has a 27.2-degree skew angle. The adjacent NEXT-D beams were connected longitudinally with UHPC and with headed #5 reinforcement at 6 in. spacing protruding from the sides of the beam flanges. For the first time in the state of Alabama, UHPC was mixed and poured on site for this bridge construction. The usage of UHPC was accommodated in the construction using a special provision developed by ALDOT. Given that the constructed bridge has a significant skew and is the first in Alabama to use UHPC in the joints, adopting a conservative design approach with headed bars was justified. However, based on prior experience with UHPC and Accelerated Bridge Construction (ABC) connections from other DOTs, it has been demonstrated that #5 straight mild steel bars, when combined with the appropriate UHPC material, should be able to fully develop their capacity within the joint width used in this bridge. This approach would help to minimize potential fabrication and installation challenges while also reducing connection costs. This conclusion is further supported by previous research from the FHWA and Iowa DOT on the use of UHPC in waffle deck connections, specifically using Lafarge® UHPC—the same material being utilized in the ongoing project in Mobile. However, the long-term performance of the connection

used in the NEXT-D project, particularly with respect to cracking and fatigue under repeated vehicular loading (1 to 2 million cycles), has not yet been thoroughly investigated.

1.2 Scope of Research

There are currently several providers of proprietary UHPC (Ultra-High Performance Concrete) materials in the U.S., with at least seven producers, including Lafarge Holcim®, VICAT®, Steelike®, Cor-Tuf®, DURA®, CeEntek®, and ALBOURGH®. In addition, several non-proprietary UHPC mix developers are emerging, particularly through PCI-funded research projects, which involve multiple PCI plants across the U.S. Some fiber companies also offer guidance for developing non-proprietary mixes using local materials to help reduce the cost of UHPC materials. Although compressive strength is often used to qualify a UHPC mix, it may not accurately reflect the bond performance, which is essential for the long-term durability of joints. This is because UHPC materials from different producers can exhibit varied early-age behaviors, such as shrinkage, and different tensile strain-hardening characteristics after cracking, both of which are crucial for ensuring the strength and reliability of connections. Therefore, a comprehensive investigation into the effects of UHPC materials from different producers (both proprietary and non-proprietary) is necessary. This will aid in standardizing joint designs and reducing costs for future UHPC applications in Alabama bridges.

The primary objective of this study is to provide ALDOT with an experimentally validated, construction- and fabrication-friendly deck connection detail between prefabricated elements using UHPC. Additionally, the study aims to assess the impact of various commercially available UHPC formulations on the long-term performance of the deck connection, particularly in relation to mechanical degradation. The study will also evaluate the performance of UHPC joints in NEXT-D beams under both static and fatigue loading conditions through experimental testing of the full-scale connection specimens.

1.3 Research Approach and Report Layout

The research approach involved the characterization of three different commercially available UHPC mix design properties (mechanical and early-age), as well as the experimental testing of four slab specimens, each measuring 1.5 feet in width and 9 feet in length, to simulate NEXT-D flanges. Additionally, four double-tee specimens were tested, modeled after NEXT-D beams, to further evaluate performance. These specimens were subjected to various testing protocols and load magnitudes, including a fatigue test with one million cycles. Key performance metrics such as joint interface openings, deflections, and strains were observed during the experimental testing to assess the effectiveness of the joint connection details using UHPC. Additionally, finite element analyses were conducted to simulate the behavior of both the slab and double-tee specimens. These analyses produced reliable and accurate models for evaluating the performance of bridges utilizing NEXT-D beams and UHPC joints.

Chapter 2 of this report provides a concise review of various deck panel-to-deck panel connection types. Chapter 3 focuses on the experimental characterization of the material properties of three commercially available UHPC mixes. In Chapter 4, the experimental testing of deck specimens with UHPC joints is detailed, including fabrication procedures, testing methods, and the resulting data. Chapter 5 covers the development and calibration of the finite element model used in this study. The final chapter presents the conclusions drawn from the research, along with recommendations for future work.

2 LITERATURE REVIEW

In current construction practice, field-installed connections between full-depth precast deck panels typically require interlacing connecting elements, such as mild steel reinforcement or headed shear studs, extending from the deck panel components. These approaches often lead to fit-up and tolerance challenges during field installation, issues that can be further exacerbated when pre- or post-tensioning is applied in both directions of the panels. Additionally, previous studies (e.g., Graybeal 2012, Issa 1995) have highlighted durability concerns related to the field-cast cementitious grout commonly used in these connections. These combined challenges negatively affect the performance of the connections, thereby compromising the overall performance of the precast deck panel system.

The following sections provide details on various panel-to-panel (both transverse and longitudinal) connections that were developed in previous research projects and successfully applied in practice for precast deck panels. These connection details have been sourced from several organizations, including the National Cooperative Highway Research Program (NCHRP), the Federal Highway Administration (FHWA), and the Precast Concrete Institute (PCI). It is important to note that, in most cases, these connections were originally developed for full-depth solid precast panels without considering the use of UHPC as the connection fill material. As a result, some of these connection designs may require modifications to incorporate UHPC effectively. Furthermore, due to the superior bond and flow characteristics of UHPC, the dimensions and reinforcement details in the connection regions may be optimized to enhance performance. Where applicable, comments and suggestions are provided to improve the constructability, performance, and cost-effectiveness of the connections when UHPC is used.

2.1 Deck panel-to-Deck panel connections with non-UHPC joint materials

Panel-to-panel connection details are crucial for effectively transferring loads between panels and distributing these loads to various components of the superstructure. These connections are subject to bending moments and vertical shear forces due to vehicular traffic. Traditionally, the edges of precast panels are designed with shear key features along the connections when two panels are joined. This shear key prevents relative vertical movement between adjacent panels under traffic loads. Historically, connections between precast bridge deck elements have included joints both with and without post-tensioning. Post-tensioned connections allowed for narrower joint widths and reduced connection areas, while non-post-tensioned joints required wider connection regions and a greater volume of grout to effectively link the precast deck panels. Although post-tensioned deck connections use less joint material, the post-tensioning process is often time-consuming and costly, creating a preference for alternatives such as mild reinforcement or shear studs. In previous field projects involving full-depth precast panels, two primary types of shear keys were typically used: match-cast shear keys with epoxy adhesive and grouted female-to-female joints filled with grout. These methods have been employed to ensure stability and effective load transfer between precast panel elements.

Figure 3 and Figure 4 show previously used deck-to-deck connections with post-tensioning, and Figure 5 and Figure 6 depict connections with mild reinforcement and no post-tensioned elements (obtained from the report FHWA-IF-09-010).[2] The connection shown in Figure 3 was first used in 1990. The post-tensioning strands in the duct are stressed after the grout has been placed, requiring special attention to sealing the connection. Figure 4 shows a transverse connection initially used in 1997. The slab decks, along with the connections, were post-tensioned longitudinally.

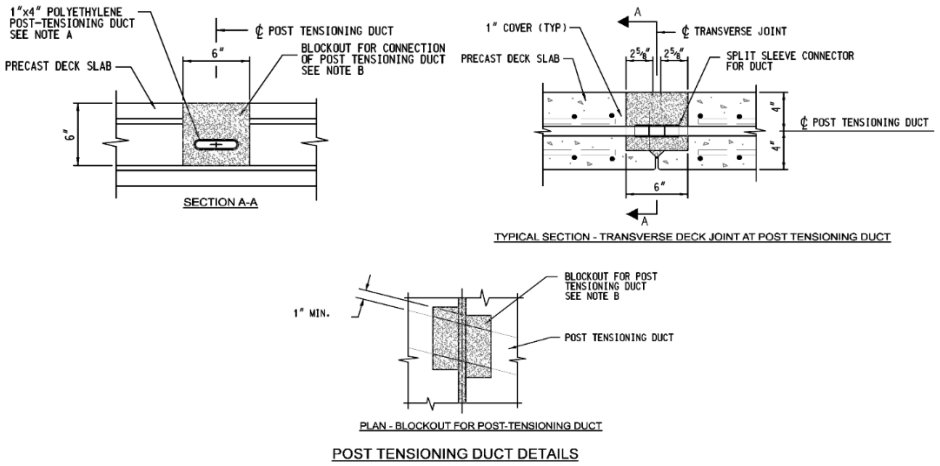

Figure 3. Deck-to-deck connection detail with post-tensioning first used in 1990

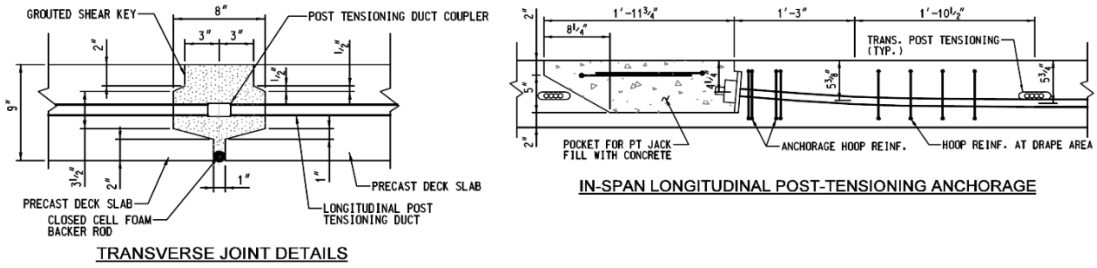

Figure 4. Deck-to-deck connection detail with post-tensioning, first used in 1997.

Figure 5 depicts a connection used in a bridge in Seymour, CT, in 2001. High-strength early-set concrete was specified for the connection, and traffic was opened one day after its construction. The joint shown in Figure 6 belongs to the Live Oak Creek Bridge (connection used in 2008), in Texas, and the research involving the development and testing of this connection is discussed under NCHRP Project 12-65.[3] In this connection detail, on one side of panel No. 6, reinforcement is embedded 6 in. into a galvanized, bulged hollow structural section (HSS 4 x 12 x 3/8 in.); on the other side of the panel, the reinforcement extends 7 ½ in., beyond the panel. A 1 in. diameter plastic pipe is attached to the top surface of the HSS tube and is used to fill the tube with grout after installation. The HSS tube has an oversized 1 ¾ in. diameter hole on the free side of the panel to help in installing adjacent panels. The HSS panels are installed such that the first panel is laid with the HSS exposed and ready to receive the protruding reinforcement from the adjacent panel. After the adjacent panel is laid, the HSS is filled with regular grout to complete the connection between panel elements. Note that installation of this connection requires tilting of the panels to avoid interference with shear connectors attached to the superstructure.

A panel-to-panel connection was developed as part of the NCHRP Project 10-71 study to develop design and construction specifications for durable CIP-reinforced concrete connections for precast deck systems. The typical details of the connection, which consist of a grouted shear key interlaced with lapped U-bar reinforcement along the length of the panels, are shown in Figure 7. Experimental studies completed on this connection indicated that the proposed longitudinal joint had sufficient strength, fatigue characteristics, and crack control for the maximum service loads determined.

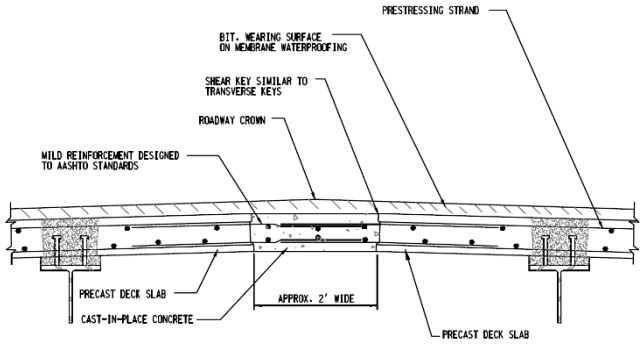

Figure 5. Deck-to-deck connection detail without post-tensioning used in Seymour, CT, in 2001.

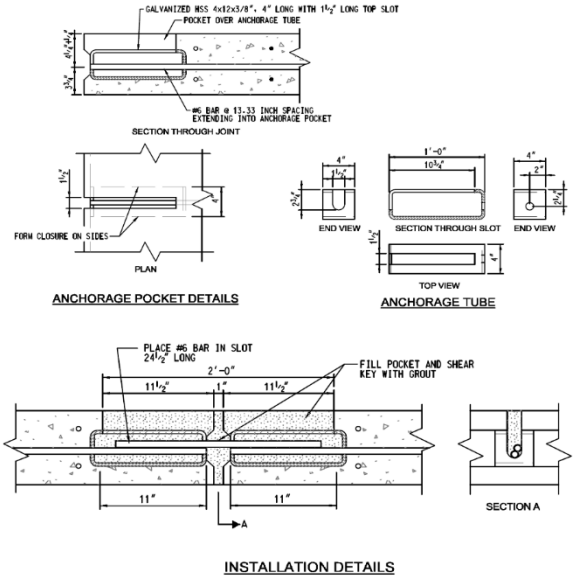

Figure 6. Deck-to-deck connection detail developed in NCHRP 584 (Badie and Tadros 2008) and used in Texas in 2008.

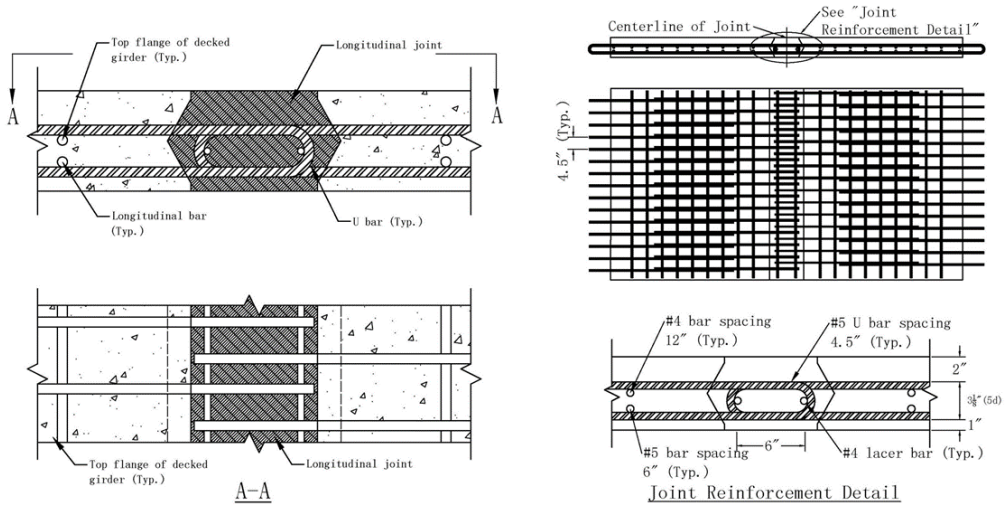

Figure 7. NCHRP 10-71 longitudinal panel-to-panel connection (French et al. 2011)

Non-UHPC deck panel joints can provide satisfactory performance when properly designed and detailed. However, most non-post-tensioned (non-PT), non-UHPC joint configurations require a substantial amount of protruding reinforcement from the precast components. This reinforcement is often difficult to place, resulting in increased labor costs. Additionally, many of these joint details necessitate the placement of supplementary reinforcement within the joint, both transverse (to facilitate development length) and longitudinal (to enhance confinement). In some cases, reinforcement bars must be threaded through 180-degree hooks. While simpler non-UHPC joint designs in terms of reinforcement can reduce complexity, they typically rely on post-tensioning, which is also labor-intensive. A frequent issue with these non-PT, non-UHPC deck joints is cracking along the joint boundaries, which can lead to water infiltration and negatively affect the long-term performance of the connection. Such cracking is often exacerbated by poor construction practices.

2.2 Connections used in adjacent butted beam systems

Butted beam systems consist of a combination of precast girders and deck elements. The PBES members are poured together in the precast yard, forming a single structural component. This concept is often used in ABC projects to avoid deck forming or deck placement, saving time during the construction process. The adjacent butted beam system is composed of four different beam types: adjacent slabs/deck beams; adjacent box beams; double-tee beams; and butted bulb tee (or deck bulb-tee) beams. The FHWA shows typical span ranges for different butted beam systems (Figure 8), which could potentially vary significantly depending on the specific state standards, number of beams, concrete strengths, and member sizes.[2] Double-tee beams have been used in pedestrian bridges and other crossings.[4] Prestressed concrete double tees are also a potentially attractive structure for short to medium range spans where speed of construction is an issue.[5] Double-tee sections used by the Florida and Texas DOTs are shown in Figure 9 and Figure 10 (Gee et al.[6]), respectively.

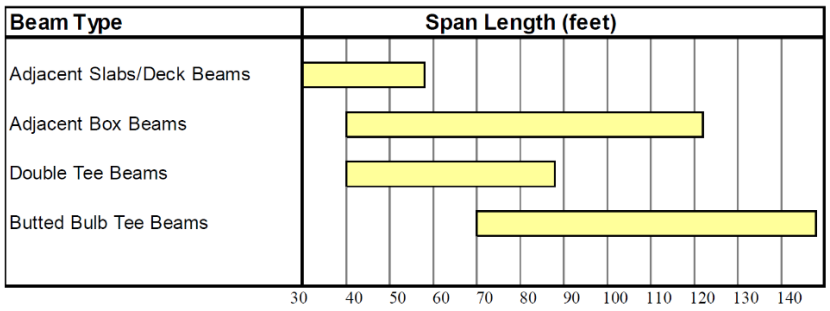

Figure 8. Typical span ranges for different butted beam systems according to the FHWA.

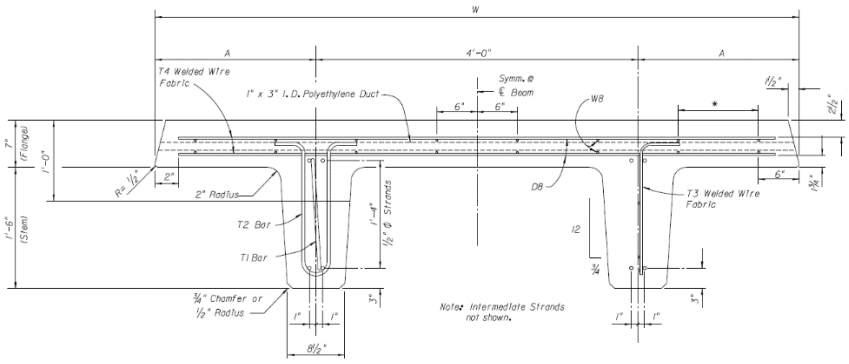

Figure 9. Double-tee section used by the Florida DOT

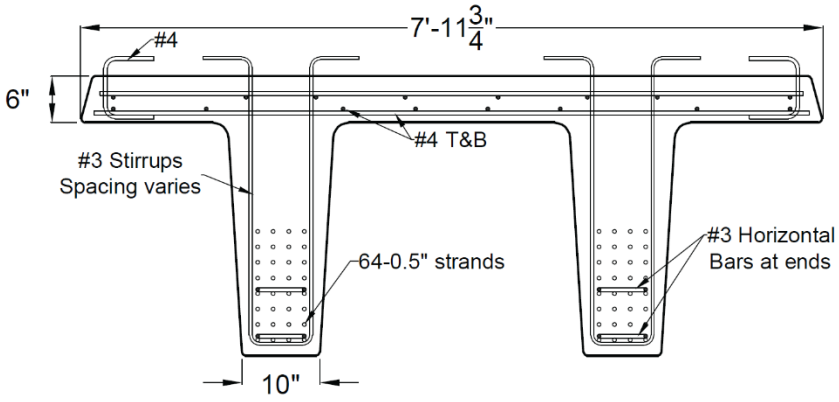

Figure 10. Double-tee section used by the Texas DOT.

Decked bulb-tee sections have been commonly used in the country by several departments of transportation to reach long spans in bridges composed of precast and prestressed concrete members. The NCHRP research report 999[7] provides examples of bulb tee sections developed by several institutions and government agencies. The Precast/Prestressed Concrete Institute (PCI) has provided standard sections in their 2014 Bridge Design Manual. Some of these sections are shown in Figure 11 and Table 1. The PCI Northeast (PCINE) has also developed bulb-tee sections that are shown in Figure 12 and Table 2.

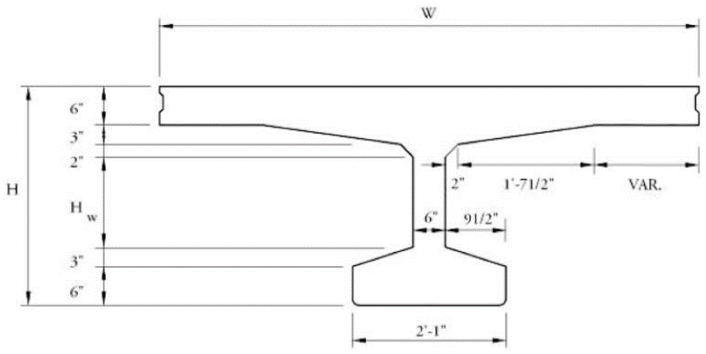

Figure 11. Deck bulb tee section provided by the PCI Bridge Design Manual

Table 1. Geometric properties of deck bulb tee sections provided by the PCI Bridge Design Manual

H (in)	H_w (in)	W (in)	Area (in^2)	Moment of inertia (in^4)	y_{bottom} (in)	Weight (kip/ft)	Maximum span (ft)
35	15	48	677	101,540	21.12	0.75	100
		72	823	116,071	23.04	0.91	78
		96	967	126,353	24.37	1.07	65
53	33	48	785	294,350	31.71	0.87	145
		72	931	335,679	34.56	1.03	121
		96	1,075	365,827	36.63	1.19	105
65	45	48	857	490,755	38.55	0.95	168
		72	1,003	559,367	41.95	1.11	148
		96	1,147	610,435	44.96	1.27	130

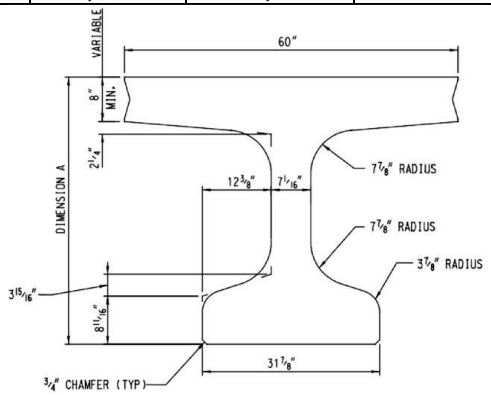

Figure 12 Deck bulb tee section designed by PCINE

Table 2. Geometric properties for deck bulb tee sections designed by PCINE

Name	Depth (in)	Flange width (in)	Area (in^2)	Moment of inertia (in^4)	y_{bottom} (in)	Weight (kip/ft)
NEDBT40	40	60	1,052	202,089	23.43	1.10
NEDBT48	48		1,109	327,115	28.07	1.16
NEDBT56	56		1,165	486,874	32.64	1.21
NEDBT64	64		1,222	683,314	37.16	1.27
NEDBT72	72		1,279	918,385	41.63	1.33
NEDBT80	80		1,335	1,193,950	46.06	1.39

The National Cooperative Highway Research Program (NCHRP) report [8] outlines connection approaches for butted beam systems. These include conventional reinforced concrete closure joints with conventional reinforcement, grouted reinforced closure pours, grout with headed reinforcement or hooked bars, ultra-high performance concrete with straight bars welded plate connections, and transverse post-tensioning. The FHWA, on the other hand, published a report[2] in 2009 informing that the states that use deck bulb tees or double-tee beams use a welded tie (or welded plate) connection combined with a grouted key. The report also states that this type of connection, even though it is the most common for double tees or bulb tees, presents several drawbacks that undermine the arguments for its usage. First, the connection is primarily designed for shear, which requires designers to treat each double-tee flange edge as a cantilever deck overhang, generating a more robust design for the flanges. Second, some designers have concerns with the long-term fatigue behavior of this type of connection, leading the FHWA to recommend the connection for bridges with lower truck volumes. Third, this connection leaves the bottom portion of the welded plate connection unprotected from the weather, which could lead to corrosion of the plate, especially in corrosive environments. Fourth, there are concerns with the grout in the keys between the beams not completely filling the void, which is the most common cause of keyway failures. Finally, the differential camber of the beams can lead to dimensional problems with the connections.

Figure 13 shows a connection detail used by the Texas DOT for double-tee beams. The connection is grouted after the connecting plates are field welded in place. A similar type of connection for double-tee beams is also depicted in Figure 14, where the welded connectors are spaced 5 ft. on center along the entire length of the beam. Figure 15 shows a connection detail used in Washington State for a deck bulb tee girder, which is the same used for double-tee beams. The welded connections are spaced a maximum of 5 ft. on center. A connection detail used by the Wyoming DOT in a bridge over Fork Crazy Woman Creek in a deck bulb tee girder is shown in Figure 16. The welded connection is spaced approximately every 6 ft.

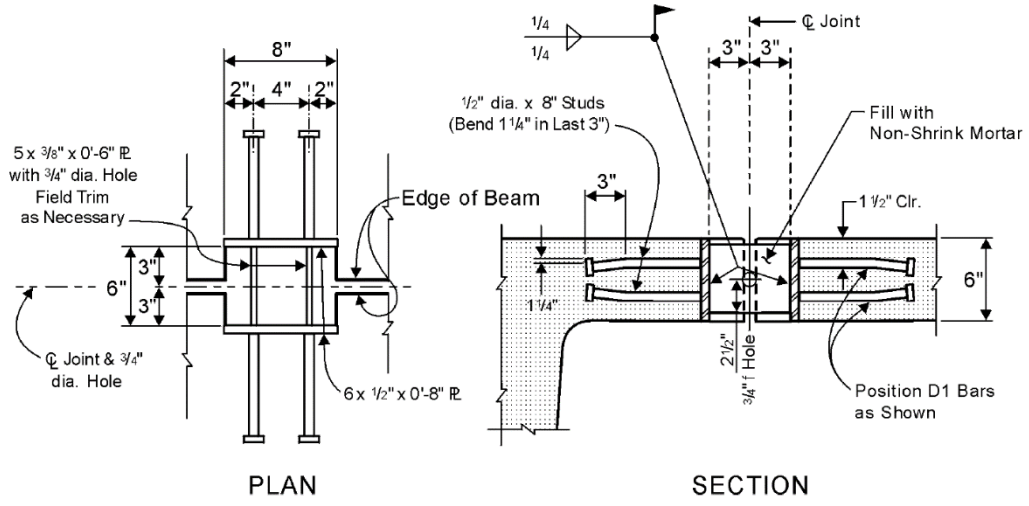

Figure 13. Welded tie connection detail for double-tee beams used by the Texas DOT.

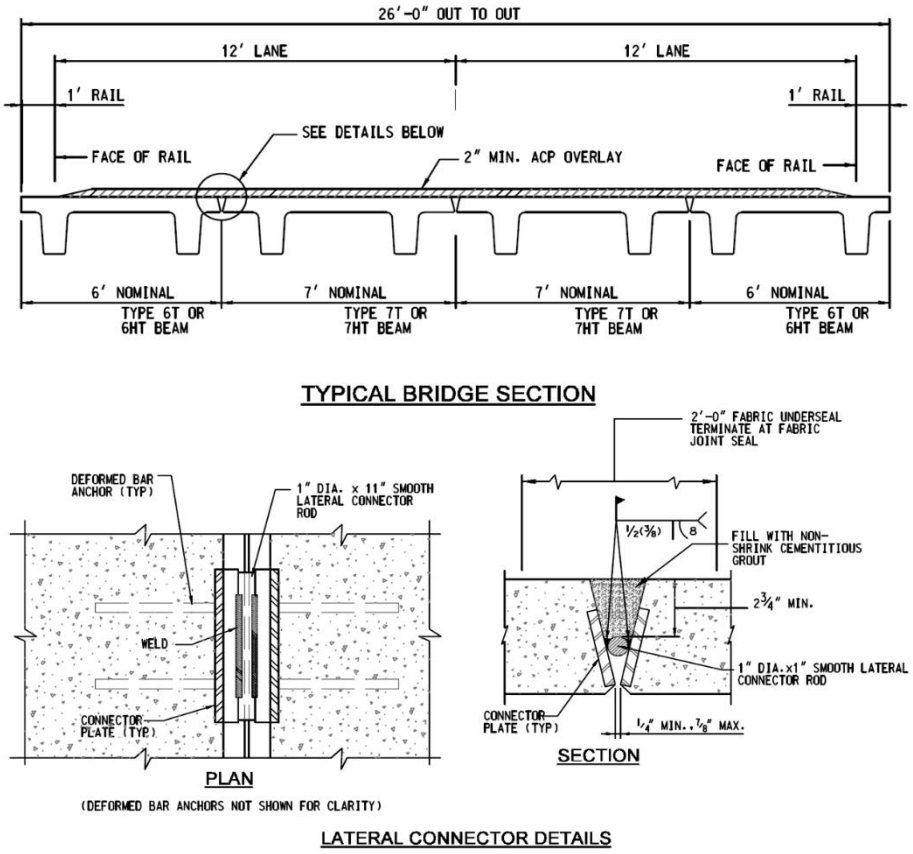

Figure 14. Welded tie connection for double-tee beams, spaced every 5 ft.

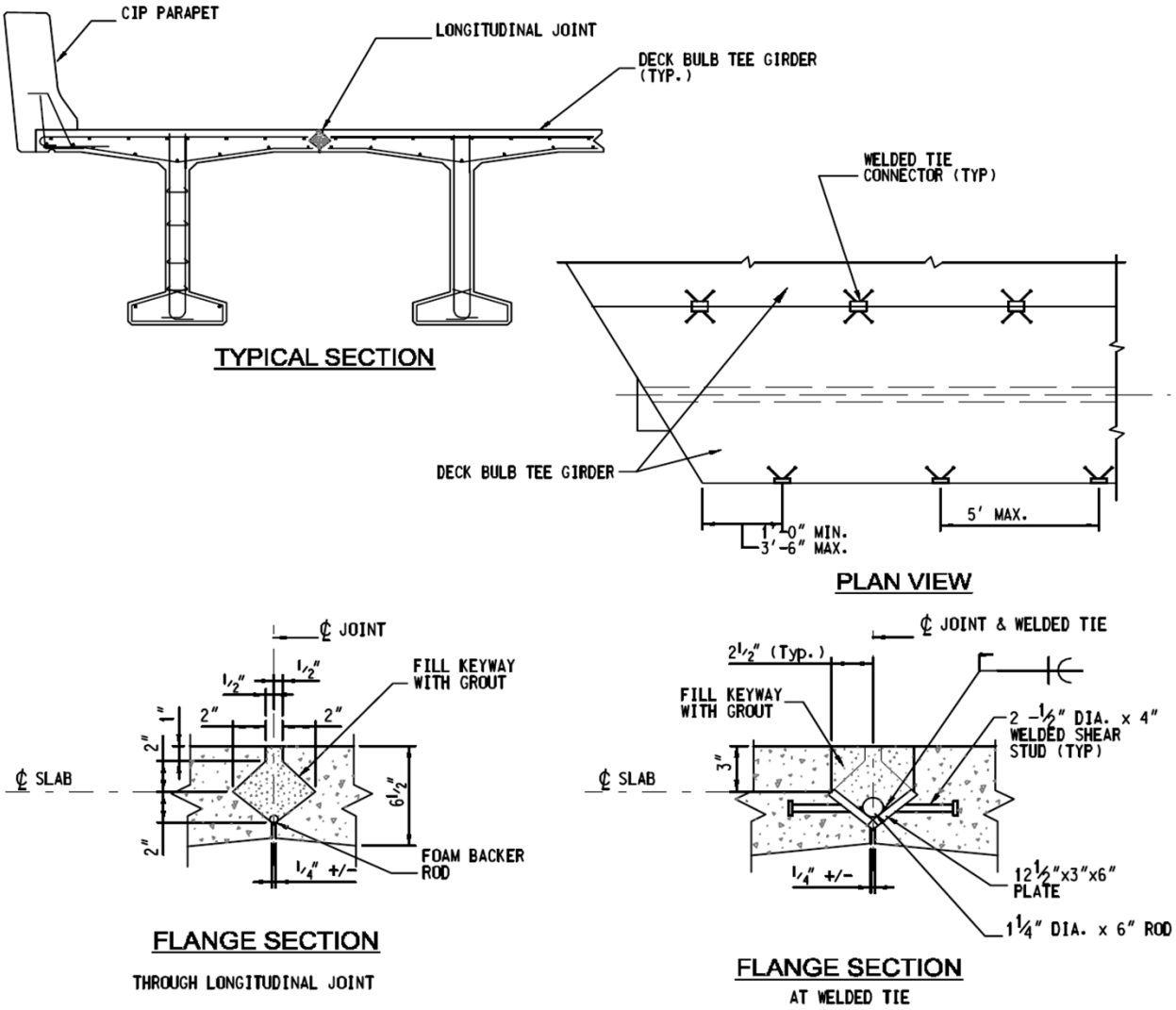

Figure 15. Welded tie connection detail for bulb tee beams used in Washington State, spaced at a maximum of 5 ft.

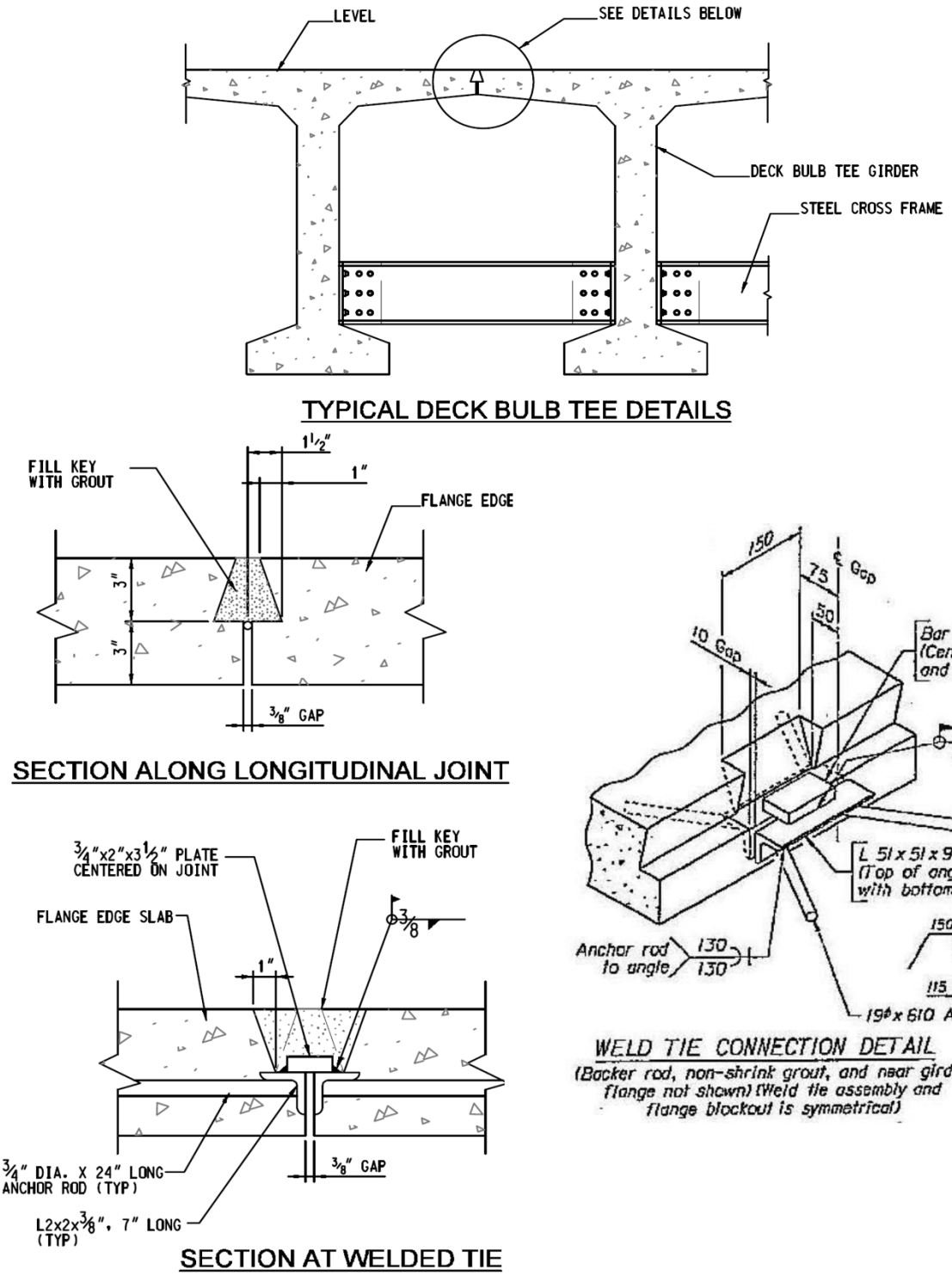

Figure 16. Welded tie connection detail for bulb tee beams used by the Wyoming DOT over Fork Crazy Woman Creek, spaced approximately every 6 ft.

2.3 UHPC Joints

Transverse deck cracking often present in the joints with traditional joint fill material discussed above has led to the development of alternate joint details utilizing UHPC. The simplest and most common detail for precast deck panel-to-panel connections involves lap splicing of mild steel reinforcing bars. In the context of Ultra-High Performance Concrete (UHPC), lap splice lengths are significantly shorter compared to those in conventional concrete. UHPC's exceptional bond strength with steel, combined with its compressive and tensile capacities, allows for simpler and more efficient designs. Shorter straight bars can be used in UHPC joints, which simplifies construction, reduces congestion of reinforcement, and minimizes labor costs. This is a major advantage in bridge construction, particularly when precast deck panels are connected in the field. UHPC's self-consolidating properties further reduce the potential for voids or defects during placement, resulting in stronger, more durable connections. In these connections, rebar from adjacent panels overlaps within a filled UHPC joint. The UHPC transfers the moment, shear, and tensile forces effectively across the joint. Typically, these connections are 6 to 8 inches (152 to 203 mm) wide, accommodating both lap splice lengths and construction tolerances (see Figure 17).

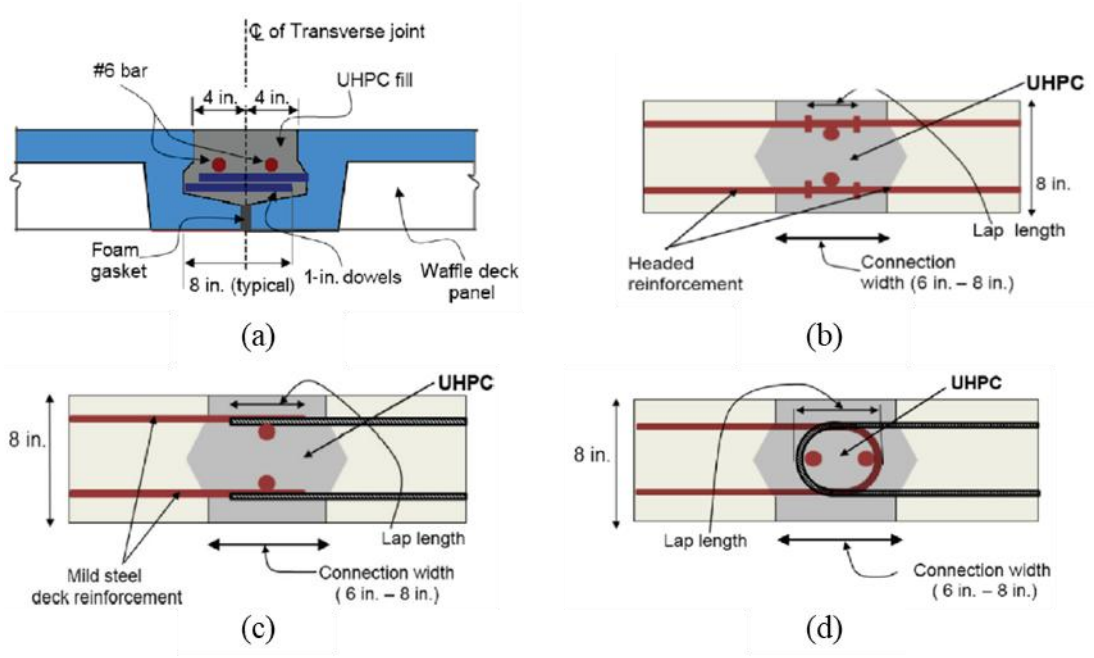

Figure 17: Common panel-to-panel UHPC connection details: (a) waffle deck panel-to-panel connection detail, (b) panel-to-panel headed connection detail, (c) panel-to-panel straight connection detail, and (d) panel-to-panel hairpin reinforcement [Aaleti and Sritharan, 2014][24].

Yuan et al. [23] proposed a novel joint detail using UHPC, without the need for post-tensioning, for connections between adjacent box beams. The aim of this design was to improve the performance of longitudinal connections, particularly in terms of strength and durability. The joint detail leverages UHPC's superior bond strength and reduced development length, providing a more efficient connection solution. Specific details of the developed joint demonstrate how UHPC simplifies construction and enhances load transfer between beams while minimizing reinforcement complexity and joint width (see Figure 18). The developed UHPC connection detail required the use of #4 reinforcement extended 5.5 inches into the joint, which provided a 4-inch splice length. Extensive large-scale experimental testing of the box beam specimens with this joint detail has

found that the UHPC connections performed well and created a robust joint region. To facilitate the use of UHPC joints and summarize the results of the work done by the FHWA, Graybeal[22] released a technical note on UHPC bridge connections. The note includes details for several different types of connections as well as the properties of several different available UHPC materials.

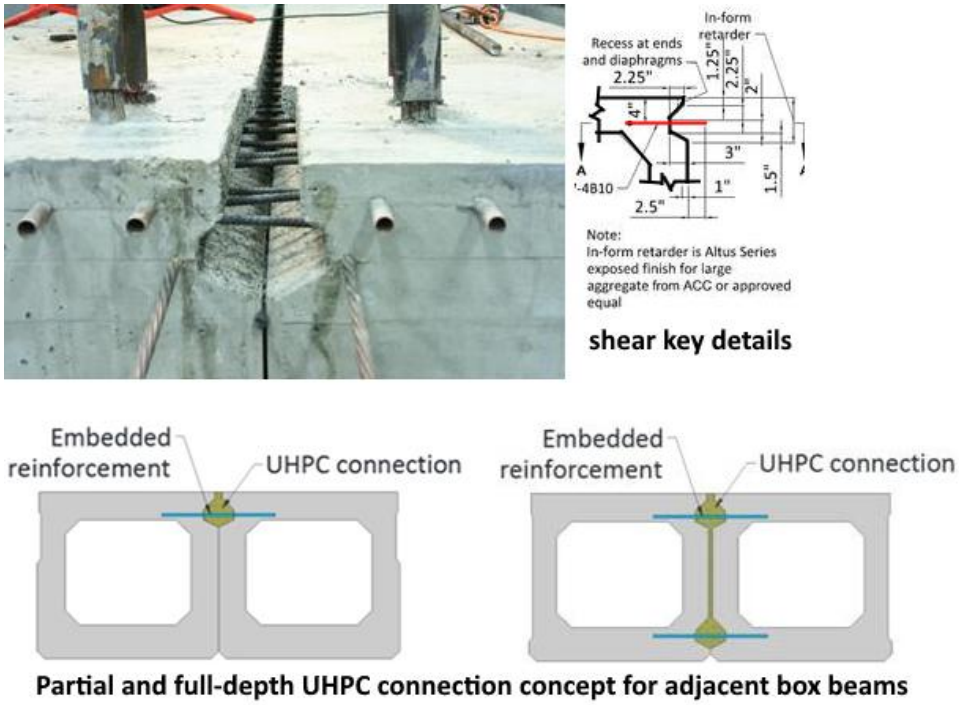

Figure 18: UHPC joint concept and shear key details developed for adjacent box beam connections, Yuan et al., 2018).

3 UHPC Material Characterization

This chapter presents a comprehensive material characterization of the ultra-high-performance concrete (UHPC) types, steel rebars, and normal concrete (NC) utilized in this study, with a focus on evaluating their structural behavior. Specifically, three different UHPC mix designs were examined to capture a range of performance attributes. Critical material properties, such as elastic modulus, compressive strength, tensile behavior, and shrinkage characteristics of the UHPC, were obtained through a combination of standardized ASTM testing procedures and tests conducted on full-scale specimens developed as part of this research project. Additionally, the stress-strain relationship of the steel rebars incorporated in the test specimens was assessed, as well as the compressive strength of normal concrete at the time of testing. Further investigations included an analysis of the joint roughness and bond behavior between UHPC and NC, which are crucial for understanding the composite behavior of these materials in structural applications.

3.1 Standard specimen geometry and fabrication

The compressive strength at different age and the elastic modulus of UHPC mixes were determined using standard 3 by 6-in UHPC cylinders, as per ASTM C1856[6]. Standard plastic cylinder molds were used to pour all UHPC cylinders (see Figure 19(a)). The tensile strength of UHPC was characterized using two different methods including, direct tension (DT) prism testing and an inverse analysis applied to four-point bending (4PB) beam results. The DT specimen dimensions were adapted based on the recommendation from the study by Graybeal and Baby.[7] The DT specimen is a 17-in. long, 2-in. square prism. The 4PB specimen is a 14-in. long, 3-in square beam, meeting the requirements of ASTM C1609[8], modified by ASTM C1856[6]. The 4PB specimen formwork was constructed with precision dimensioned wood (Figure 19(b)). As shown in Figure 19(c), a computerized numerical control (CNC) machine was used to ensure precision in the fabrication process of the DT wooden formwork shown in Figure 19(d). The formwork of both the DT and 4PB specimens was covered with a plastic waterproof adhesive layer. This process prevented any absorption of water from the UHPC mixture by the wood formwork, which could adversely impact the hydration process and material properties.

Shrinkage of the UHPC was measured using three different types of instrumentation. First, shrinkage beams were fabricated in accordance with ASTM C157[9]. The beams had a 3-in. square cross section and an 11.25-in. length, and their length change was measured using a length comparator device. As seen in Figure 19(e), steel molds were used to pour the shrinkage beams. Secondly, concrete strain gauges (SG) were placed at the center of UHPC cylinders (Figure 19(f)) and UHPC joints in slab and double-tee specimens and used to measure the shrinkage strains. Finally, a demountable mechanical strain gauge (DEMEC) was also used to measure strains on the surface of the UHPC poured in the joints of the slab specimens. The bond strength between UHPC and normal concrete was tested in direct tension using a UHPC -NC composite specimen. The bond specimens were fabricated with a constant 6-in. (152 mm) square cross section, and 6-in. (152 mm) long UHPC blocks were poured on a NC block with the same rough surface as the slab and double-tee specimens at the joint. Threaded rods with a diameter of 5/8 in. (16 mm) were embedded in the NC and UHPC blocks to perform the pullout test. Figure 19(g) shows a formwork used to pour UHPC for the bond specimens. Longitudinal #5 rebars used in the joints of slab and double-tee specimens were also tested in tension to obtain the stress-strain behavior of the steel reinforcement. Figure 20 shows the specimen geometries and dimensions used in the material characterization study after the demolding process.

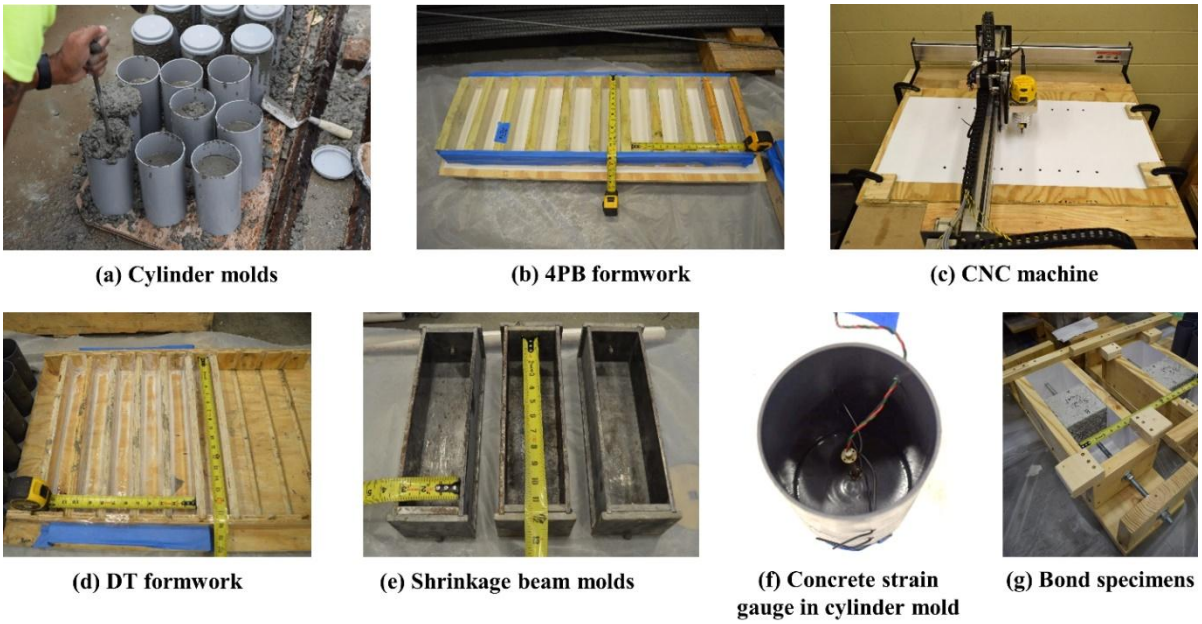

Figure 19. Formwork construction and assemble for material characterization specimens

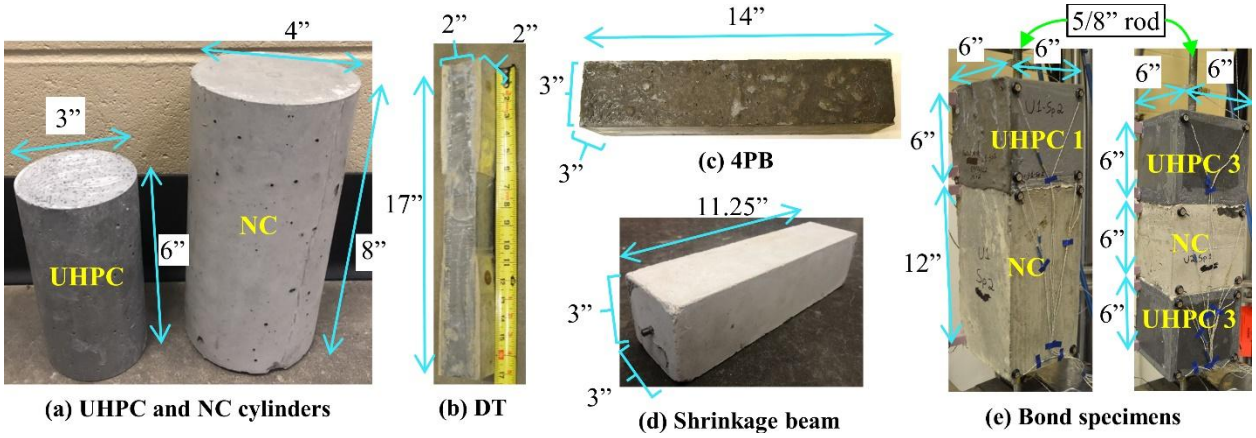

Figure 20. Specimen geometries of different test specimens used for UHPC material characterization

3.1.1 Casting and curing

Three commercially available UHPC formulations were used in this experimental investigation. These formulations consisted of premixed cementitious materials, water, admixture, and steel fibers. The three mix designs for each UHPC type (UHPC 1, UHPC 2, and UHPC 3) are detailed in Table 3. All steel fibers used in this study measured 0.5 inches in length and 0.008 inches in diameter. Figure 21 illustrates the different premix materials, steel fibers, and UHPC cylinders corresponding to each UHPC type.

A standard horizontal shear mixer as shown in Figure 21(d) was used for mixing. The three UHPC types used in this study followed the same mixing procedures as recommended by their respective manufacturers. he UHPC batch used for casting slabs or double-tee specimens was also used for material characterization specimens to assess the structural behavior of the concrete. As depicted

in Figure 21(e), UHPC was poured from one side of the formwork for both double-tee (DT) and four-point bending (4PB) specimens, allowing the material to flow freely and promote a preferential orientation of the fibers along the specimen length, perpendicular to the anticipated crack formation. This pouring technique was also applied to the shrinkage beam specimens. All specimens involved in the material characterization study underwent the same curing process as the slab and double-tee specimens. From the time of pouring until testing, all specimens were stored under consistent laboratory temperature and humidity conditions.

(a) Cementitious premixture (b) Steel fibers (c) UHPC cylinders

(d) Shear horizontal mixer (e) Flow direction of UHPC

Figure 21. UHPC materials and cylinders, shear horizontal mixer, and flow direction of UHPC

Table 3. Mix proportions of three commercially available UHPCs

Material	lb/yd^3 (kg/m^3)		
	UHPC 1	UHPC 2	UHPC 3
Premixture	3600 (2136)	3594 (2132)	3514 (2085)
Water	252 (150)	374 (222)	303 (180)
HRWRA[1]	36 (21)	32 (19)	42 (25)
Accelerator	-	-	20 (12)
Steel fibers	264 (157)	256 (152)	333 (198)
Percentage of steel fibers by volume	2%	2%	2.5%

[1]HRWRA = high-range water-reducing admixture

Several specimen types were tested in the material characterization investigation, including samples from all three UHPC types and rebars from slab as well as double-tee specimens. Table 4 displays the test matrix for all UHPC samples and specimens evaluating the joint interface.

Table 4. Test matrix containing number of tested UHPC and joint interface specimens

Test type	UHPC 1	UHPC 2	UHPC 3
Compressive strength	3 per data point	3 per data point	3 per data point

Elastic modulus at time of testing	3 for slab specimens 2 for double-tee specimens	3	2
DT	10	10	8
4PB	10	10	10
Shrinkage beams	3	3	3
DEMEC[1]	2	2	-
Cylinders with concrete SG measuring shrinkage	1	-	1
Joints with concrete SG measuring shrinkage	4	2	2
Tensile strength of bond specimens	2	-	2
Macrotexture depth of bond specimens	2	-	2

3.1.2 Compressive strength and Elastic Modulus

All the UHPC and NC cylinders tested for both compressive strength and elastic modulus results were loaded under a load rate of 145 ± 7 psi/s and 35 ± 7 psi/s, respectively, following the testing methodology suggested by ASTM C1856[6] for UHPC and ASTM C39[10] for normal concrete. A pair of surface strain gauges were applied on some of the UHPC cylinders used to obtain their strain in the direction parallel to the applied load, as permitted by ASTM C469[11], while other cylinders had a concrete strain gauge placed in the cylinder mold to capture their strain. The elastic modulus of the cylinders was calculated with the strain from the strain gauges and a load cell placed under the samples. The strain gauges and load cell were connected to a data acquisition system that recorded the data during testing. The specimens were loaded until approximately 40% of their peak compressive strength at least three times to determine their average elastic modulus. The UHPC cylinders were end-ground and tested without caps, whereas the NC cylinders were not end-ground, but unbonded caps were used on the bottom and top ends of the sample. Figure 22(a) shows a surface strain gauge used in one of the cylinders, Figure 22(b) displays a UHPC cylinder with a concrete strain gauge embedded in it, and Figure 22(c) shows the cylinder mounted in the hydraulic compression frame for elastic modulus testing.

The UHPC and normal concrete cylinder specimens were tested using a hydraulic compression frame using load control protocols. During testing, surface and concrete strain gauges were used to obtain local strains at specific locations in the specimens. Additionally, a non-contact displacement measurement system was used to obtain local displacements, strains, and deflections of some specimens based on the movement of light-emitting diode (LED) markers attached to the samples. All data for the material characterization specimens was recorded at a frequency of 20 Hz.

The compressive strength of all UHPC used in this study was periodically recorded from the day of casting to 28 days of age. Figure 23(a) displays the compressive strength curve over time for the three UHPC types used. The compressive strength of all UHPC types and NC and elastic modulus of UHPC were obtained at the time of testing. Figure 23 (b) shows the compressive stress-strain curve used to obtain the elastic modulus of the tested UHPCs. It can be seen that the stress-strain response of UHPC in compression is nearly linear until the peak strength. Table 5 shows the measured compressive strength and elastic modulus values for different concrete types at the time of testing. The results in Table 5 are shown with the precision recommended by ASTM C39[10] (10 psi

or 0.1 MPa) and ASTM C469[11] (50 ksi or 200 MPa) for compressive strength of concrete, and elastic modulus, respectively.

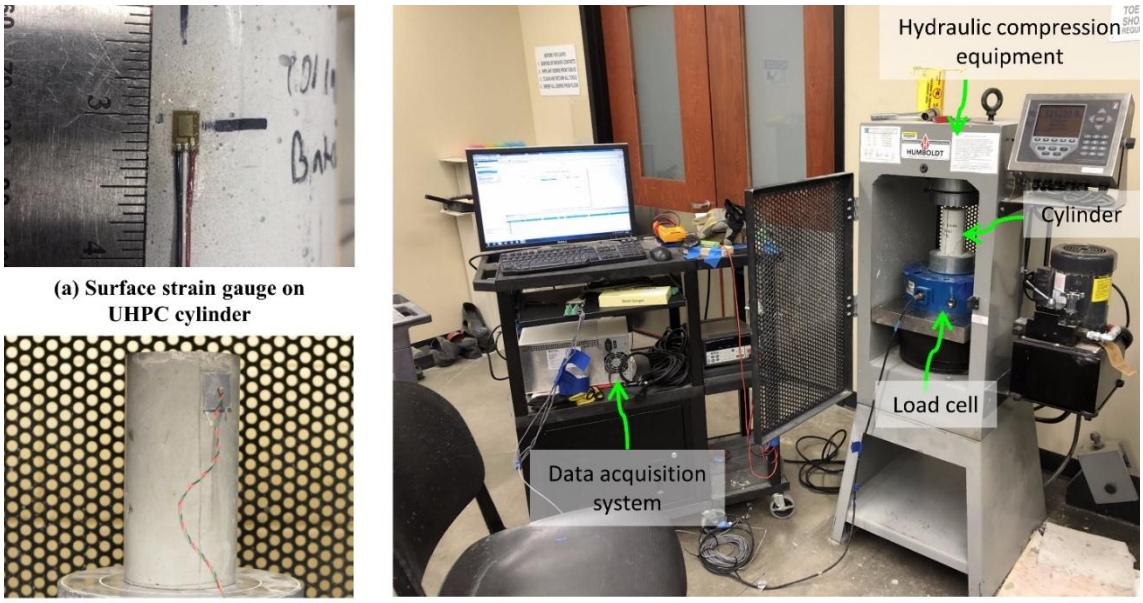

(a) Surface strain gauge on UHPC cylinder

(b) UHPC cylinder with concrete strain gauge

(c) Test setup for elastic modulus testing of concrete cylinders

Figure 22. Concrete cylinder strain gauges and test setup for elastic modulus testing.

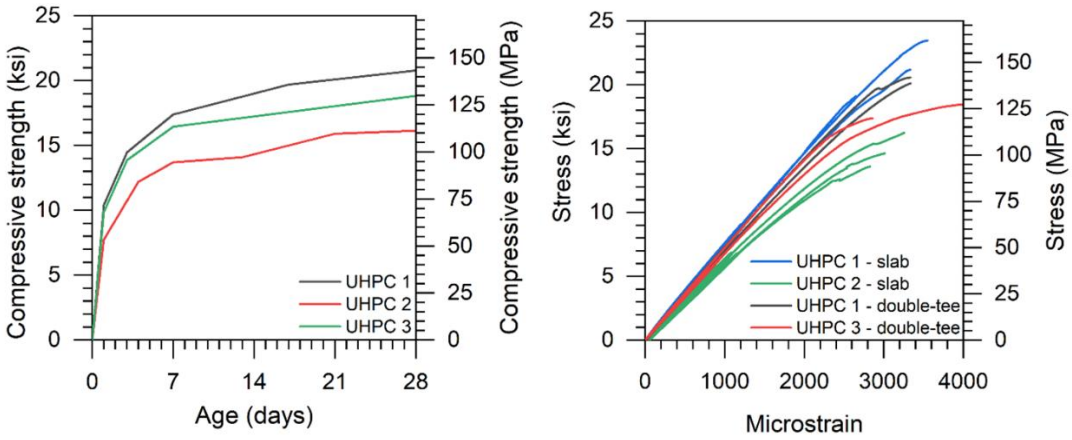

(a) Compressive strengths of UHPC types over time

(b) Compressive stress-strain curves of UHPC types at the time of testing

Figure 23. Compressive strength behavior of the different used UHPC types.

Table 5. Concrete compressive strengths at the time of testing

Concrete type	Compressive strength ksi (MPa)		Elastic modulus ksi (MPa)	
	Slabs	Double-tees	Slabs	Double-tees
UHPC 1	21.26 (146.9)	20.41 (140.6)	7,550 (52,200)	7,100 (48,800)
UHPC 2	16.14 (111.0)	-	5,950 (41,000)	-
UHPC 3	-	18.83 (129.6)	-	7,000 (48,000)
NC	7.15 (49.6)	9.72 (66.9)	-	-

3.1.3 UHPC Tension Behavior

There are currently several testing methods in the literature to evaluate the tensile strength of fiber reinforced concrete, but there is still a lack of agreement on which method is most suitable for UHPC. Two different test methods, including direction tension (DT) test and four-point bending (4PB) test, were used to characterize the UHPC tension behavior as there are currently no recommended standard test method. These test methods were chosen based on the ongoing industry efforts in this arena. The tensile strengths of the different UHPC types in this study were obtained from DT prisms and 4PB beams. While the DT results are directly obtained by dividing the applied load by the specimen's cross-sectional area, the tensile strength resultant from the 4PB specimens is calculated based on an inverse analysis from the moment-curvature response of the specimens. All DT, and 4PB tests were performed under displacement control using closed-loop servo-hydraulic testing frames. During testing, surface and concrete strain gauges were used to obtain local strains at specific locations in the specimens. Additionally, a non-contact displacement measurement system was used to obtain local displacements, strains, and deflections of some specimens based on the movement of light-emitting diode (LED) markers attached to the samples. All data for the material characterization specimens was recorded at a frequency of 20 Hz.

3.1.3.1 Direct Tension Test

A set of tapered aluminum plates were glued on opposite sides at both ends of the DT specimens using metal/concrete epoxy to minimize stress concentrations while the prisms were gripped by tension testing apparatus (Figure 24(a)). After gripping, the specimen was pulled at a constant displacement rate of 1×10^{-4} in./s until failure, as suggested by Graybeal and Baby[7]. The axial strain developed during testing of each DT specimen was obtained using LEDs placed over a 4 in. gauge length, capturing the elongation of each one of the four edges of the specimen. Figure 24(b) shows a specimen mounted in the testing frame with LEDs placed on each face of the prism. A total of 10 specimens per UHPC type were tested.

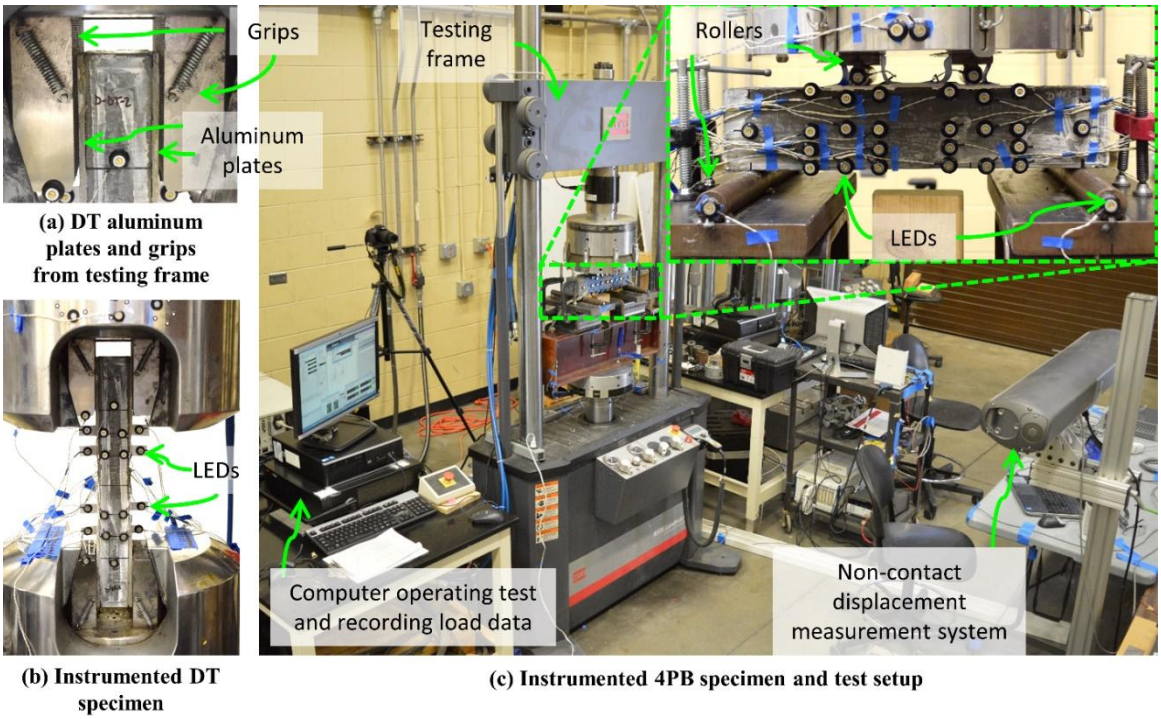

Figure 24. DT and 4PB instrumentation and test setup

To generate the DT tensile strength results, the average axial stress and the average axial strain were calculated according to Equation 1 and Equation 2, respectively.

$$f_t = \frac{T}{A} \tag{1}$$

$$\varepsilon_t = \frac{\Delta_L}{L} \tag{2}$$

Where f_t is the average tensile axial stress; T is the tensile load recorded by the testing frame; A is the average cross-sectional area based on caliper measurements at three cross-section locations; ε_t is the average axial strain; Δ_L is the average length change measured by four pairs of LEDs; and L is the gauge length equal to 4 in.

The stress-strain responses of the three different UHPC types used in this study are shown in Figure 25(a), and their peak stresses are displayed in Table 6. For simplification purposes, in Figure 25(a), "U" refers to UHPC, "avg" to average, and "sp" to individual specimen. Figure 25(b) shows the typical failure observed in the DT specimens. The observed tensile responses consist of three distinct phases: elastic, strain hardening, and strain softening. The elastic phase refers to the elastic straining of the composite UHPC section observed from the beginning of the test until the UHPC paste reaches its tensile strength and first cracking occurs. The second phase, which occurs between the breaking point and peak stress, is distinguished by the UHPC's strain hardening. The last phase, which occurs from peak load to the end of response, is associated with crack localization in the specimen. A similar tensile behavior was also observed by Wille et al.[16].

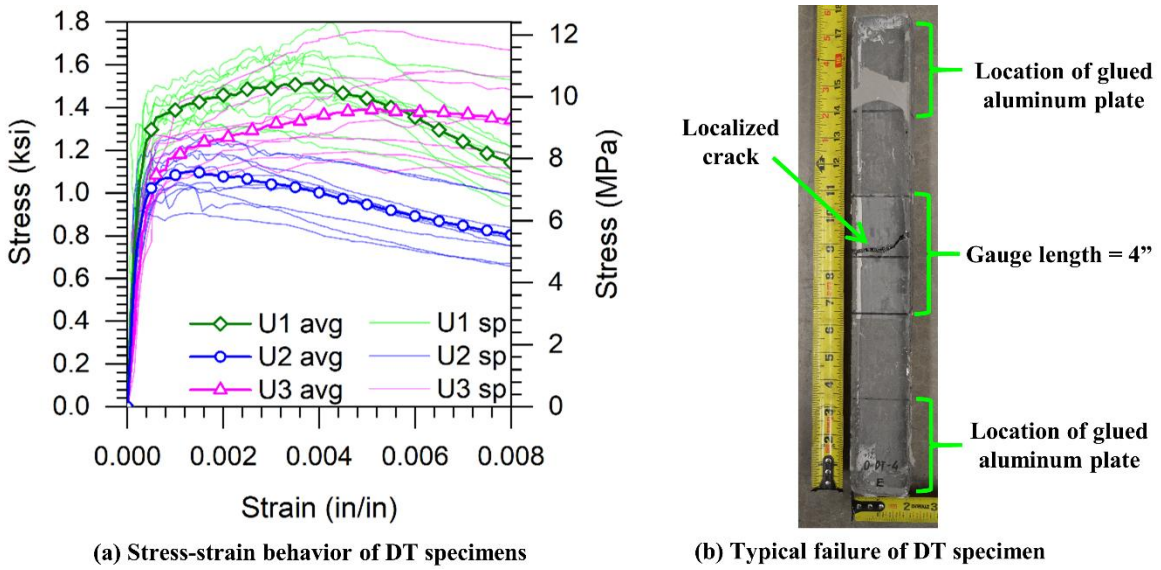

(a) Stress-strain behavior of DT specimens

(b) Typical failure of DT specimen

Figure 25. Measured Tensile stress-strain behavior of UHPC using DT method

Table 6. Peak tensile strengths of UHPC Mixes

Specimen	Peak tensile strength, ksi (MPa)		
	UHPC 1	UHPC 2	UHPC 3
DT-1	1.45 (6.45)	1.27 (5.65)	1.39 (6.18)
DT-2	1.62 (7.21)	1.05 (4.67)	1.57 (6.98)

DT-3	1.80 (8.01)	1.06 (4.72)	1.26 (5.60)
DT-4	1.57 (6.98)	0.93 (4.14)	1.76 (7.83)
DT-5	1.47 (6.54)	1.05 (4.67)	1.19 (5.29)
DT-6	1.34 (5.96)	1.04 (4.63)	1.16 (5.16)
DT-7	1.65 (7.34)	1.20 (5.34)	1.54 (6.85)
DT-8	1.67 (7.43)	1.25 (5.56)	1.35 (6.01)
DT-9	1.55 (6.89)	1.19 (5.29)	-
DT-10	1.36 (6.05)	1.14 (5.07)	-
Average	1.55 (6.89)	1.12 (4.97)	1.40 (6.24)
Standard deviation	0.14 (0.64)	0.11 (0.48)	0.21 (0.92)
Coefficient of variation	9.4 %	9.8 %	14.8 %

3.1.3.2 Four-point Bending Test

The 4PB beams were simply supported over a 12 in. span and were loaded at the two loading points that divide the span into 4-in. thirds under displacement control at a rate of 5.9×10^{-4} in./s (0.0015 mm/s). The load was recorded by the testing frame, and the three-dimensional (3D) optical tracking system, which recorded the movement of the LED markers, captured the beam local deformations. Several LEDs were arranged in a grid along the length and over the depth of the beam on its side facing the non-contact tracking system. The LEDs were used to calculate strains through the depth of the specimens in the constant bending moment region. The instrumented simply supported specimens and test setup used in the 4PB beams are shown in Figure 24(c). The same test setup was used for the DT specimens in another testing frame. The experimental results for the 4PB specimens were processed, and an inverse analysis was conducted to provide a stress-strain curve that could be compared directly to the direct tension stress-strain response.

In order to indirectly determine the UHPC stress-strain response for a particular specimen, inverse analysis of UHPC four-point bending tests requires measurement of the curvature of the beam.[17-19] The utilized method in this study, however, does not calculate the beam curvature indirectly from the midspan deflection or the load point deflection; rather, it obtains the beam curvature from observed axial strains using the aforementioned non-contact measurement device with LED markers. An experimental moment-curvature response was generated using the curvature determined from LED data and the bending moment calculated from the applied load.

In the proposed inverse analysis, moment-curvature response is determined for each 4PB beam using an assumed UHPC stress-strain behavior, as depicted in Figure 26(a). In the compression zone, the stress-strain relationship is assumed to be bilinear, whereas in the tension zone, it is assumed to be tetra linear. The variation of strain across the depth of the beam is assumed to vary linearly, as shown in Figure 26(b). The stress-strain response and elastic modulus of UHPC was obtained from cylinder compression testing results, as shown in Section 3.1.2**Error! Reference s ource not found.**. The calculated moment-curvature response is compared with the experimental response to determine whether they closely match with each other. If they do not match, the stress-strain response is modified and a new comparison between the moment-curvature curves is performed until a match is found. Once agreement is reached, it is decided that the predetermined stress-strain behavior accurately represents the tension behavior of the UHPC.

The inverse analysis in this investigation was performed on all of 4PB specimens. The typical failure of the 4PB specimens is shown in Figure 27(a). Figure 27(b) shows the observed experimental moment versus midspan deflection of the beams with their average response. Figure 27(c) displays the comparison between the experimental and calculated moment-curvature responses for one selected specimen of each UHPC type, and Figure 27(d) shows the UHPC stress-strain responses

obtained from the inverse analysis procedure with their average response. The results for the peak loads and stresses are summarized in Table 7.

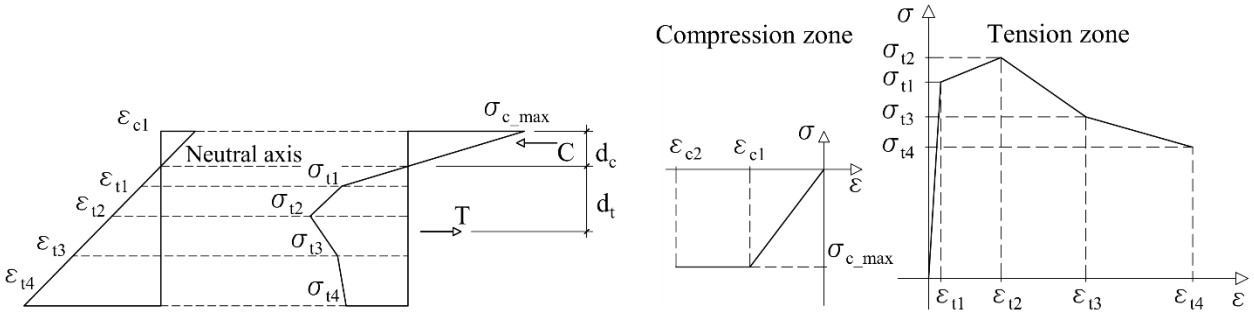

(a) Strain and stress profiles over the beam depth when $\varepsilon_c = \varepsilon_{c1}$ and $\varepsilon_t = \varepsilon_{t4}$

(b) Assumed stress-strain curve

Figure 26. Stress and strain assumptions for inverse analysis procedure

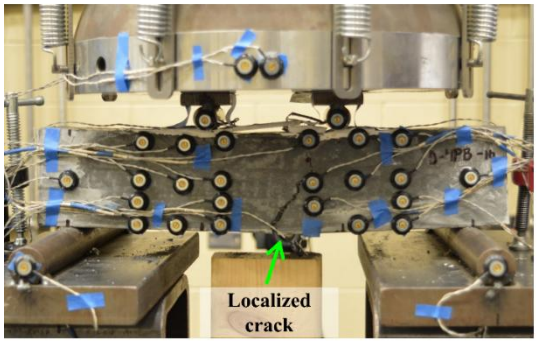

(a) Typical failure of 4PB specimens

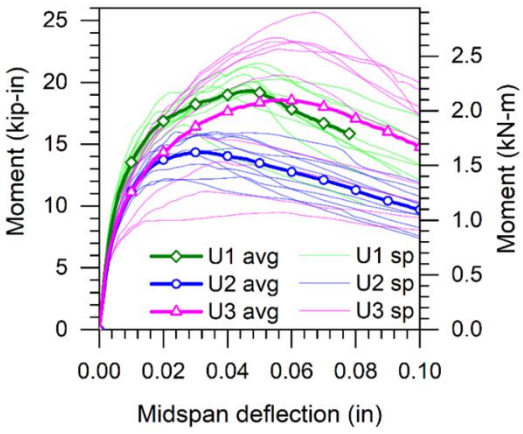

(b) Experimental moment vs. midspan deflection

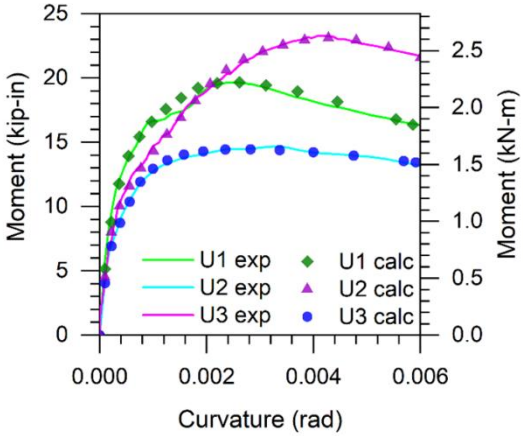

(c) Moment-curvature responses

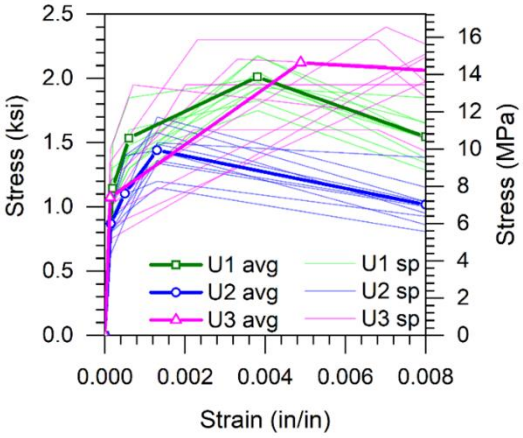

(d) Stress-strain response obtained from inverse analysis

Figure 27. Typical observed failure in 4PB specimens and calculated inverse analysis results

Table 7. 4PB specimens peak loads and tensile strengths

Specimen	Peak load, kip (kN)			Peak tensile strength, ksi (MPa)		
	UHPC 1	UHPC 2	UHPC 3	UHPC 1	UHPC 2	UHPC 3
4PB-1	12.21 (1.38)	20.25 (2.29)	23.27 (2.63)	1.15 (7.93)	2.01 (13.86)	1.60 (11.03)
4PB-2	16.02 (1.81)	16.58 (1.87)	22.72 (2.57)	1.66 (11.45)	1.80 (12.41)	1.95 (13.44)
4PB-3	15.88 (1.79)	19.78 (2.24)	23.62 (2.67)	1.50 (10.34)	2.10 (14.48)	2.30 (15.86)
4PB-4	12.35 (1.40)	20.08 (2.27)	25.67 (2.90)	1.20 (8.27)	2.23 (15.38)	1.95 (13.44)
4PB-5	14.53 (1.64)	21.27 (2.40)	20.57 (2.32)	1.49 (10.27)	2.19 (15.10)	2.35 (16.20)
4PB-6	14.27 (1.61)	21.56 (2.44)	23.31 (2.63)	1.44 (9.93)	1.95 (13.44)	2.05 (14.13)
4PB-7	15.84 (1.79)	20.65 (2.33)	15.81 (1.79)	1.58 (10.89)	2.05 (14.13)	2.15 (14.82)
4PB-8	16.00 (1.81)	19.14 (2.16)	13.60 (1.54)	1.70 (11.72)	1.93 (13.31)	2.40 (16.55)
4PB-9	13.40 (1.51)	19.20 (2.17)	11.21 (1.27)	1.34 (9.24)	-	-
4PB-10	14.67 (1.66)	19.67 (2.22)	9.48 (1.07)	1.36 (9.38)	1.85 (12.76)	2.35 (16.20)
Average	14.52 (1.64)	19.82 (2.24)	18.93 (2.14)	1.44 (9.94)	2.01 (13.87)	2.12 (14.63)
Standard deviation	1.39 (0.16)	1.32 (0.15)	5.56 (0.63)	0.17 (1.19)	0.14 (0.95)	0.25 (1.71)
Coefficient of variation	9.6%	6.7%	29.4%	12.0%	6.8%	11.7%

3.1.4 Shrinkage Behavior

The shrinkage beam specimens for all three UHPC mixes had their length change monitored at multiple time intervals from 24 h after casting to 28 days. The length change readings were obtained using a length comparator device according to ASTM C157[9]. Based on the initial length of the specimen and the variation of length over time, it is possible to calculate the concrete strain resulting from the shrinkage process. The variation of length is calculated with respect to a reference steel rod, which is kept in the same room as the specimens to avoid incorrect strain variations due to temperature change. Figure 28(a) shows the reading device with the steel rod mounted in it and Figure 28(b) displays a shrinkage beam having its length change measured. It is important to note that, by following the methodology described by ASTM C157[9], length changes were not obtained from casting time to the age of 1 day of the specimens. This time period, however, could be captured by concrete strain gauges in UHPC cylinders and joints connected to a data acquisition system. The concrete strain gauges recorded the UHPC shrinkage approximately during the first five days after the pour. The DEMEC device was only used to capture surface strains of the UHPC used in the slab specimens. Pre-tapped stainless steel disks were attached to the UHPC surface using cyanoacrylate adhesive. The disks were arranged in a two-dimensional grid of 5.9 in. using a setting out bar on the top and sides of the UHPC used in the joint. Similarly to the shrinkage beam measurements, the strains measured based on the local movement of disks due to concrete shrinkage were monitored several times over the span of 28 days. Figure 28(c) shows the top surface of one of the slab specimens with steel disks on its surface, and Figure 28(d) shows the DEMEC used to measure the strain between disks. The UHPC cylinders with a concrete strain gauge used to obtain their elastic modulus also had their strain due to shrinkage monitored during the first several days after their casting.

As mentioned in Section 3.1, the shrinkage of UHPC in this study was measured using three distinct techniques: shrinkage beams, the DEMEC device, and concrete strain gauges in UHPC cylinders and joints. Shrinkage beams were used to measure the shrinkage of each of the three UHPC types from the ages of 1 day to 28 days. After verifying that the DEMEC measurements were consistent with the results of the shrinkage beams in the slab specimens, it was determined that

shrinkage beams would be sufficient to capture the shrinkage strains in the double-tees. Concrete strain gauges placed in the center of the cylinders and joints of all specimens captured the initial shrinkage behavior of the UHPC from the moment it was poured until approximately 5 days later.

(a) Steel rod mounted on length change reading device

(b) Specimen mounted on length change reading device

(c) Specimen with pre-drilled steel disks attached on its surface

(d) DEMEC device used to measure strain between disks

Figure 28. Instrumentation used to monitor shrinkage of shrinkage beams and UHPC joint.

Figure 29 categorizes and illustrates all the shrinkage data collected in this investigation for the three different UHPCs into specimen and UHPC types. The UHPC shrinkage readings obtained from shrinkage beams and cylinders with concrete strain gauges, which were not captured directly from the joint, were plotted with the corresponding slab or double-tee specimens containing that specific UHPC type. The measured shrinkage strains varied between 400 to 800 microstrains for all three UHPC mixes.

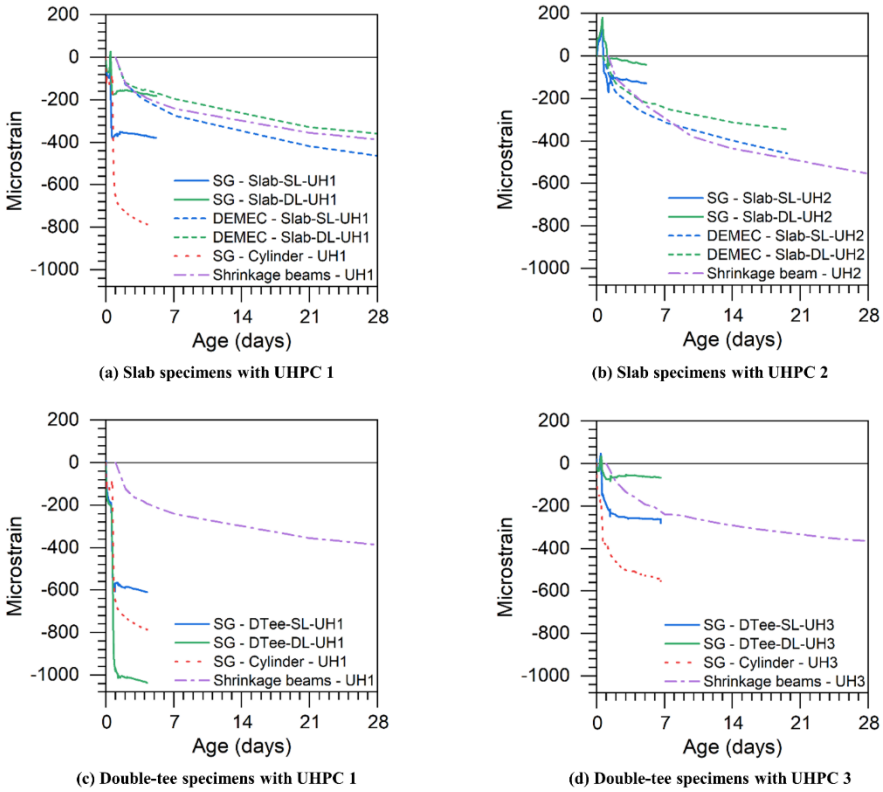

(a) Slab specimens with UHPC 1

(b) Slab specimens with UHPC 2

(c) Double-tee specimens with UHPC 1

(d) Double-tee specimens with UHPC 3

Figure 29. Measured shrinkage strains in the three UHPC mixes

3.1.5 UHPC-NC Bond Behavior under Tension

Before UHPC was poured on NC to form the bond specimens, the roughness of the NC blocks was determined by having their macrotexture depth calculated according to ASTM E965[12]. Sand passing a No. 50 sieve and retained in a No. 100 sieve was poured onto the NC clean surface and the material was carefully spread with a rubber circular disk, filling the surface voids flush with the aggregate particles. The macrotexture depth was then calculated with the known volume of the used sand and the measured NC concrete block surface area. Figure 30(a) and Figure 30(b) show NC joint interfaces before and after the use of the material on the concrete surface.

Threaded rods with a diameter of 5/8 in. (16 mm) were embedded in the NC and UHPC blocks and used to apply tension at the bond interface. The rods were gripped by the tension testing frame and pulled at a constant displacement rate of 2×10^{-4} in./s (5.08×10^{-3} mm/s). The interface opening was captured by the non-contact displacement measurement system, which recorded the movement of LEDs placed near the UHPC/NC interface on each of the four corners of the UHPC and NC blocks. Figure 30(c) shows a bond specimen mounted on the testing frame.

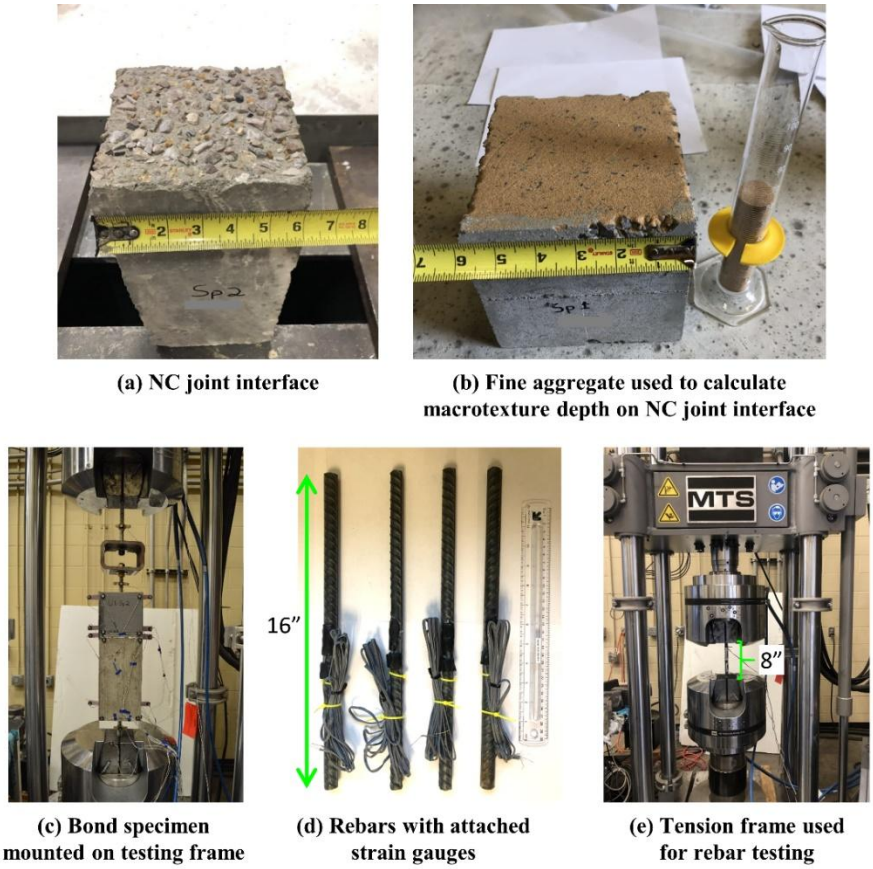

(a) NC joint interface

(b) Fine aggregate used to calculate macrotexture depth on NC joint interface

(c) Bond specimen mounted on testing frame

(d) Rebars with attached strain gauges

(e) Tension frame used for rebar testing

Figure 30. Test setup and details of bond specimens and rebars

The macrotexture depth of each of the four bond specimens was measured, and the average result is shown in Table 8. Only the UHPC types (UHPC-1 and UHPC-3) used in the double-tee specimens were included in the UHPC-NC interface bond strength tests. Two specimens per each UHPC type were tested. The measured bond stress vs. the interface opening response for all the bond specimens is shown in Figure 31(a). It was observed that the interface gap opening from the

moment loading is applied on the specimen until failure is less than the accuracy of the used non-contact measurement displacement system, which is 0.004 in. (0.1 mm). Due to this fact, the interface opening behavior seen in Figure 31(a) can be described as a mixture of the actual specimen behavior and data noise of the used equipment. The peak load, however, was accurately measured by the testing frame load cell. The peak bond stress was obtained by dividing the peak load by the measured squared concrete cross section and is summarized in Table 8. Figure 31(b) displays the tested bond specimens and their failure locations. The measured interface bond strength under direct tension is around 2.5 to 3.5 $\sqrt{f_c'}$, which is nearly 62% to 87% of the tensile strength of regular concrete.

Table 8. Bond specimen macrotexture depth test results

Specimen	Average macrotexture depth in. (mm)	Peak bond stress ksi (MPa)
U1-sp1	0.073 (1.85)	0.33 (2.28)
U1-sp2	0.077 (1.96)	0.36 (2.48)
U3-sp1	0.077 (1.96)	0.24 (1.65)
U3-sp2	0.075 (1.91)	0.23 (1.59)

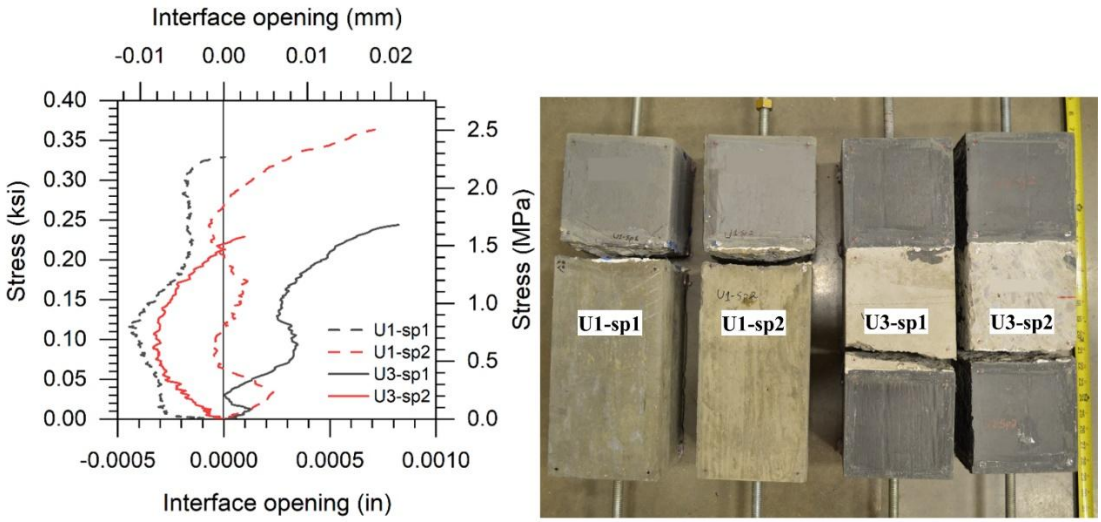

(a) Bond stress vs. interface opening

(b) Failure of bond specimens

Figure 31. UHPC-NC bond specimen response in tension and observed failure locations.

4 EXPERIMENTAL TESTING OF SLAB AND DOUBLE-TEE SPECIMENS

The long-term durability of transverse joints in adjacent precast concrete beams and slabs is a significant concern for state highway departments, particularly as the trend towards Accelerated Bridge Construction (ABC) grows. With the increasing replacement of aging bridges and the demand for new infrastructure, the use of precast concrete bridges will become more prevalent. The original shear key design used for NEXT D beams incorporated headed bars (see Figure 32a), which adds additional costs when compared to using a straight rebar. During the project duration, another NEXT-D beam bridge with UHPC in the joints, was designed to be used on a county bridge. This design had bottom flange reinforcement in NEXTD beam extend into the joint region and the adjacent beams were connected using UHPC in the joint (see Figure 32b). The shear key detail is critical for ensuring continuity between precast units while eliminating the need for additional transverse post-tensioning or structural topping over the precast elements. Further testing is necessary to evaluate the strength and stiffness of the current shear key configuration, including its shape and reinforcing details, under various loading scenarios. Previous studies have primarily focused on the performance of shear keys under conditions involving high moments. However, for the NEXT-D beam examined in this study, it is important to account for the presence of large shear forces and relatively small bending moments—an aspect that has not been sufficiently investigated in prior research. The experiments detailed in this chapter are designed to thoroughly evaluate the performance of the shear key in terms of its stiffness, strength under static loading, and durability under fatigue conditions.

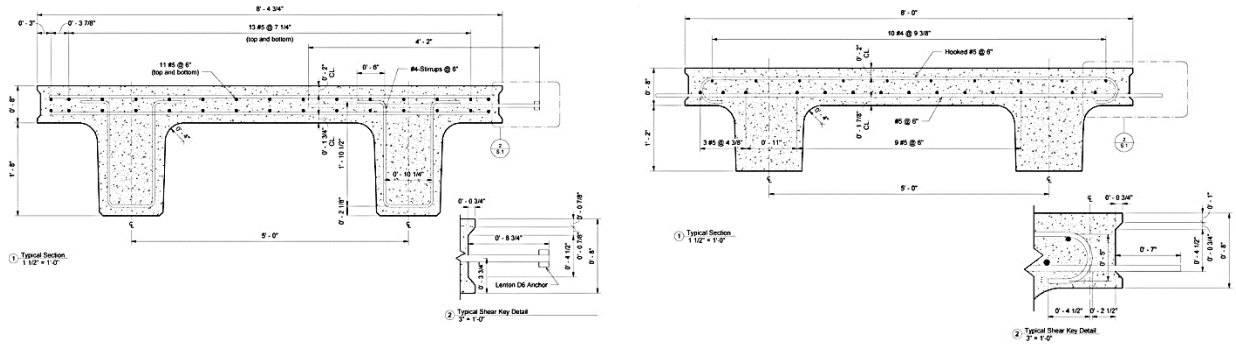

a) NEXT-D beam used in Mobile Bridge

b) NEXT-D beam used in County Bridge

Figure 32: Schematics of NEXT D beams used in bridge projects

Graybeal (2010b) conducted studies on diamond-shaped shear keys using Ultra-High Performance Concrete (UHPC) as the joint material, focusing on long-term fatigue damage. However, the shear key shape and reinforcing details in those studies differ from those considered in the present investigation. An experimental research program was undertaken to evaluate the structural behavior of the longitudinal shear key and its influence on bridge system design. The experiments focused on assessing the capacity and load-deformation characteristics of the shear key under static loading, as well as the reduction in strength and stiffness after up to 1 million loading cycles to evaluate fatigue performance. Since the shear key is designed to provide transverse continuity, and its performance is highly dependent on stiffness, a series of tests were designed to analyze the connection's behavior under varying load conditions.

This chapter presents the details of the experimental testing conducted on slab and double-tee specimen tests with different joint reinforcement details, UHPC materials and loading conditions. The loading protocols, locations of applied load, and instrumentation used for the slab and double-tee specimens tested in this study, the structural performance of the specimens are described.

4.1 Specimen dimensions and Joint details

The test specimens used in this experimental investigation to simulate UHPC joint connections in NEXT-D beam bridges were designed based on the actual cross-sectional details of the bridge beams used in real-world projects. The NEXT beams in these projects feature an 8-inch thick flange, with #5 Grade 60 reinforcement used for both longitudinal and transverse flange reinforcement. In one bridge, a #6 headed dowel bar with a standard Lenton D6 anchor head extended 8 inches into the joint region, while in another, the #5 bottom flange reinforcement from the beam extended 6.25 inches into the joint region (see Figure 32). The experimental investigation was done in two phases to minimize the costs and fine tune the experimental design parameters pertaining to UHPC mixes and joint reinforcement details. In Phase-1 of the testing, a 1.5-ft wide, 8 in. slab specimens to represent the flanges of NEXT D beams were used, with no headed reinforcement as joint reinforcement. In Phase-II of the testing, double-tee specimens made of 26 in. deep NEXT D beams with 8 in. thick flanges were used. The interface geometry between NC and UHPC is the same for the slab specimens and was slightly modified for the double-tee specimens to accommodate the prefabricated steel formwork shapes available at a local precast plant. The modification is a minor 1/8-in. (3.2-mm) change in the joint interface geometry that can be seen in Figure 33 and Figure 34. The specimens tested to simulate UHPC joint connections bridges using NEXT-D beams had the following geometry and connection details:

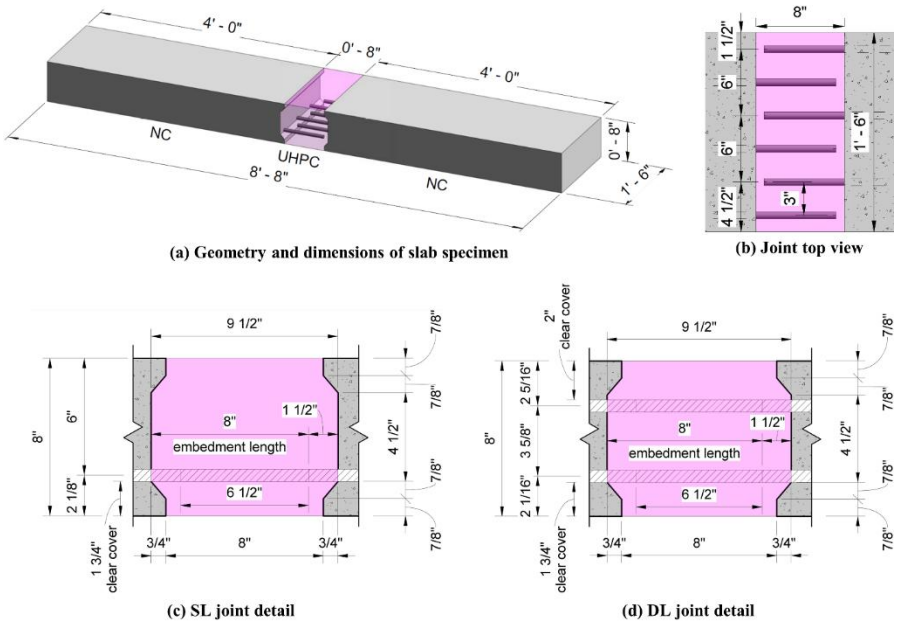

Figure 33. Phase-I slab specimen dimensions and joint details

Phase-I Slab specimens: The specimens were fabricated and tested before the construction of the double-tee elements and were designed to simulate a NEXT-D beam without its webs, consisting only of the beam's flange. These prismatic specimens measured 104 inches in length, 18 inches in width, and 8 inches in depth. Four slab specimens were constructed to evaluate the effects of two different UHPC types (UHPC 1 and UHPC 3) and two joint reinforcement layouts (single layer vs.

double layer). The specimens were divided into two groups: double-layer (DL) and single-layer (SL) slabs, with two specimens in each group.

The SL specimens feature a single layer of six rebars located near the bottom surface of the slab, extending into the UHPC joint, along with an additional layer of three rebars with 180º hooks embedded solely in the normal concrete (NC). These rebars have a clear cover of 2 inches from the top surface and 2.5 inches (64 mm) from the joint interface. The DL specimens share the same bottom-layer rebar configuration as the SL slabs, but the top-layer rebars are straight, with the same joint embedment length as the rebars in the bottom layer. All reinforcement used in the slab specimens consisted of #5 rebars. Figure 33 shows the specimen dimensions and joint details, including reinforcement lengths and interface shape.

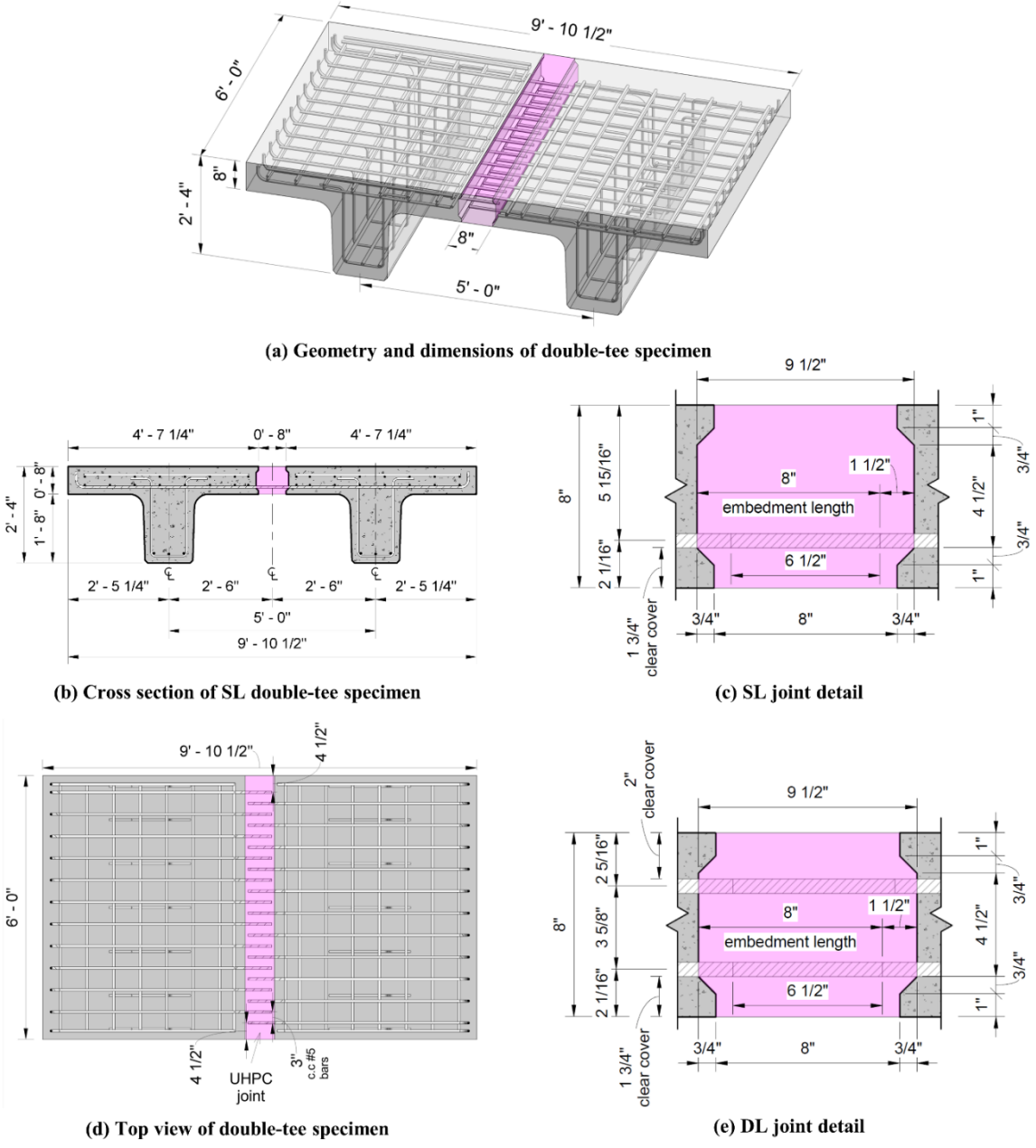

Figure 34. Double-tee specimen dimensions and joint details

Phase-II Double-tee specimens: the double-tee beams had a 5-ft. (1524-mm) span between the centerlines of the webs, a total height of 2 ft. 4 in. (711 mm), a length of 6 ft. (1829 mm), and a width of 9 ft. 10.5 in. (3010 mm). Similar to the slab specimens, the double-tees were grouped according to the number of layers of rebar embedded in the UHPC joint. Specimens with a single rebar layer crossing the joint interface are referred to as SL specimens, whereas double-tees with two layers of rebars present in the joint are categorized as DL specimens. The double-tee geometry and connection details of SL and DL specimens are depicted in Figure 34. More details regarding the reinforcement of the double-tees are provided in Section 4.2.

4.2 Test Specimen Fabrication and Material Properties

The construction process of the slab specimens for Phase-I study took place in the Large Scale Structures Laboratory at The University of Alabama. Dimensional lumber and plywood sheets were used for all slab specimen formwork, for both NC and UHPC pours. The normal concrete used in the slab specimens was mixed and poured using a ready-mix concrete truck, and concrete vibrators were used to aid the pouring process. The normal concrete slab specimen parts were cast first, and after 28 days of curing, the sections were assembled with the appropriate joint width between them for UHPC joint pour. Due to the small length of the joint (18 in.) compared to the joint length in a real-world bridge, during the UHPC pour a plastic waterproof adhesive layer was used to prevent any absorption of water from the plywood, preventing possible interference in the hydration process of the joint. Figure 35(a) shows a typical formwork used for the construction of the NC slab components, and Figure 35(b) shows a formwork used for the UHPC joint pour. In order to improve the bond between NC and UHPC at the joint, a commercially available in-form retarder was applied to the formwork in the joint regions. The retarder was applied on the whole joint interface of the slab formwork (Figure 35 (c)). After casting, the specimens were covered with plastic sheets to minimize water evaporation and were left to cure in the laboratory for 24 hours. The formwork was removed 24 hours post-casting, and the joint region was pressure washed to remove unhydrated concrete, which had been affected by the retarder application, creating a roughened surface in the joint area. Figure 37(a) illustrates the joint interface roughness during the power washing, showing half of the joint region after washing. Following this, the slabs were relocated outdoors to simulate field curing conditions. Burlap was placed over the specimens, as shown in Figure 37(b), with a plastic tarp covering them to help retain moisture. The burlap was kept wet by watering it twice a day for the first 14 days after casting.

For the Phase-II double-tee specimens, standard NEXT D formwork was utilized from a local precast plant. The casting of these specimens adhered to the typical procedures employed for NEXT bridge beams. In accordance with standard full-scale bridge construction practices, the retarder was not applied to the entire depth of the joint region. Instead, it was selectively applied only at the center of the joint interface of the double-tee formwork, as depicted in Figure 35(d). The wooden formwork used for the UHPC joint pour of the double-tee specimens is shown in Figure 35(e). The formwork for the double-tee specimens was provided and assembled by the local precast plant. Steel forms were used for the joint interface and bottom sections, while wood was used for the sides. Both normal concrete (NC) components of each double-tee specimen were identical, and the mild steel reinforcement details placed in the formwork for these laboratory specimens are shown in Figure 36. Similar to the slab specimens, the double-tee specimens featured only #5 rebars crossing the joint interface, spaced at intervals of 3 inches (76 mm). The NC used to cast the double-tee specimens was mixed in a concrete precast plant and used their standard ALDOT bridge mix used for full-scale bridge girders. The specimens were poured with the aid of mechanical equipment and vibrators (Figure 37(c)). Concrete cylinders were poured for material testing according to ASTM

C31[14] (Figure 37(d)). Similar to the slab specimens, a retarder was applied on part of the formwork (see Figure 35(d)) prior to the casting of concrete. Pressure washing was then applied on the joint surface of the specimens 24 hours after casting to create a rough surface at the joint interface to increase the bond strength between NC and UHPC. After the pour, the double-tee specimens were covered with plastic sheets to minimize water evaporation from the concrete, and heaters were used to accelerate the curing process of the specimens.

(a) NC formwork for slab specimens

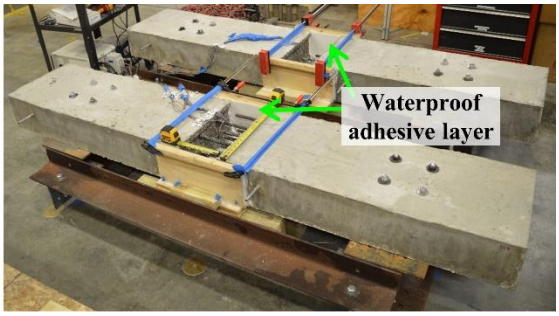

(b) UHPC joint formwork for slab specimens

(c) Joint surface in NC formwork for slab specimens

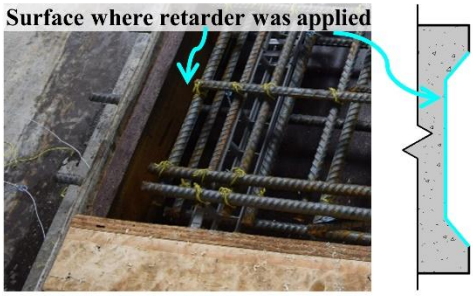

(d) Joint surface in NC formwork for double-tee specimens

(e) NC formwork for double-tee specimens

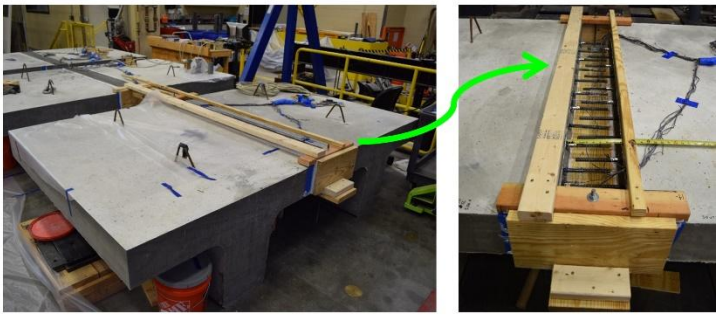

(e) Double-tee specimen with UHPC joint formwork

Figure 35. Formwork used for slab and double-tee specimens

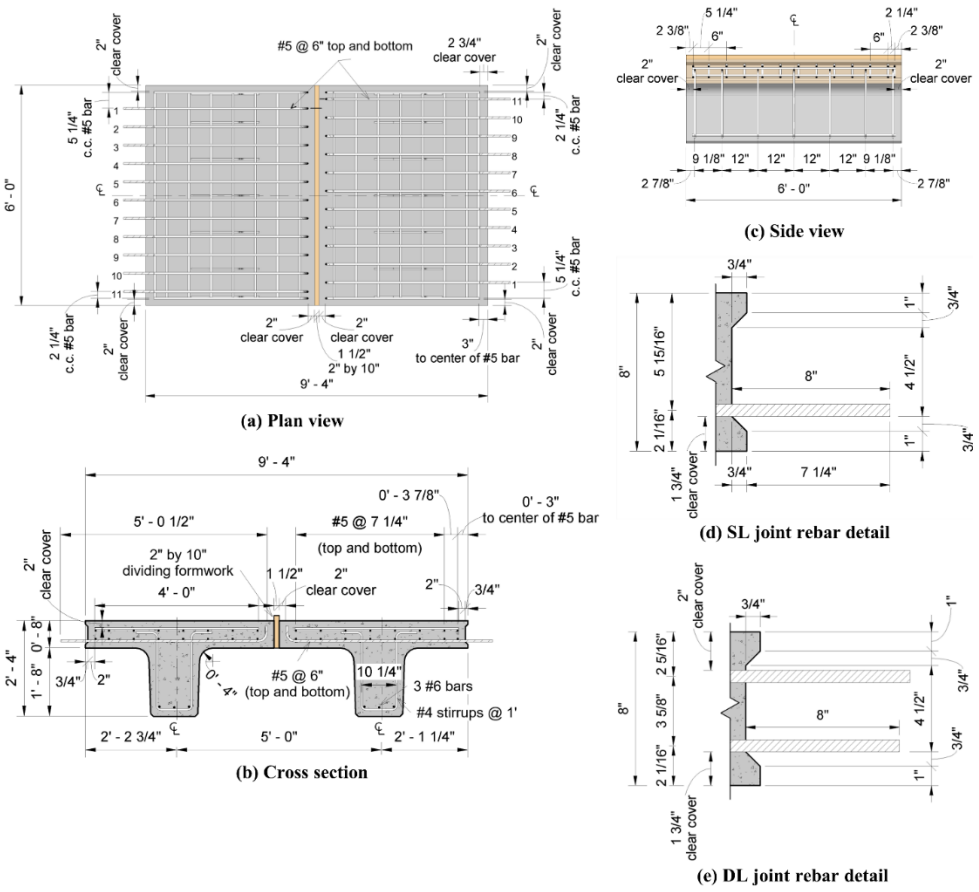

Figure 36. Details of mild steel reinforcement placed in double-tee formwork

Figure 37. Casting and curing of normal concrete slab and double-tee components and UHPC joints.

The UHPC mixing, casting, and curing processes for both the slab and double-tee specimens were identical, with the exception that, due to the larger volume of UHPC needed for joints in the double-tee specimens, two mixers were used simultaneously, as opposed to one that was used to pour the slab specimens. UHPC was poured from one side only of the joint, allowing the material to freely flow to the opposite side. The temperature of the mix was kept below 80 ºF (26.7 ºC) at all times. Figure 37(e) and Figure 37(f) show the pouring of the slab and double-tee UHPC joints, respectively. Similar to the NC curing process, the joints were also covered after casting to reduce water evaporation from the UHPC. The measured material properties for the test specimens are provided in Chapter 3.

4.3 Test matrix and Load Protocols

The performance of the UHPC joints in the slab and double-tee specimens was examined using several different types of tests. A total of four slab specimens and four double tees were tested in this study. All the load protocols described in this section apply to all the specimens of their respective shape (either slab or double-tee (i.e., DTee)) and rebar configuration (either SL or DL). Table 9 presents the test matrix, including the UHPC types used for the slab and double-tee specimens. The name of each specimen tested in this experimental program is shown in Table 10.

Table 9. Test matrix for slab and double-tee specimens

Specimen type	Rebar layer configuration	UHPC 1	UHPC 2	UHPC 3	Total
Slab	Single layer (SL)	1 specimen	1 specimen	-	2
	Double layer (DL)	1 specimen	1 specimen	-	2
Double tee	Single layer (SL)	1 specimen	-	1 specimen	2
	Double layer (DL)	1 specimen	-	1 specimen	2
Total		4 specimens	2 specimens	2 specimens	8

Table 10. Naming Scheme used for test specimens

Specimen type	Rebar layer configuration	UHPC 1	UHPC 2	UHPC 3
Slab	Single layer (SL)	Slab-SL-UH1	Slab-SL-UH2	-
	Double layer (DL)	Slab-DL-UH1	Slab-DL-UH2	-
Double tee	Single layer (SL)	DTee-SL-UH1	-	DTee-SL-UH3
	Double layer (DL)	DTee-DL-UH1	-	DTee-DL-UH3

For each specimen, a service load test, a fatigue test, an overload test and a failure load test were conducted. The overload was defined as a factor of the service level load, which will cause very minimal damage to panel or joint. The failure load was defined as a factor of the service load, which will cause a significant cracking or failure of the panel and joints. All the service, overload, and ultimate load tests were performed using monotonic increments of loads, and these tests were paused during loading to the target values for visual inspection of any damage to the test system, including formation of cracks. The fatigue and overload load values for service load tests were calculated based on the current AASHTO standard truck wheel load, from the AASHTO LRFD Bridge Design Specifications[15]. For the fatigue test, the specimens were subjected to 1 million cycles at a frequency of 2 Hz using a sinusoidal loading profile. The fatigue tests were periodically paused to monitor any possible progressive damage to the specimens and to apply ramp-shaped loading programs to evaluate the stiffness of the system. The maximum load applied during the stiffness

measurement tests was the same as the peak load of their corresponding fatigue test. Table 11 and Table 12 show the test matrix and summarize the details of the loading protocol, including the order of tests, test description, location of applied load, area of contact of the applied load, and maximum load of the slab and double-tee specimens, respectively. All the tests controlled by closed loop servo-hydraulic actuators (all except failure test in slab specimens and final overload test in DTee specimens) had a minimum load value of 0.50 kip (2.22 kN) at all the time to ensure that the actuator doesn't lose contact with the test specimens as number of cycles increased.

Table 11. Details of Test matrix and load protocols used for slab specimens

Test ID	Test description	Location of applied load	Peak load kip (kN)	Loading shape	Number of cycles
S1	Fatigue test	9 in. (229 mm) from center of joint	6.04 (26.9)	Sinusoidal	1,000,000
S2	Stiffness measurement test	9 in. (229 mm) from center of joint	6.04 (26.9)	Ramp	3 per test
S3	Overload test	9 in. (229 mm) from center of joint	12.1 (53.8)	Ramp	3
S4	Failure test	Center of joint	Varied per specimen	Load applied manually	2

Table 12. Details of Test matrix and load protocols used for double-tee specimens

Test ID	Test description	Location of applied load	Peak load kip (kN)	Loading shape	Number of cycles
D1	Fatigue test	9 in. (229 mm) from center of joint	21.3 (94.7)	Sinusoidal	1,000,000
D2	Stiffness measurement test	9 in. (229 mm) from center of joint	21.3 (94.7)	Ramp	3 per test
D3	Overload test	9 in. (229 mm) from center of joint	28.0 (124.6)	Ramp	3
D4	Overload cyclic test	9 in. (229 mm) from center of joint	28.0 (124.6)	Sinusoidal	1,500
D5	Final overload test	9 in. (229 mm) from center of joint	64.0 (284.7)	Load applied manually	4

The peak load value for the slab fatigue test (TEST-S1) was initially calculated using half of the design truck live load ($P_{des}/2$) for each axle provided by AASHTO[15], then multiplied by the dynamic load allowance factor of 1.33, which is an increment to be applied to the static wheel load to account for the wheel load impact from moving vehicles. Subsequently, the resultant load was multiplied by the ratio of the specimen width to the equivalent interior strip (obtained from the AASHTO equivalent strip method) calculated according to the specimen span and the sign of the bending moment generated by the load. Since the boundary conditions used during the testing resulted in a simply supported condition, a positive moment was generated at all times. This procedure was adopted due to the significantly reduced width of the slab specimens compared to full-sized NEXT beams. The peak load of overload test, TEST-S3 was obtained by doubling the peak load of the fatigue tests. After the fatigue, stiffness measurement, and overload tests were performed, the slab specimens were subjected to a final failure test (TEST-S4). The loading during tests S4 was paused periodically to capture and monitor crack formation and propagation as the load increased. During the failure load tests, slab specimens Slab-SL-UH1, Slab-SL-UH2, Slab-DL-UH1, and Slab-DL-UH2 were

loaded until their midspan deflection reached 2 in. (51 mm), 2.5 in. (64 mm), 1.8 in. (46 mm), and 2 in. (51 mm), respectively.

The double-tee specimens had their peak load for tests D1 and D2 calculated similarly to the slab tests S1 and S2, with the exception that the only factor applied to $P_{des}/2$ was the dynamic load allowance factor of 1.33. The peak loads for the overload test (D3) and the overload cyclic test (D4) were obtained by multiplying $P_{des}/2$ by the dynamic load allowance factor of 1.75. Subsequently, a final overload test was operated on each double-tee specimen. The test consisted of three cycles of 48 kip (213.5 kN) each, which created a bending moment that surpassed the calculated cracking moment of the system, and one cycle with a peak load of 64 kip (284.7 kN), which was lower than the calculated ultimate capacity of both SL and DL specimens. The test was paused at load values 15 kip (66.7 kN), 35 kip (155.7 kN), 48 kip (213.5 kN), and 64 kip (284.7 kN) to observe and monitor the formation of cracks and crack propagation on the specimens.

During the fatigue test (TEST S1) for all of the slab specimens, static stiffness measurement tests (TEST S2) were periodically performed after different number of load cycles to monitor the change in stiffness of the system. Typically, stiffness tests (S2) for all the specimens were operated every 200,000 cycles during fatigue tests (S1). However, the number of cycles between tests S2 was occasionally modified in order to minimize any possible idle time during the fatigue experiment. It was observed that, since the change in stiffness of the slab specimens was not significant, for the double-tee specimens, D2 tests were performed every 500,000 cycles during D1 tests. Table 13 and Table 14 show when tests S2 and D2 were performed during fatigue tests (S1 and D1) for slab and double-tee specimens, respectively.

Table 13. S1 cycle number in which test S2 was performed

Test S2 number	S1 cycle number for each slab specimen			
	Slab-SL-UH1	Slab-DL-UH1	Slab-SL-UH2	Slab-DL-UH2
1	0	0	0	0
2	100,000	135,000	200,000	200,000
3	300,000	300,000	400,000	400,000
4	500,000	450,000	600,000	600,000
5	700,000	700,000	800,000	800,000
6	865,000	835,000	1,000,000	1,000,000
7	1,000,000	1,000,000	-	-

Table 14. D1 cycle number in which test D2 was performed

Test D2 number	D1 cycle number for each slab specimen			
	DTee-SL-UH1	DTee-DL-UH1	DTee-SL-UH3	DTee-DL-UH3
1	0	0	0	0
2	500,000	500,000	500,000	500,000
3	1,000,000	1,000,000	1,000,000	1,000,000

4.4 Test setup and Instrumentation

This section presents the details of the test setup, instrumentation, and equipment used to operate and monitor the performance of the slab and double-tee specimens during testing. Several different types of instruments were used for this study, including linear variable differential transducers (LVDTs), string potentiometers, load cells, strain gauges, and LEDs (used with the non-

contact displacement measurement system). For tests S1, S2, S3, D1, D2, D3, and D4, 35-kip (156-kN) capacity closed-loop servo-hydraulic actuator was used to conduct the experiments with load control protocols described in Section 4.3. Hydraulic jacks with a load capacity of 206-kip (916-kN) were used for tests S4 and D5. The load for these tests was applied manually with a hydraulic hand pump connected to the loading jack.

All the strain gauges used in the slab specimens were placed at the joint location. Surface strain gauges were applied on rebars protruding from the NC into the UHPC. These gauges were placed either at the center of the joint or as close as possible to the joint interface. A pair of concrete strain gauges were placed in the joint of each specimen. One concrete gauge was placed at the center of the joint, while the other was positioned below the first one, at the same height as the bottom rebar layer. After casting, four surface strain gauges were also applied on the sides of the joints, two on each side at heights of 2 1/16 in. (52 mm) (same height as the bottom rebar layer) and 7 5/8 in. (194 mm) (or 3/8 in. (9.5 mm) from the top surface). Figure 38 shows the location of the strain gauges used in the slab specimens.

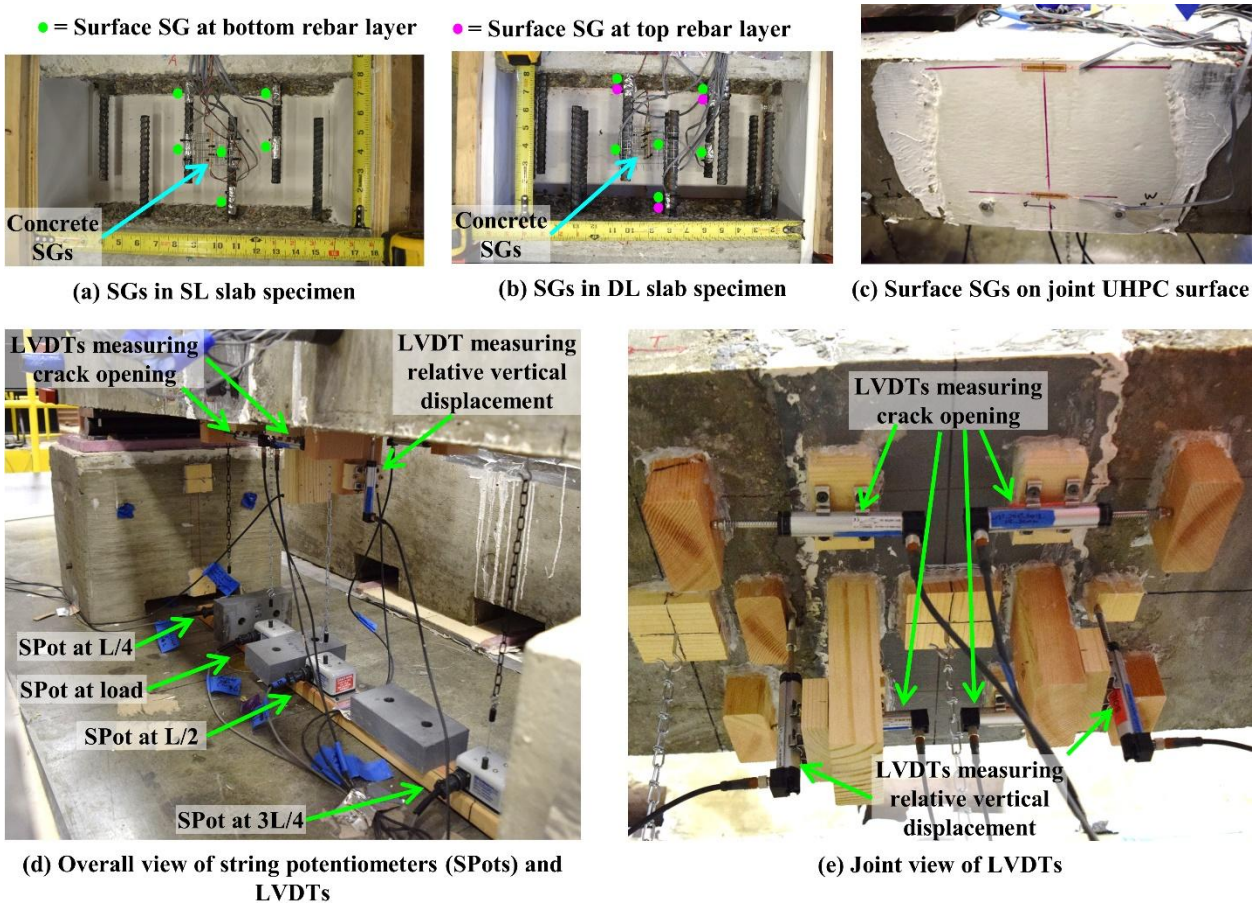

(a) SGs in SL slab specimen

(b) SGs in DL slab specimen

(c) Surface SGs on joint UHPC surface

(d) Overall view of string potentiometers (SPots) and LVDTs

(e) Joint view of LVDTs

Figure 38. Instrumentation details used in all four slab specimens during Tests S1, S2, and S3

During tests S1, S2, and S3, the slab specimens were simply supported over a span (L) of 5 feet 8 inches, representing the distance between the faces of the webs of two adjacent NEXT beams. A 1 in. thick and 3 in. wide steel plate on top of a 3-in. (76-mm) diameter steel rollers, which allowed free rotation at those locations were used as supports for these slab specimens. String potentiometers were used to capture the deflection of the slab at the locations L/4, L/2 (midspan),

3L/4, and at the location of the center of the applied load, which was at 9 in. (229 mm) from midspan (approximately at 0.37L). All string potentiometers were positioned at half the specimen width at their respective locations along the span length. The crack opening at the bottom surface of the slab on both sides of the joint interface was monitored using a total of four LVDTs. Each pair of the instruments was placed on each joint interface location, and each LVDT in its pair was placed 10 in. (254 mm) apart from one another. The relative vertical movement at the joint between UHPC and NC was also monitored by attaching one LVDT on each side of the joint, centered along the specimen width. The loading was applied at a distance of 9 in. (229 mm) from the center of the specimen, such that the edge of the loading area coincided with the edge of one of the joint interfaces. Figure 38 shows the instrumentation used during the slab tests S1, S2, and S3, and Figure 39 shows the test setup with the steel loading beam and the 10 in. by 10 in. (254 mm by 254 mm) neoprene pad used on the specimens.

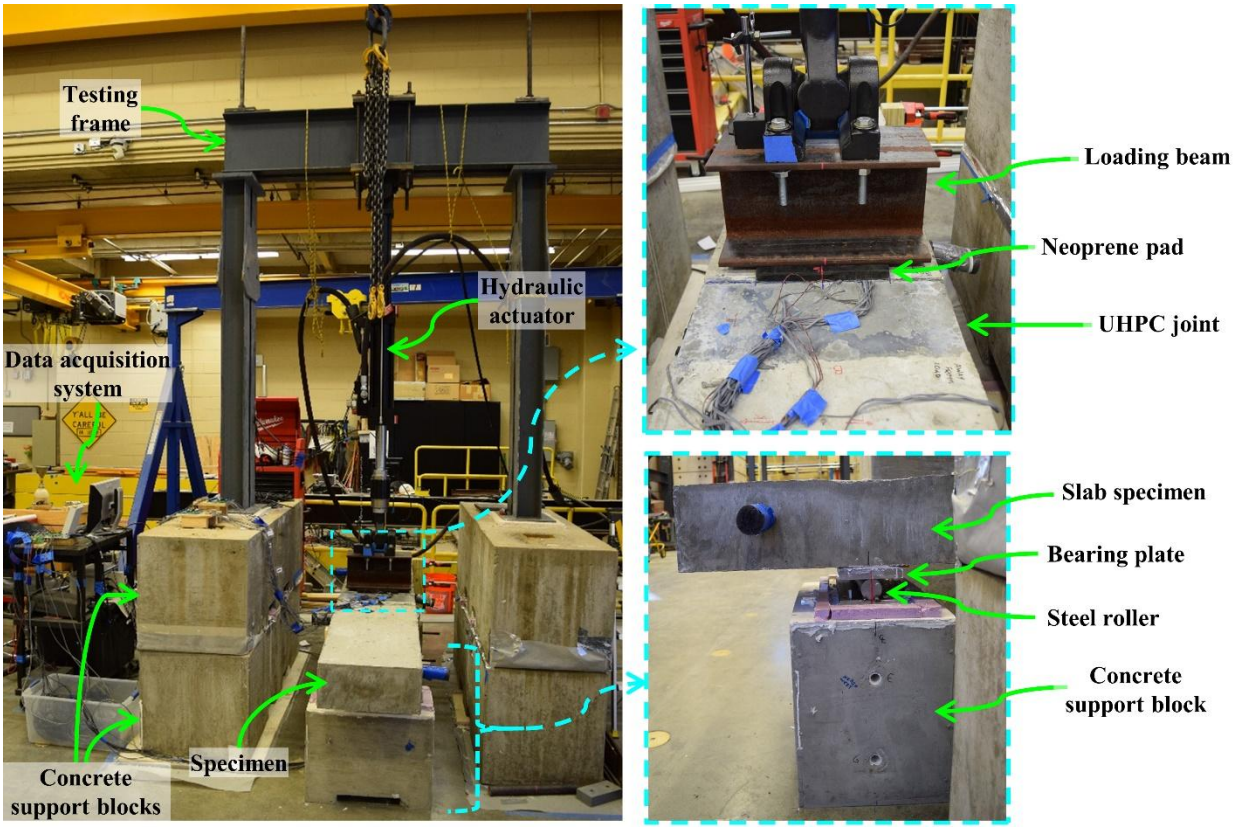

Figure 39. Test setup used for the slab specimens tests S1, S2, and S3

The supports locations were moved during failure test, S4, for all the slab specimens, to avoid a potential shear failure. For this test, the slab specimens were simply supported over a span of 8 ft. 2 in. (2489 mm), and the load was applied at the center of the specimen. A in. thick neoprene pad measuring 4 in. (102 mm) by 14 in. (356 mm) was used to distribute the load over the top joint surface. The same instrumentation as used during tests S1, S2, and S3 was also used during test S4, with the addition of LEDs, a non-contact measurement system to capture deflection along the beam length and joint opening along the specimen depth at the joint interface location. The pairs of LEDs placed to measure the joint opening were spaced 2 in. (51 mm) apart along the joint depth. Figure 40 shows the test setup used for test S4 for all the slab test specimens.

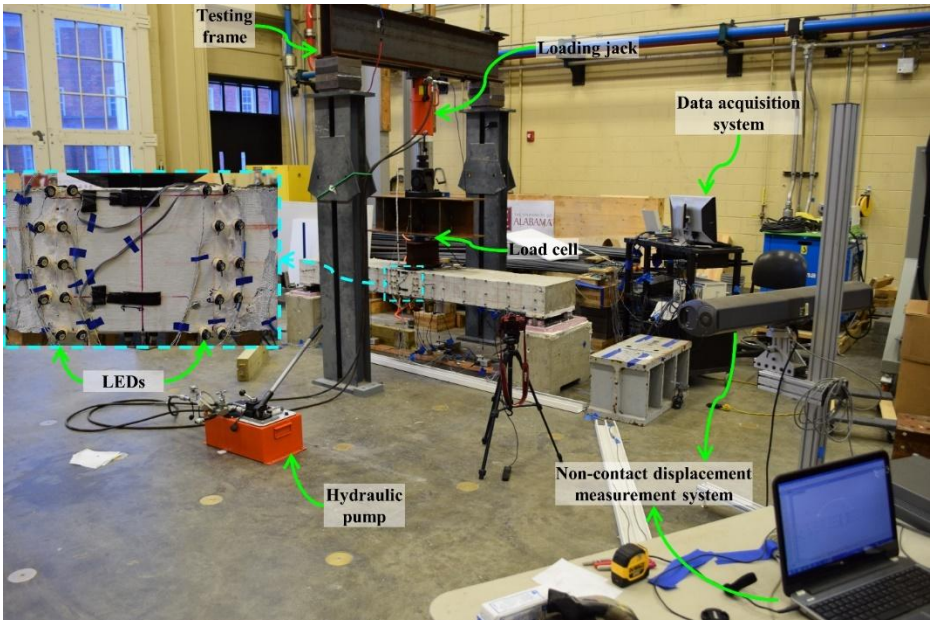

Figure 40. Test setup used for Test S4 for all the slab test specimens.

The double-tee (DTee) specimens were instrumented with concrete strain gauges placed in the UHPC joint and surface strain gauges placed on rebars at several locations. The location of the applied strain gauges in these specimens is depicted in Figure 41, with concrete strain gauges showed in red and steel gauges showed in blue. No surface strain gauges were applied on rebars at the top rebar layers in the specimens with two layers of rebar. The instrumentation used on the double-tee specimens remained the same throughout their different tests. Similarly to the slab specimens, the double-tee specimens had string potentiometers monitoring their deflection at multiple locations and LVDTs capturing the joint opening (placed horizontally) and relative vertical displacement between UHPC and NC (placed vertically). Due to the fact that a horizontal and a vertical LVDT could not fit at the same location along the joint longitudinal axis as a string potentiometer, the LVDTs had to be spaced 2.5 in. (64 mm) apart from the string potentiometers. Figure 42 provides the location of the string potentiometers and LVDTs used on the double-tee specimens.

The test setup for tests D1, D2, D3, and D4 was similar to the one for S1, S2, and S3. A 35-kip hydraulic actuator was used to apply the load at a location of 9 in. (229 mm) from the center of the specimen in the direction perpendicular to the joint longitudinal axis. A 10 in. by 10 in. by 8 in. (254 mm by 254 mm by 203 mm) UHPC prism was cast and used as a loading block, and a 10 in. by 10 in. (254 mm by 254 mm) neoprene pad was used to evenly distribute the load from the actuator to the specimen. The neoprene pad used for testing measured 10 inches by 10 inches, which is half the size of a standard wheel load dimension (10 inches by 20 inches). This reduced pad size was intentionally selected to apply maximum loading over the joint, creating a more conservative test condition. By concentrating the load over a smaller area, the testing imposed higher stresses than would occur under a full wheel load in real-world conditions, ensuring a more rigorous assessment of joint performance. Two double-tee specimens were tested simultaneously using two separate testing frames to meet the testing schedule requirements. Figure 43 illustrates the test setups employed for each specimen. Each specimen was equipped with instrumentation connected to one of two independent data acquisition systems, which operated separately throughout the testing process.

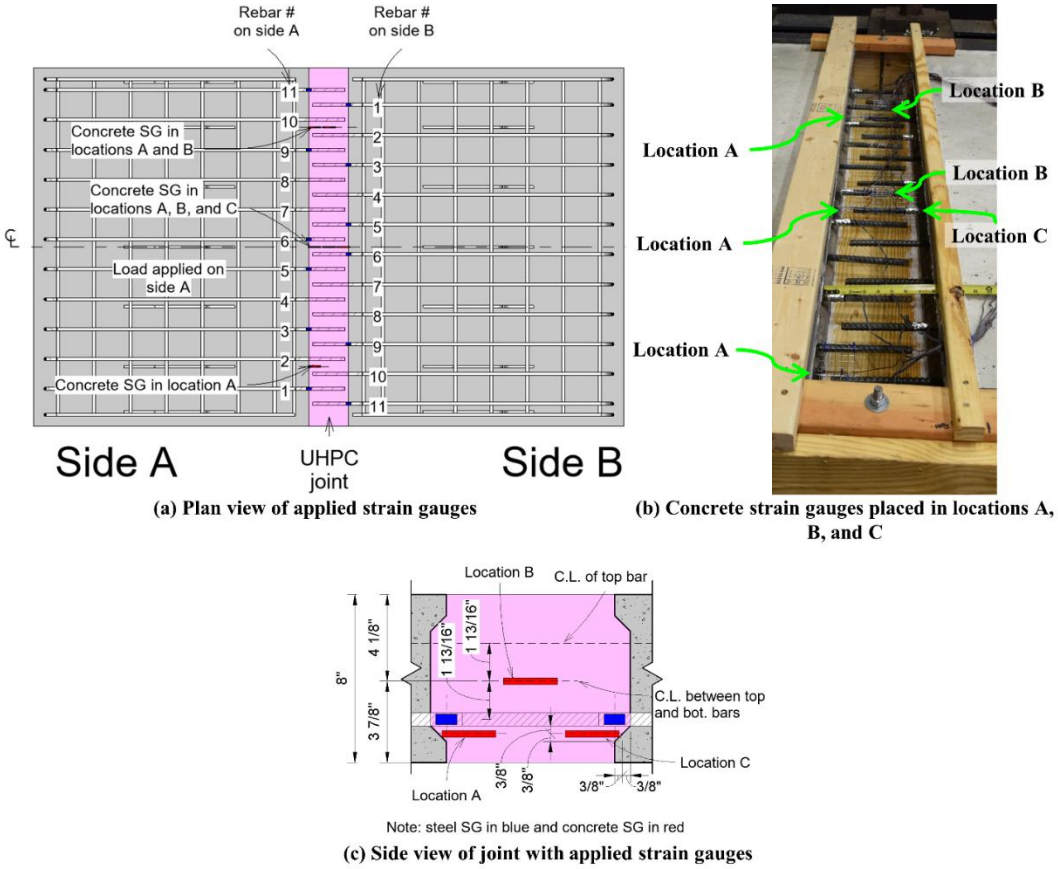

(a) Plan view of applied strain gauges

(b) Concrete strain gauges placed in locations A, B, and C

(c) Side view of joint with applied strain gauges

Figure 41. Strain gauges applied in the joint of double-tee specimens

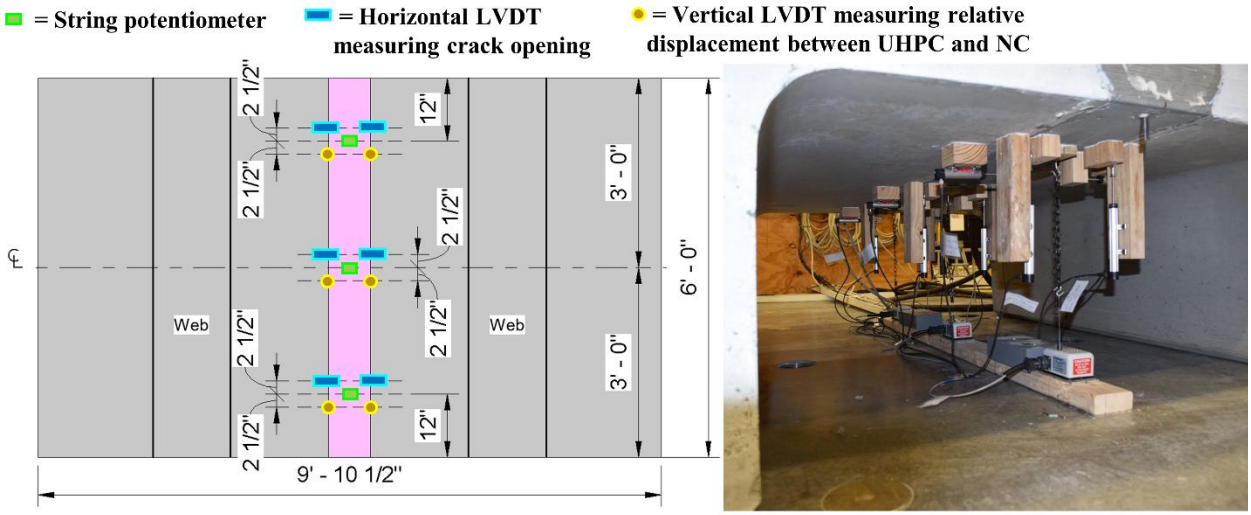

(a) Bottom view of locations of string potentiometers and LVDTs

(b) String potentiometers and LVDTs placed on specimen

Figure 42. Location of string potentiometers and LVDTs during all double-tee tests

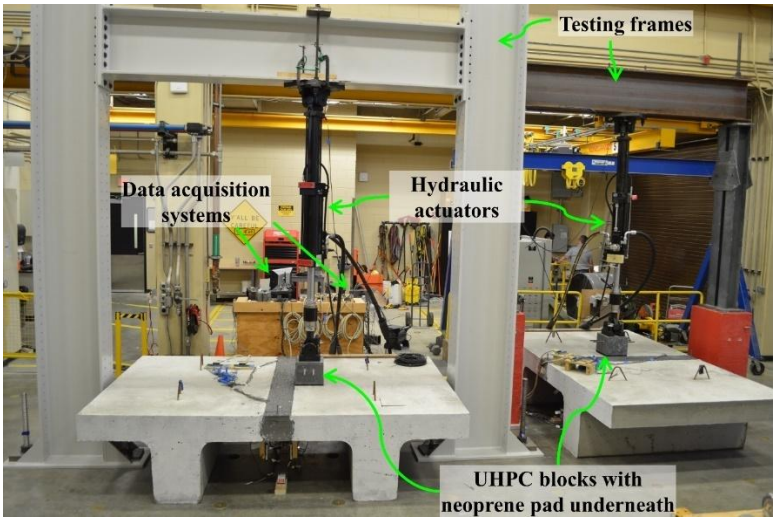

Figure 43. Test setup used for double-tee specimens Tests D1, D2, D3, and D4

All tests D5 were conducted using the same testing frame. A manually operated 206-kip (916-kN) hydraulic loading jack was used to load the double-tee specimens. As previously mentioned, the instrumentation remained the same as used in tests D1, D2, D3, and D4. Figure 44 shows the test setup used for tests D5.

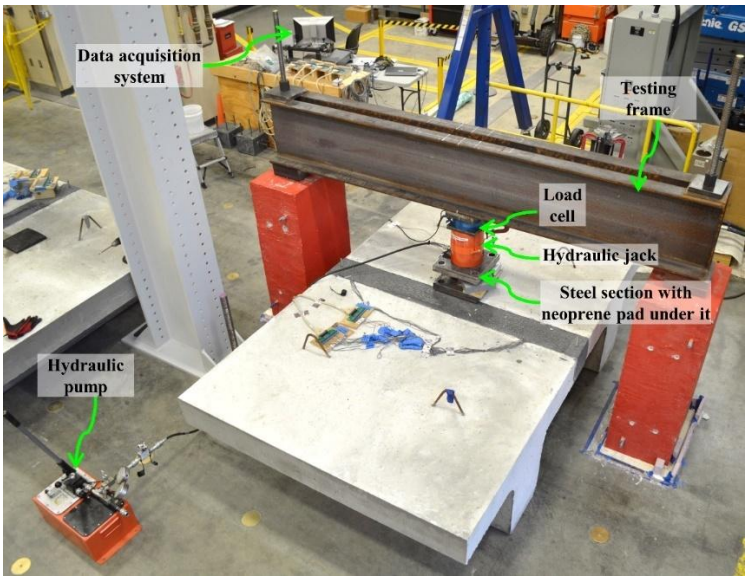

Figure 44. Test setup used for Test D5 of all the double-tee specimens.

4.5 Observations and Results from the Slab Specimen Tests

This section presents the experimental results for all the four slab specimen under different tests. The measured vertical relative displacement between NC and UHPC at the joint interface using LVDTs were smaller the sensitivity of the instrument during all the tests. Due to this observation, the responses of these LVDTs are not presented in the results.

The initial objective for the boundary conditions of the slab specimens was to create a fixed support on both sides, replicating the restraint provided by the flange-to-web connection to the top flange of the double-tee specimens. To achieve the desired boundary conditions, the first specimen, Slab-SL-UH1, was supported directly on a 24 in. (610 mm) by 15 in. (381 mm) concrete block, providing a contact area of 18 in. (457 mm) by 15 in. (381 mm), with the 15 in. (381 mm) dimension aligned along the span. A layer of gypsum cement paste was applied between the specimen and the concrete block to ensure even load distribution across the support. Additionally, four 5/8-in. (16-mm) threaded rods were used to secure the specimen to the support block, while four steel angles, two on each side of the supports, were installed to minimize rotation at the support points. The initial support system for specimen Slab-SL-UH1 is shown in Figure 45. However, after conducting preliminary tests and comparing the experimental deflections with theoretical calculations, it was determined that the boundary conditions more closely resembled a simply supported case rather than the intended fixed-fixed scenario. As a result, the threaded rods and steel angles were removed, though the specimen continued to be supported directly on the concrete blocks. The other three specimens, Slab-DL-UH1, Slab-SL-UH2, and Slab-DL-UH2, were supported as shown in Figure 39. It was later concluded that the considerably low strains and joint opening results shown in this section from Slab-SL-UH1 when comparing to the other three specimens were due to the fact that the former specimen was supported on the 15-in. (381-mm) wide support blocks, and hardened gypsum cement connected the specimen and support blocks to a certain degree.

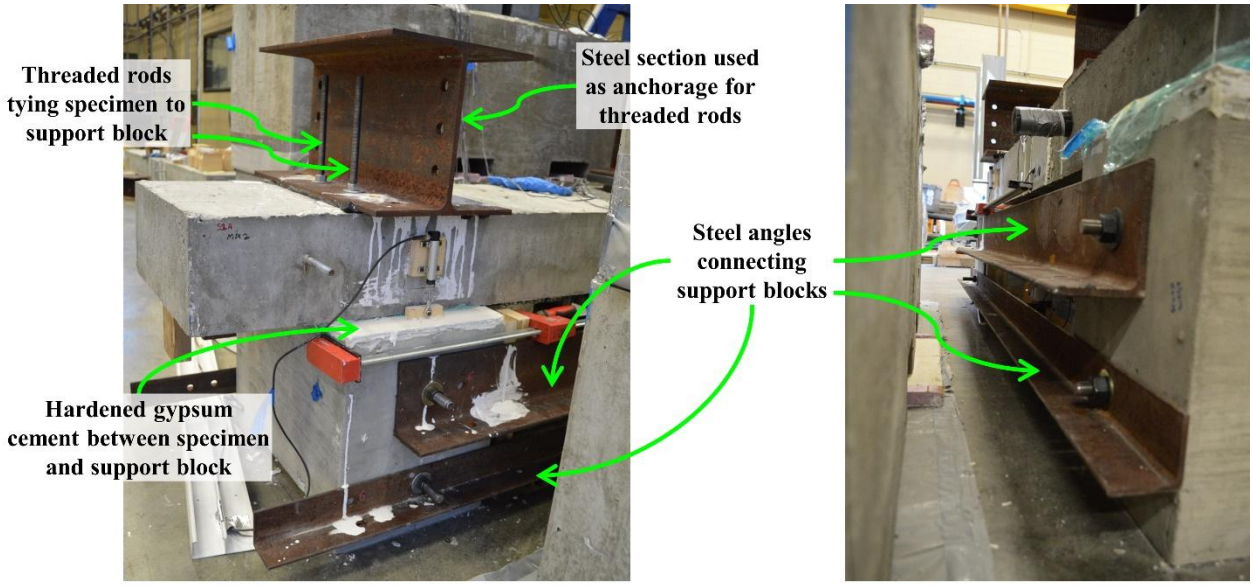

(a) Initial support configuration

(b) Steel angles connecting the two concrete support blocks

Figure 45. Initial boundary condition configuration used for specimen Slab-SL-UH1

4.5.1 Test S1 – Fatigue Tests for 1,000,000 cycles

All slab specimens were subjected to 1,000,000, load-controlled cycles with an applied load of 6.04 kip (26.87 kN) at a frequency of 2 Hz. The test lasted several days, and during that period the specimens were monitored with the intent of capturing potential cracking, specifically at the joint region. It was observed, however, that no cracks were developed during the tests S1 in any of the four slab specimens. All data was continuously recorded at a frequency of 20 Hz. Following the testing, a computer program was developed to reduce the size of the data files, making the data processing and plotting more manageable and compatible with the available computational

resources. From the raw data, 10 cycles (equivalent to 5 seconds) of data were extracted for every 1,800 cycles (or 15 minutes) and combined. The necessary calculations were then performed, and the results were plotted and are presented in this section. This section shows the response of each instrument based on the difference of their corresponding values read at the peak (6.04 kip or 26.78 kN) and valley (0.50 kip or 2.22 kN) of the cyclic loading. The difference in deflections in the slab specimens with single and double layers of rebar present in the joint are shown in Figure 46 and Figure 47, respectively. It was observed that the difference in deflections was lower than 0.014 in. (0.36 mm), which corresponds to a span ratio of approximately L/4,860.

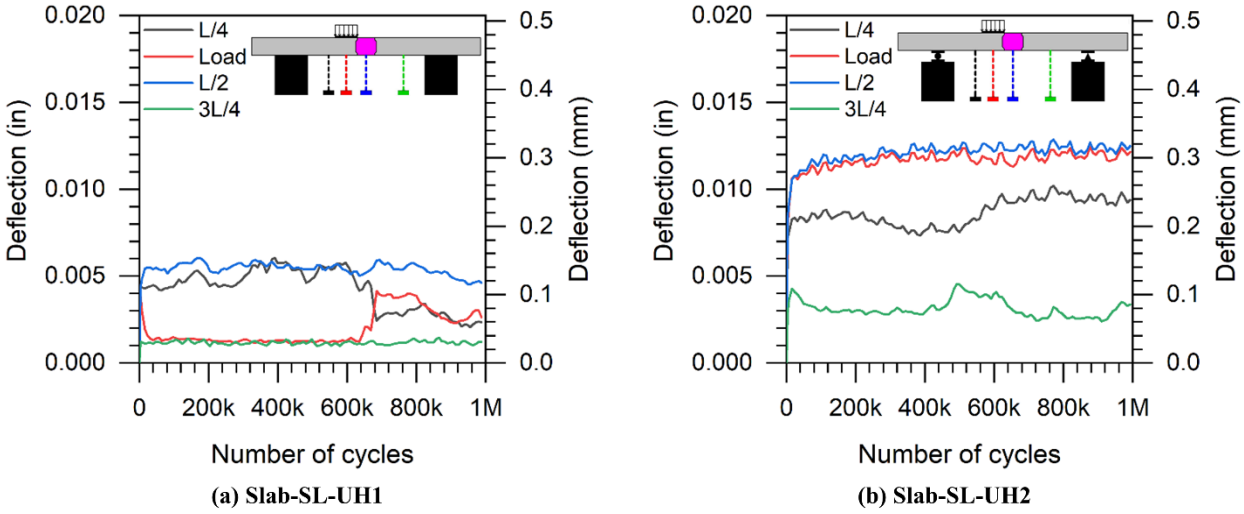

(a) Slab-SL-UH1 (b) Slab-SL-UH2

Figure 46. Difference in deflections of Slab-SL specimens

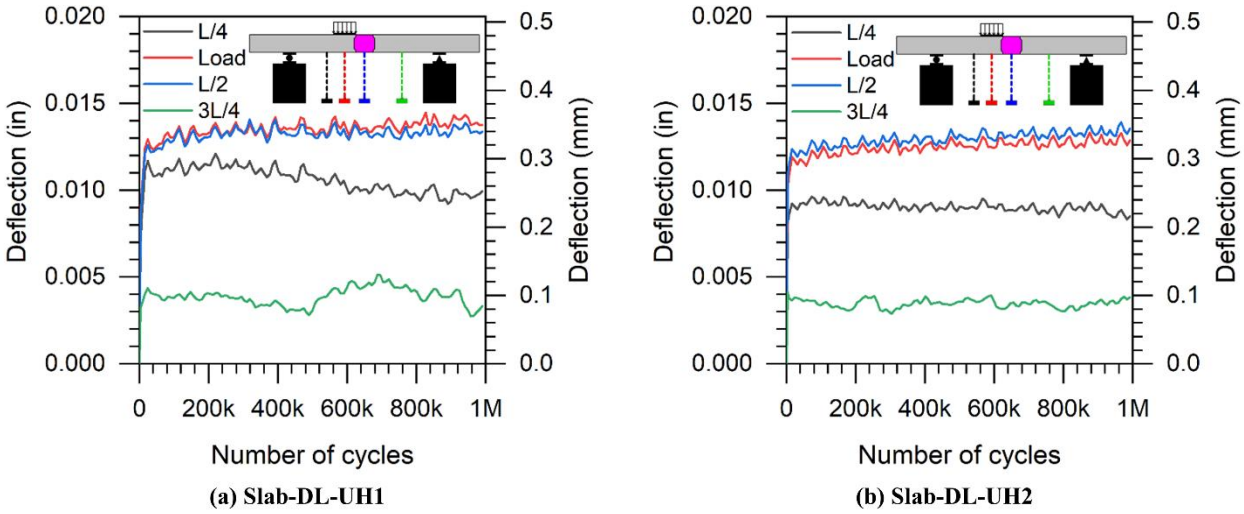

(a) Slab-DL-UH1 (b) Slab-DL-UH2

Figure 47. Difference in deflections of Slab-DL specimens

A schematic showing all strain gauges applied on the slab specimens is depicted in Figure 48. In addition, the figure shows the naming of each strain gauge according to their location in the specimen joint. The steel and concrete strain responses of the specimens Slab-SL-UH1, Slab-DL-UH1, Slab-SL-UH2, and Slab-DL-UH2 are shown in Figure 49, Figure 50, Figure 51, and Figure 52, respectively. It is important to note that specimen Slab-SL-UH1 was loaded on Side B, while the other

three slab specimens were loaded on Side A (see Figure 48). The strain response values of the strain gauges on side B are therefore greater than those on side A for specimen Slab-SL-UH1, and the opposite is true for the other specimens. Based on all strain responses, it was observed that both the steel and UHPC materials were in their respective elastic regions at all times. Furthermore, it was determined that fatigue loading did not result in a significant change in the strains captured by any strain gauge. The maximum observed change in strain was close to 350 microstrain, which corresponds to only approximately 17% of the yield strain of steel reinforcement.

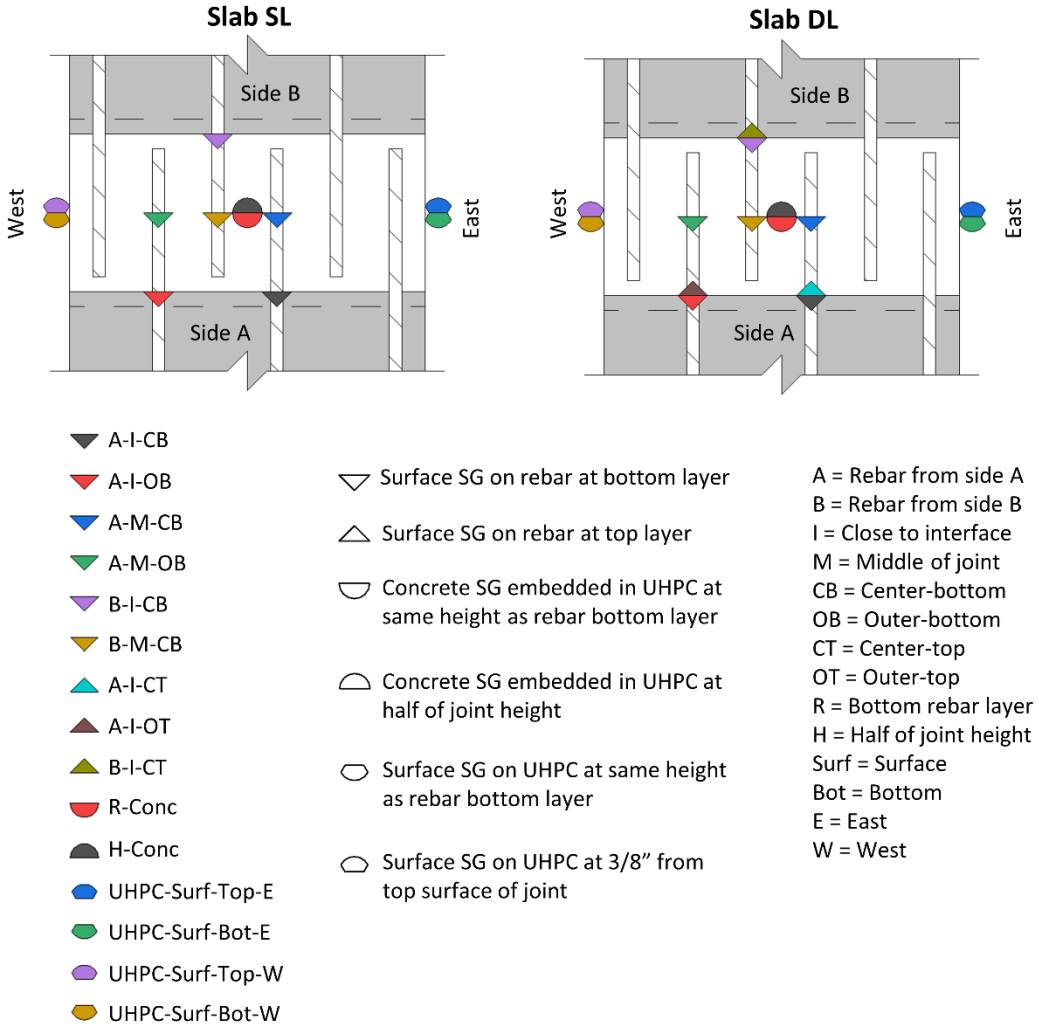

Figure 48. Schematics of strain gauges applied on slab specimens

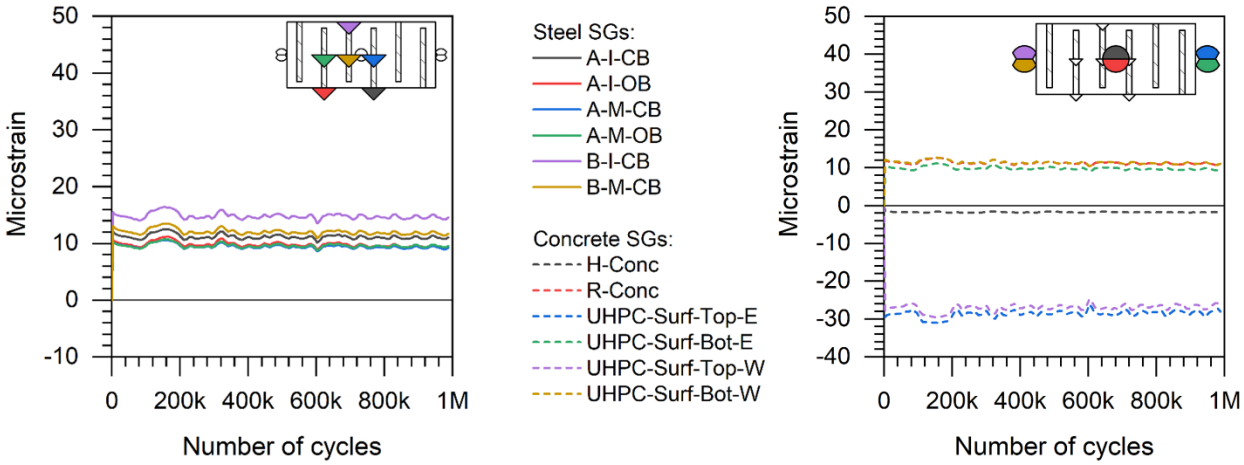

(a) Difference in steel strain gauge responses

(b) Difference in concrete strain gauge responses

Figure 49. Strain responses of specimen Slab-SL-UH1 during fatigue test S1

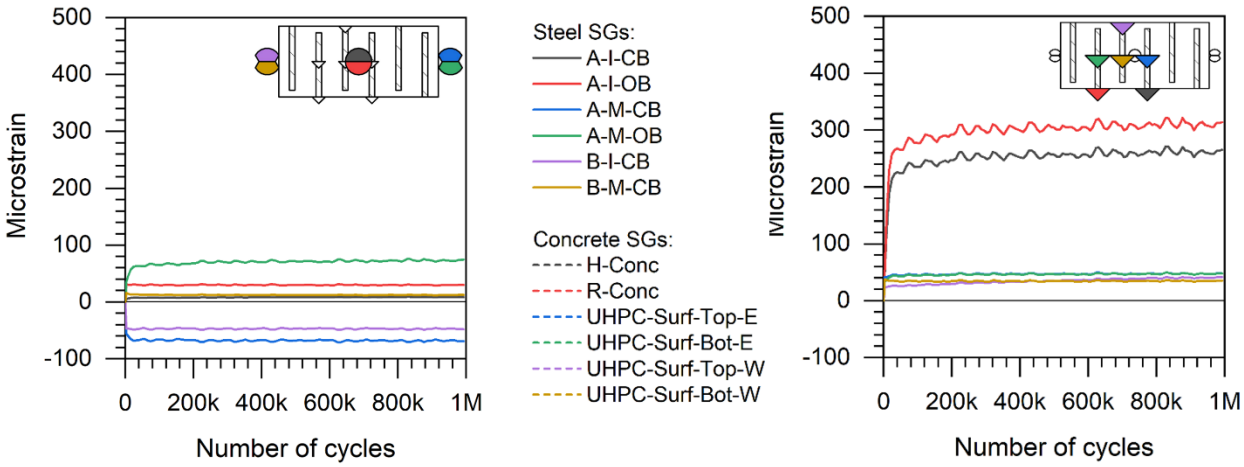

(a) Difference in steel strain gauge responses

(b) Difference in concrete strain gauge responses

Figure 50. Strain responses of specimen Slab-SL-UH2 during fatigue test S1

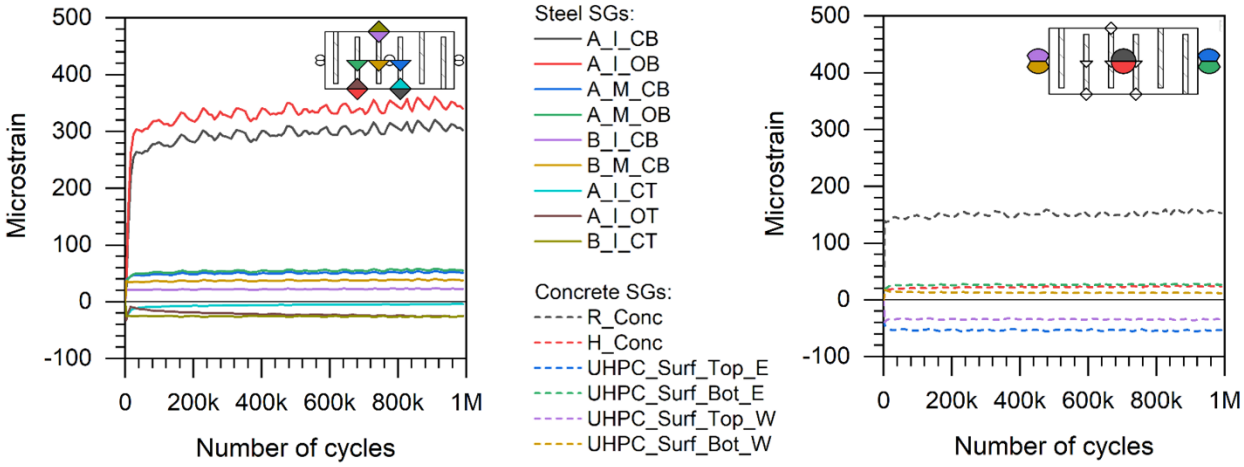

(a) Difference in steel strain gauge responses

(b) Difference in concrete strain gauge responses

Figure 51. Strain responses of specimen Slab-DL-UH1 during fatigue test S1

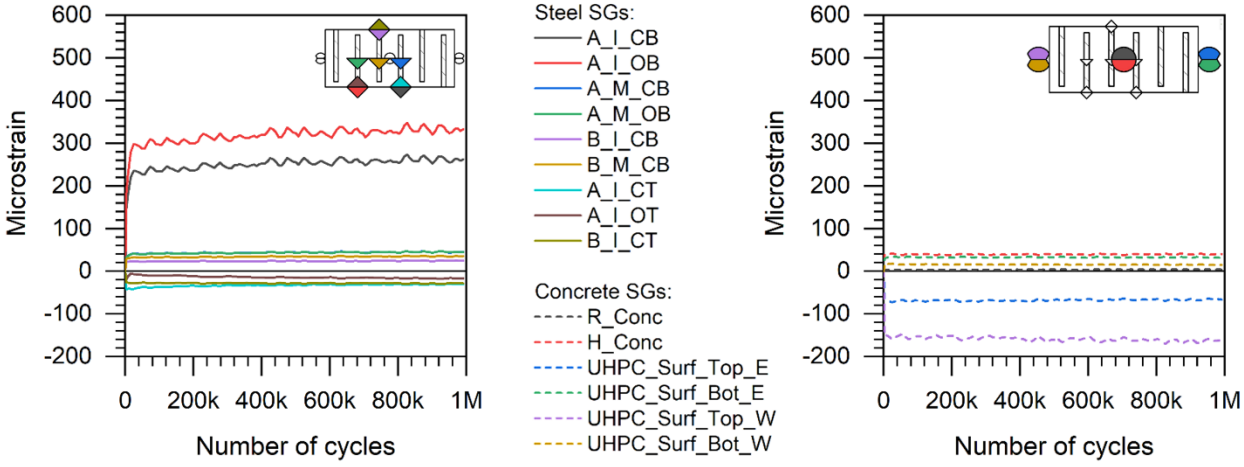

(a) Difference in steel strain gauge responses

(b) Difference in concrete strain gauge responses

Figure 52. Strain responses of specimen Slab-DL-UH2 during fatigue test S1

As previously mentioned, the interface joint opening between NC and UHPC was measured at four locations by four LVDTs. The LVDT locations were named Southeast (SE), Southwest (SW), Northeast (NE), and Northwest (NW), which agree with the West and East directions shown in Figure 48. The load was applied at the South location for all specimens at a distance of 9 in. (229 mm) from the center of the joint or 5 in. (127 mm) from the edge of the joint. The difference in the joint opening readings in the slab specimens with a single and double layer of reinforcement are shown in Figure 53 and Figure 54, respectively. In all cases, the difference in displacement was lower than 0.004 in. (0.10 mm).

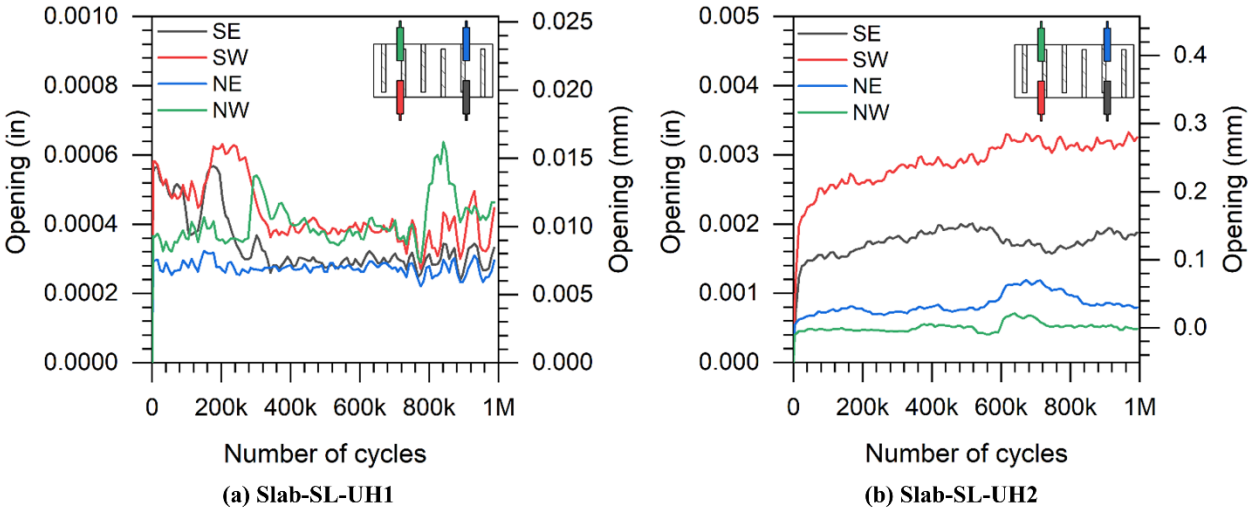

(a) Slab-SL-UH1 (b) Slab-SL-UH2

Figure 53. Difference in joint opening of Slab-SL specimens

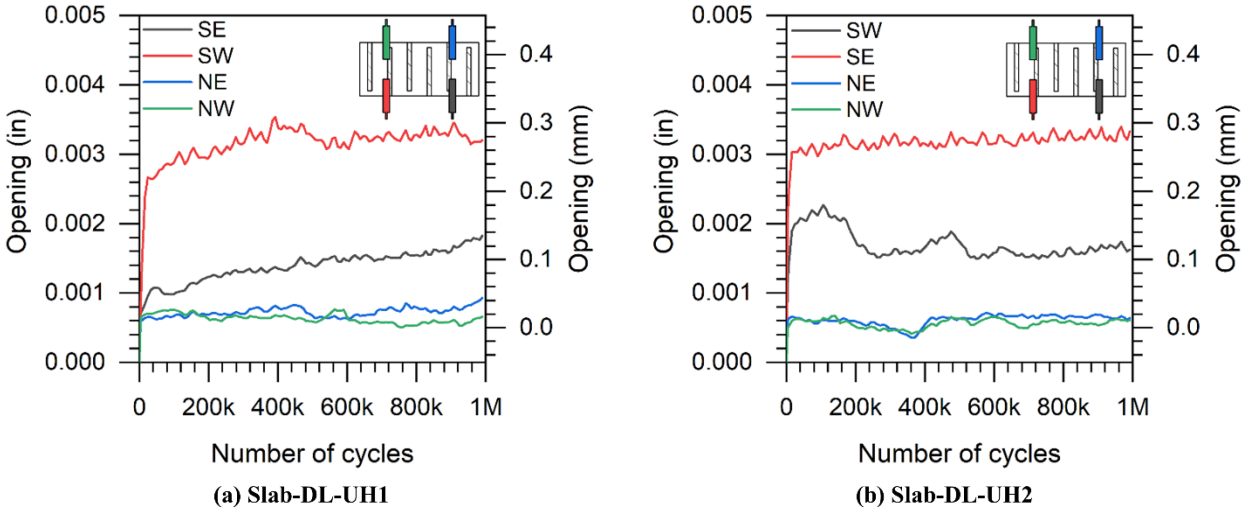

(a) Slab-DL-UH1 (b) Slab-DL-UH2

Figure 54. Difference in joint opening of Slab-DL specimens

4.5.2 Test S2 – Stiffness Measurement Test

Tests S2 were periodically conducted to monitor the change in stiffness of the system over the course of operation of test S1. Tests S1 were periodically paused so a test S2 could be performed on a given specimen. While section 4.5.1 showed the response of every instrument placed on the specimens, this section presents selected instruments to represent the change in stiffness of the systems. The selected instruments were the string potentiometer under the applied load, the steel SG A-I-CB (B-I-CB for Slab-SL-UH1), the concrete SG R-Conc, and the average joint opening of all four LVDTs combined. The beginning of every data set from every test S2 had its first data point as zero in the x-axis. This ensured an easier comparison of the change in stiffness (or slope of the graph) of the system when comparing different tests S2 on the same specimen.

Figure 55 shows the response of the string potentiometer placed under the applied load during tests S2 for all the slab specimens. With the exception of Slab-SL-UH1, which had a different support configuration, all the other slab specimens experienced a similar deflection response after the fatigue test S1 began.

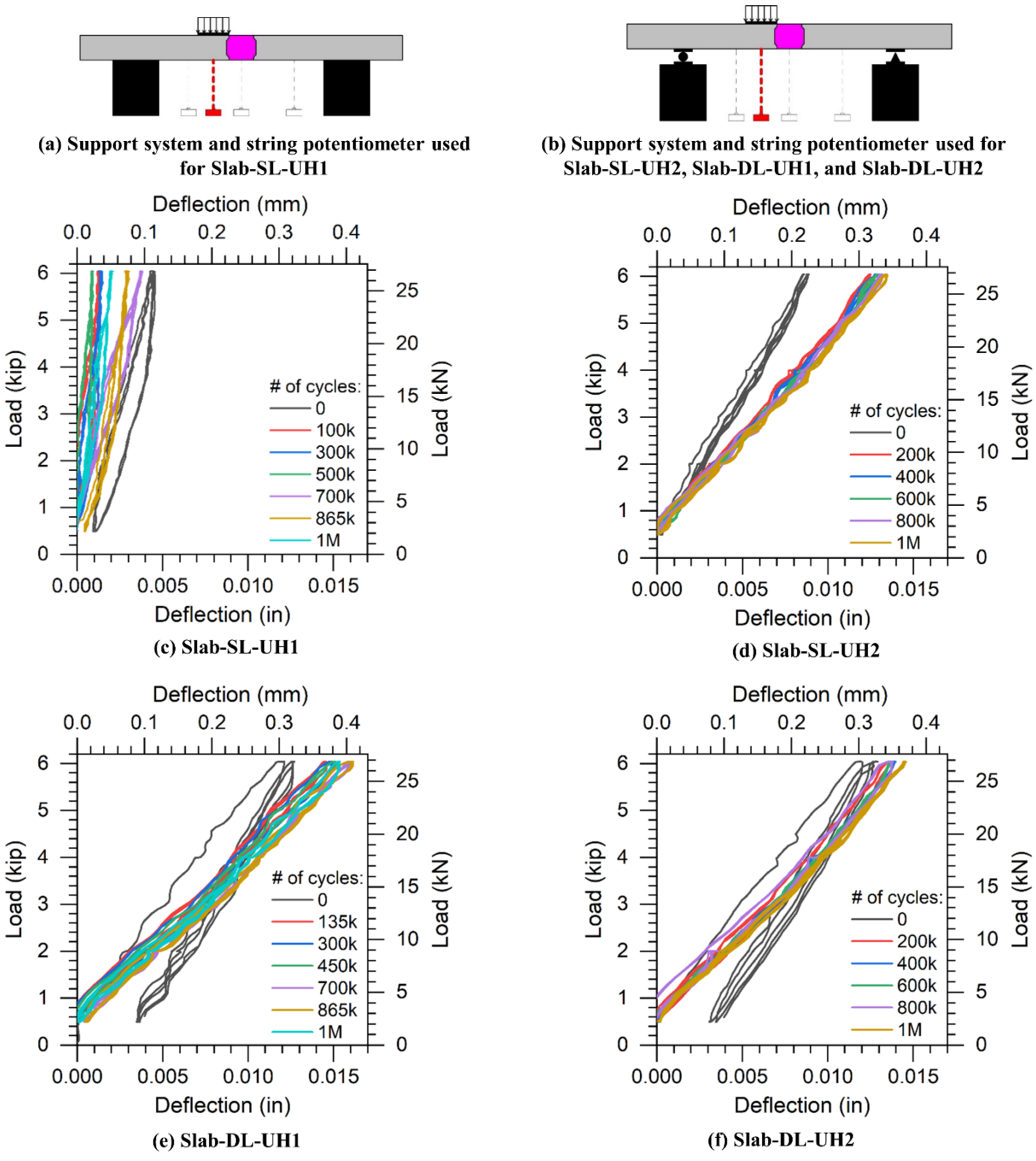

Figure 55. String potentiometer responses during tests S2

Figure 56 shows the variation in strain during tests S2 captured by the strain gauge placed at the center rebar, at the bottom rebar layer, and closest to the applied load. Since Slab-SL-UH1 was loaded on side B, the strain gauge response displayed comes from B-I-CB, whereas in the other specimens, the response from A-I-CB is shown. It was observed that the highest variation of strain

occurred between 0 and 200,000 cycles, and that the variation in strain over the remaining tests S2 was minimal compared to the first test S2 performed at 0 cycles from test S1. In all cases, the variation in strain did exceed 300 microstrains.

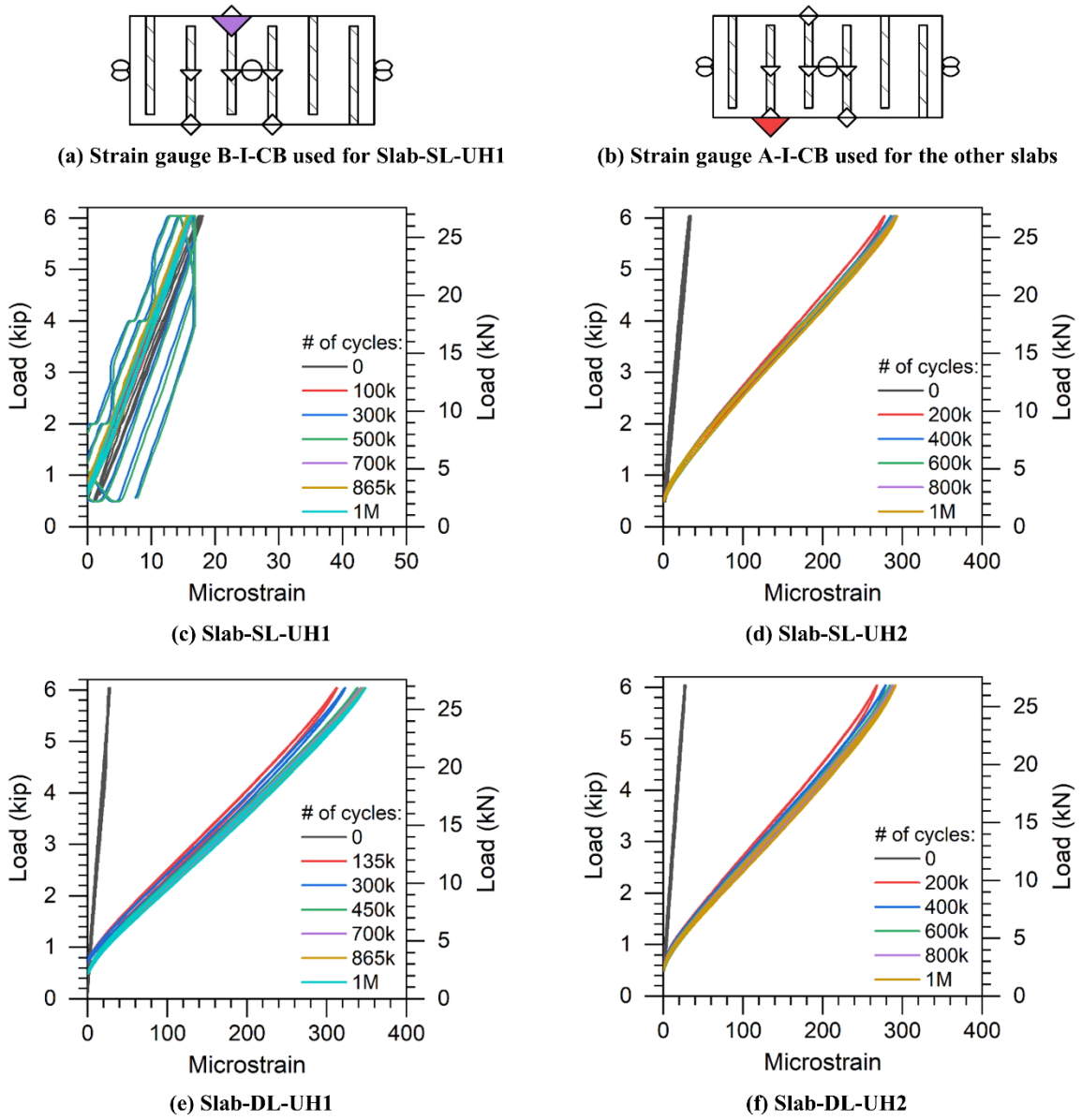

Figure 56. Strain responses during tests S2

The average joint opening of all four LVDTs placed at the joint interfaces during tests S2 is shown in Figure 57. The observed responses followed the same pattern observed in Figure 55 and Figure 56, in which the highest variation between tests S2 was between the first test (at 0 cycles) and the second one. Moreover, as seen previously, the response captured from Slab-SL-UH1 is lower than the other three specimens. The variation in average joint opening, for all cases, was less than 0.002 in. (0.05 mm).

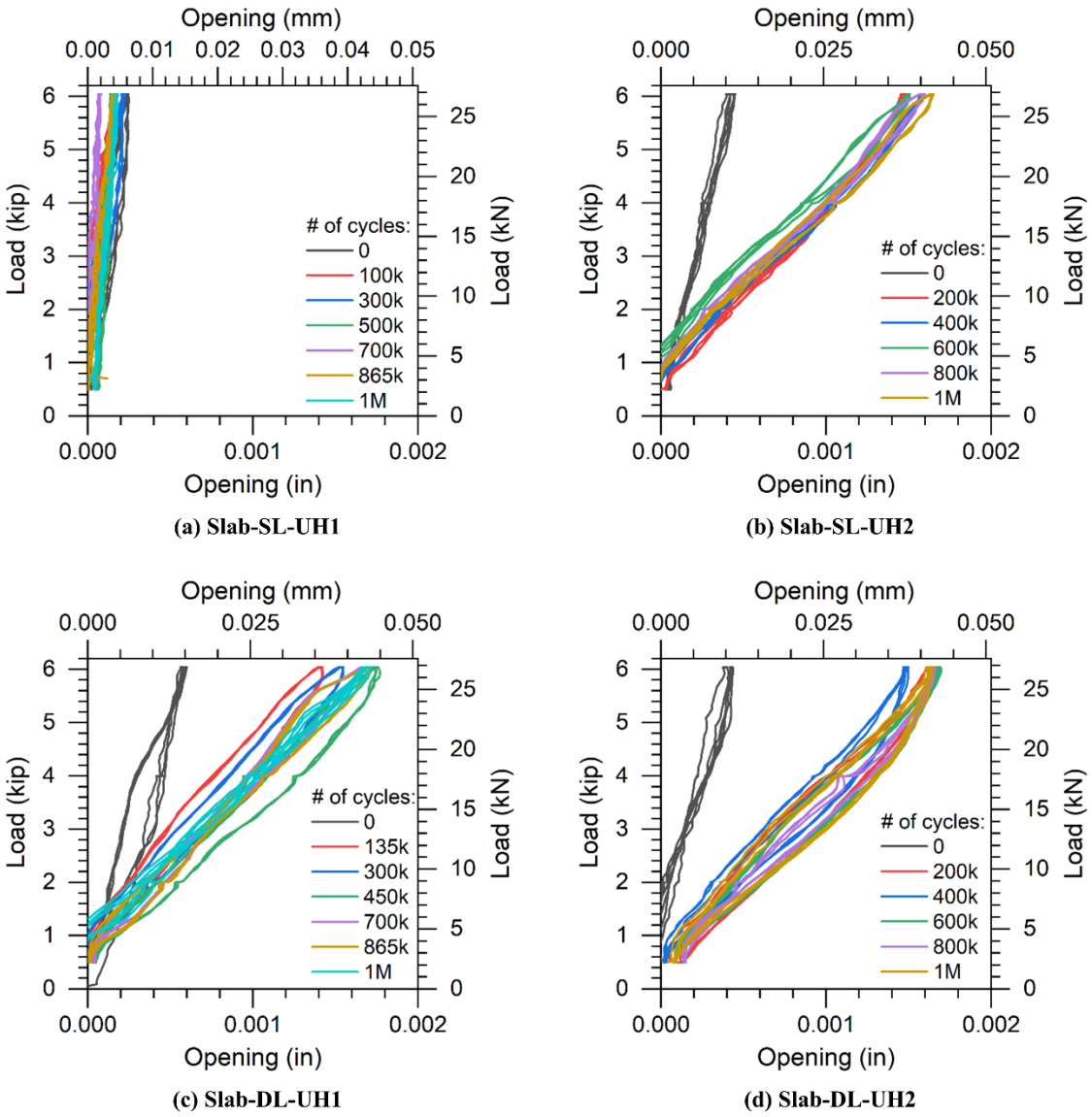

Figure 57. Average joint opening responses during tests S2

4.5.3 Test S3 – Overload test

The overload tests, or tests S3, were performed on the slab specimens after all the fatigue loading (test S1) and stiffness measurement tests (tests S2) were completed. The specimens were subjected to a load that was double the amount applied in tests S1 and S2. From the measured responses such as deflection (Figure 58(c)), strain (Figure 58(d)), and average joint opening (Figure 58(e)), significant residual values are shown by each instrument response, inferring that the applied load of 12.1 kip (53.8 kN) was sufficient for the specimen to observe some degree of nonlinearity at the joint location. Cracking was detected only in specimens Slab-DL-UH1 and Slab-DL-UH2. The cracks on both specimens followed the same pattern: parallel to the joint, at the bottom of the specimen, and on the side where the load was applied. The typical cracking is shown in Figure 59.

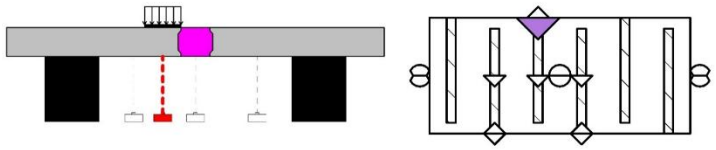

(a) String potentiometer and steel strain gauge B-I-CB used to show response of Slab-SL-UH1 in test S3

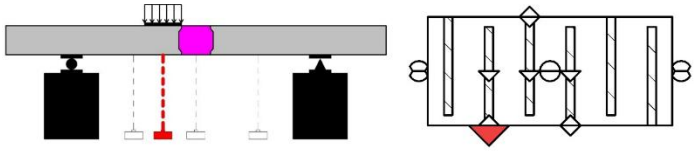

(b) String potentiometer and steel strain gauge A-I-CB used to show responses of Slab-SL-UH2, Slab-DL-UH1, and Slab-DL-UH2 in test S3

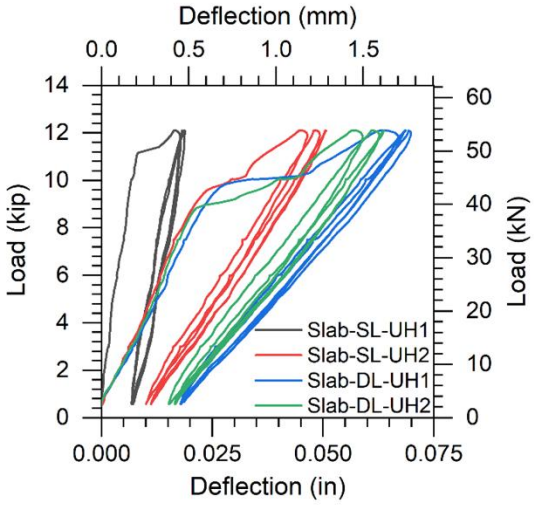

(c) String potentiometer responses

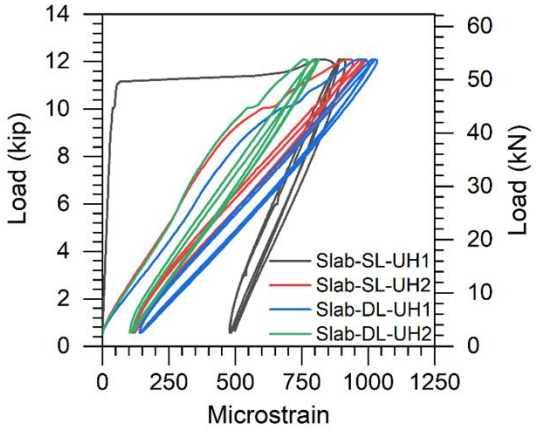

(d) Steel strain gauge responses

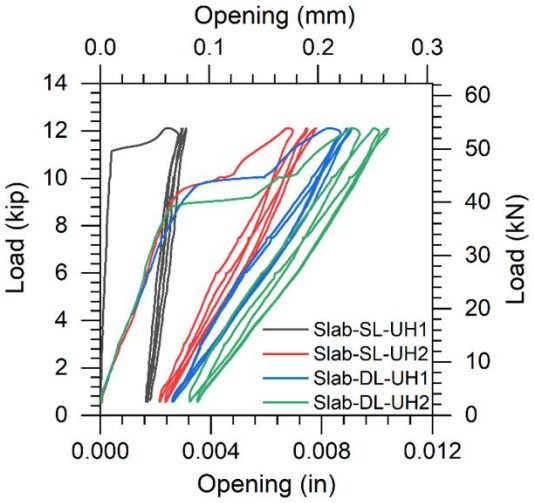

(e) Average interface joint opening responses

Figure 58. Slab specimens response during test S3

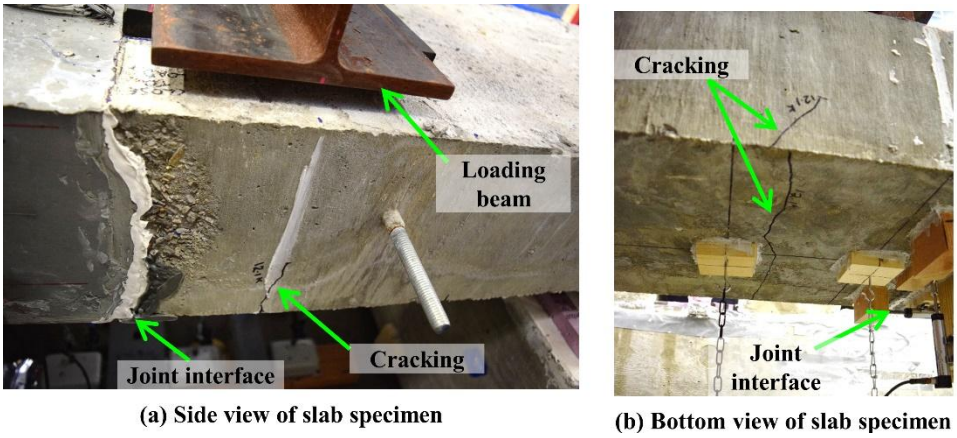

(a) Side view of slab specimen (b) Bottom view of slab specimen

Figure 59. Typical cracking in Slab-DL specimens during test S3

4.5.4 Test S4 – Failure test

Unlike tests S1, S2, and S3, the failure tests involved supporting the slab specimens over an extended span of 98 in. (2489 mm) instead of the previous 68 in. (1727 mm). This adjustment was made to reduce the likelihood of shear failure. The load was applied at the center of the specimen over an area measuring 4 in. (102 mm) by 14 in. (356 mm). The slabs were continuously loaded until a midspan deflection of approximately 2 in. (51 mm) was achieved, in order to assess their ultimate capacity. During the testing of specimen Slab-SL-UH2, a partial malfunction occurred in the voltage supplier connected to the data acquisition system, which compromised the readings from most of the voltage-based instruments, such as string potentiometers and LVDTs. As a result, no LVDT data is presented in this section for this specimen (Slab -SL-UH2), and only the string potentiometer data from the instrument at midspan, directly under the applied load, is shown. The joint opening at the interface, typically measured by the LVDTs during all slab tests, was measured in test S4 using a non-contact displacement measurement system, with LEDs placed adjacent to the interface

The peak loads captured during tests S4 for the specimens Slab-SL-UH1, Slab-SL-UH2, Slab-DL-UH1, and Slab-DL-UH1 were 20.27 kip (90.17 kN), 21.45 kip (95.41 kN), 22.28 kip (99.11 kN), and 22.72 kip (101.06 kN), respectively. The load at which first cracking was observed in NC was 8 kip (35.6 kN) for Slab-SL-UH1, 12 kip (53.4 kN) for Slab-SL-UH2, 8 kip (35.6 kN) for Slab-DL-UH1, and 12.5 kip (55.6 kN) for Slab-DL-UH2. The deflections observed during testing are shown in Figure 60. Figure 61 displays the strains captured in the Slab-SL specimens, and Figure 62 shows the strains in the Slab-DL specimens. It was observed that, in all specimens, the bottom-layer steel reinforcement at the interface location yielded based on the responses of strain gauges A-I-CB, A-I-OB, and B-I-CB.

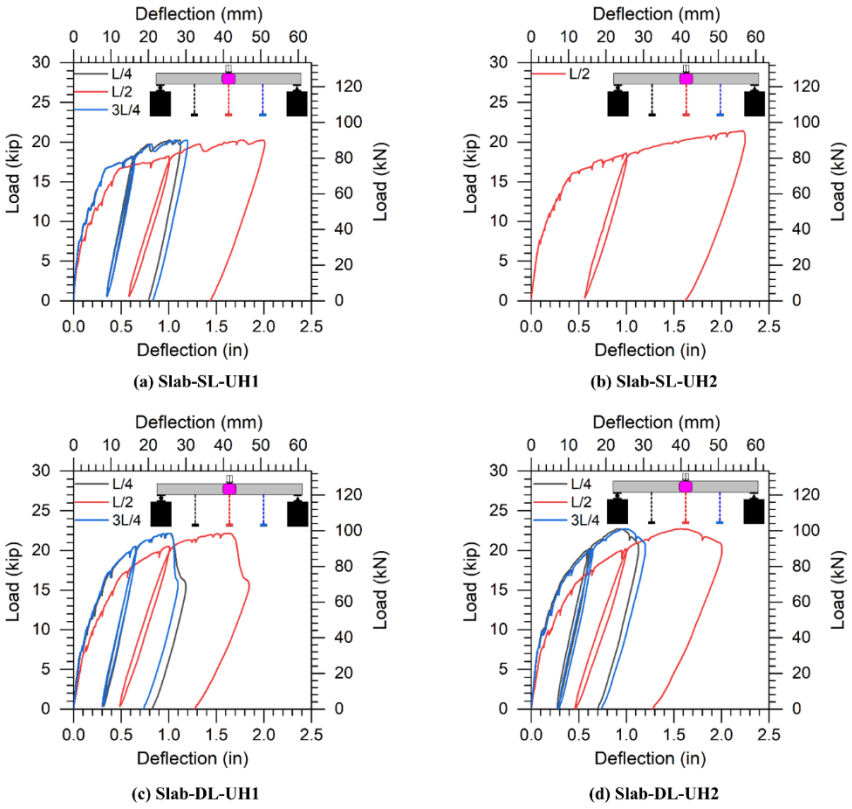

Figure 60. Measured string potentiometer deflections in all slab specimens during tests S4

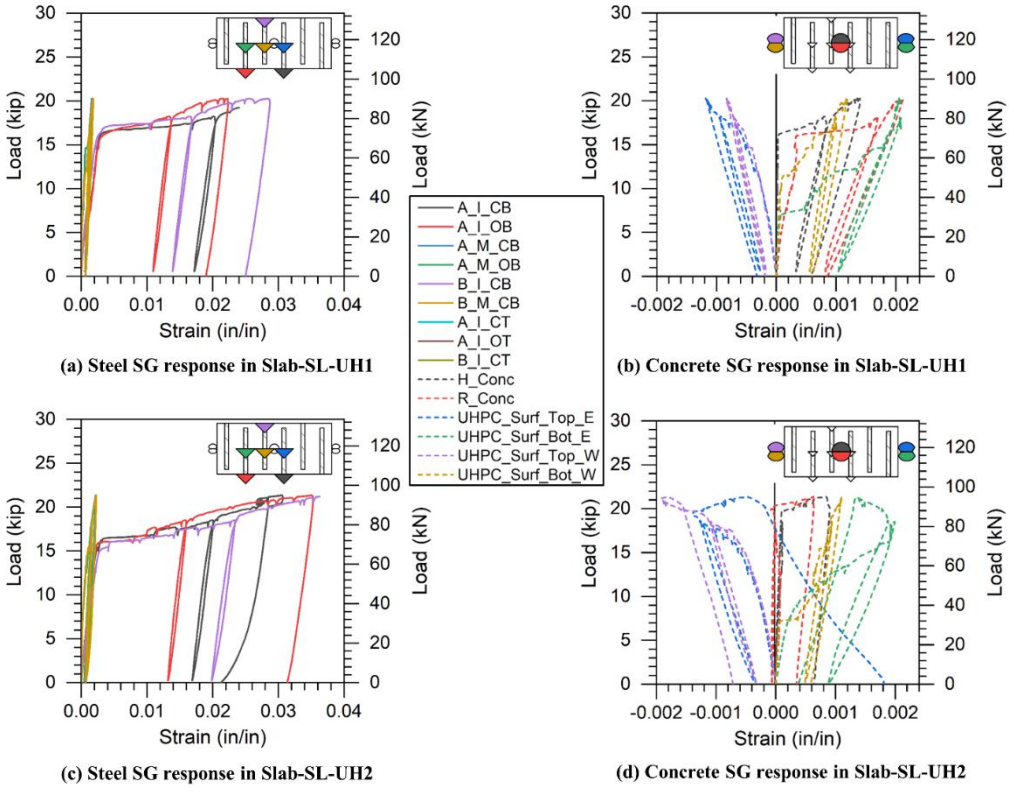

Figure 61. Measured strain gauge responses of Slab-SL specimens during tests S4

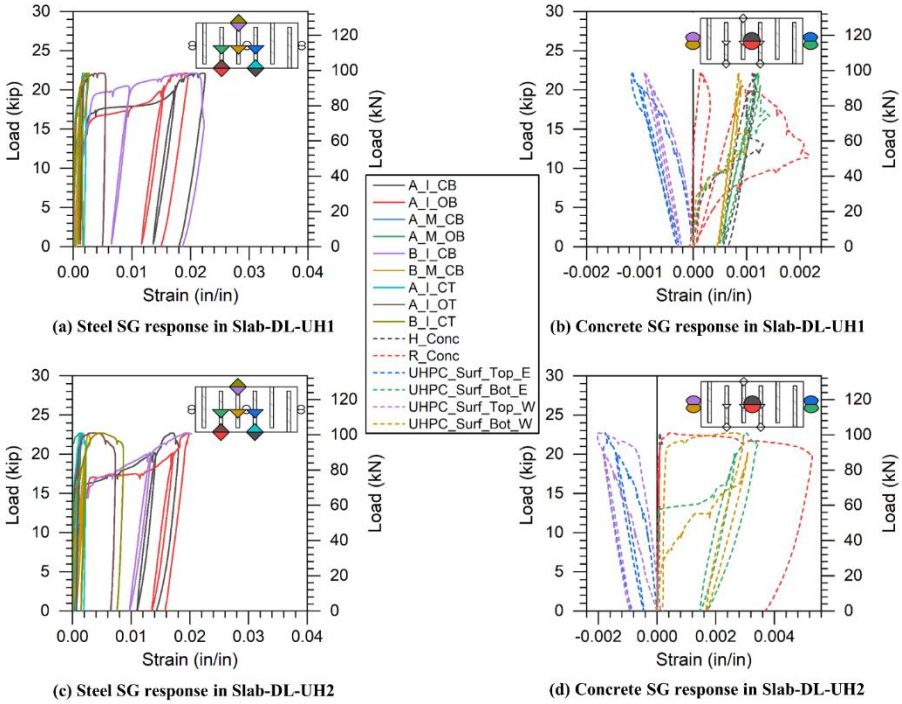

Figure 62. Measured strain gauge responses of Slab-DL specimens during tests S4.

The joint interface opening read by LVDTs is shown in Figure 63. It is important to note that the specimens observed significant cracking in the NC close to the joint interface, creating the possibility that certain LVDTs captured the opening of the joint in combination with crack openings that were formed near the interface. This can be observed, for instance, in the specimen Slab-DL-UH2 in Figure 63(c), in which LVDT NE captured a peak opening more than two times the peak opening of the other LVDTs placed on that specimen. The LEDs placed at the joint interface along the specimen depth were positioned on the side surface of the specimen, whereas the LVDTs were fixed on the bottom surface of the specimen. Even though both instruments had an initial gauge length of approximately 1 in. (25 mm), the area of contact of each LVDT with the NC was significantly larger than that of each LEDs. Due to the difference in location of the two instruments on the specimen and the disparity in area of contact, when a crack formed in the NC near the joint, there was the possibility that it was captured by one instrument, but not the other. This led to different opening responses of the crack opening at the bottom of the joint between the two instrument types. The joint interface opening of the slab specimens captured by LEDs is shown in Figure 64, Figure 65, Figure 66, and Figure 67. Those figures also show the cracking damage at the front and back of the specimens.

It was also observed that, when a major crack formed outside of the gauge length of a given LED pair, the response of that specific pair was significantly lower than that of a pair that captured the opening of the crack. This led, in some cases, to an opening from an LED pair at a higher height being more significant than that of a pair at a lower height that did not capture a major crack. This can be observed, for instance, on the left side of the joint in specimen Slab-SL-UH2 (see Figure 65(a) and (c)), where a crack was formed outside of the bottommost LED pair, but inside the initial gauge length of the other LED pairs on that side of the joint.

Figure 68 shows all the slab specimens after all testing (S1, S2, S3, and S4). Bending moment-generated cracks in the NC and UHPC can be seen in the figure along the specimen length. The depiction sides A and B are also displayed in the figure. Chalk lines were used to create a grid on the

specimen for better visual placement of the crack locations. The grid lines are spaced 2 in. (51 mm) vertically and 4 in. (102 mm) horizontally.

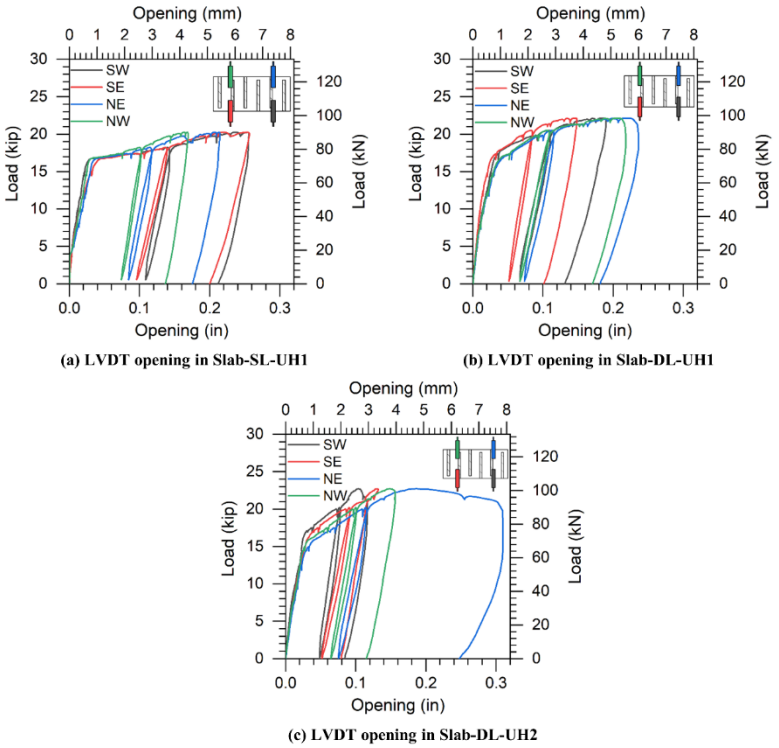

(a) LVDT opening in Slab-SL-UH1

(b) LVDT opening in Slab-DL-UH1

(c) LVDT opening in Slab-DL-UH2

Figure 63. Measured Joint opening in slab specimens using LVDTs during tests S4

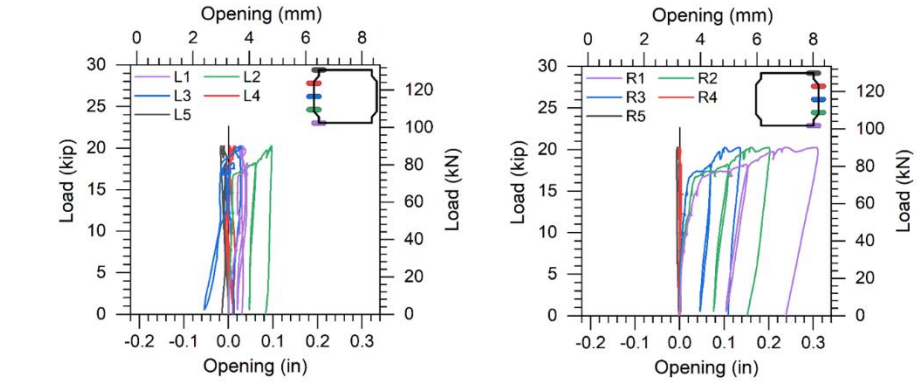

(a) LED opening on the left side of Slab-SL-UH1

(b) LED opening on the right side of Slab-SL-UH1

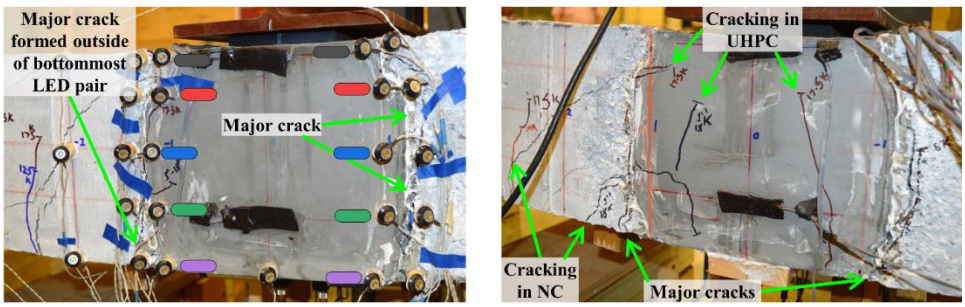

(c) Joint damage at the front of Slab-SL-UH1

(d) Joint damage at the back of Slab-SL-UH1

Figure 64. Measured LED joint opening and joint cracking of specimen Slab-SL-UH1

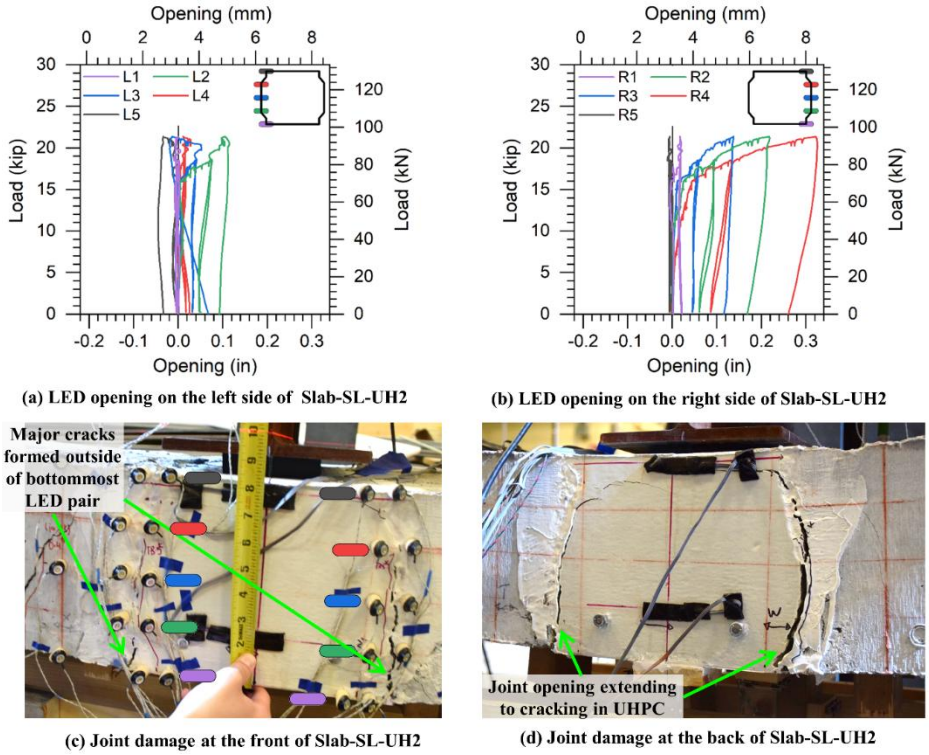

(a) LED opening on the left side of Slab-SL-UH2

(b) LED opening on the right side of Slab-SL-UH2

(c) Joint damage at the front of Slab-SL-UH2

(d) Joint damage at the back of Slab-SL-UH2

Figure 65. Measured LED joint opening and joint cracking of specimen Slab-SL-UH2

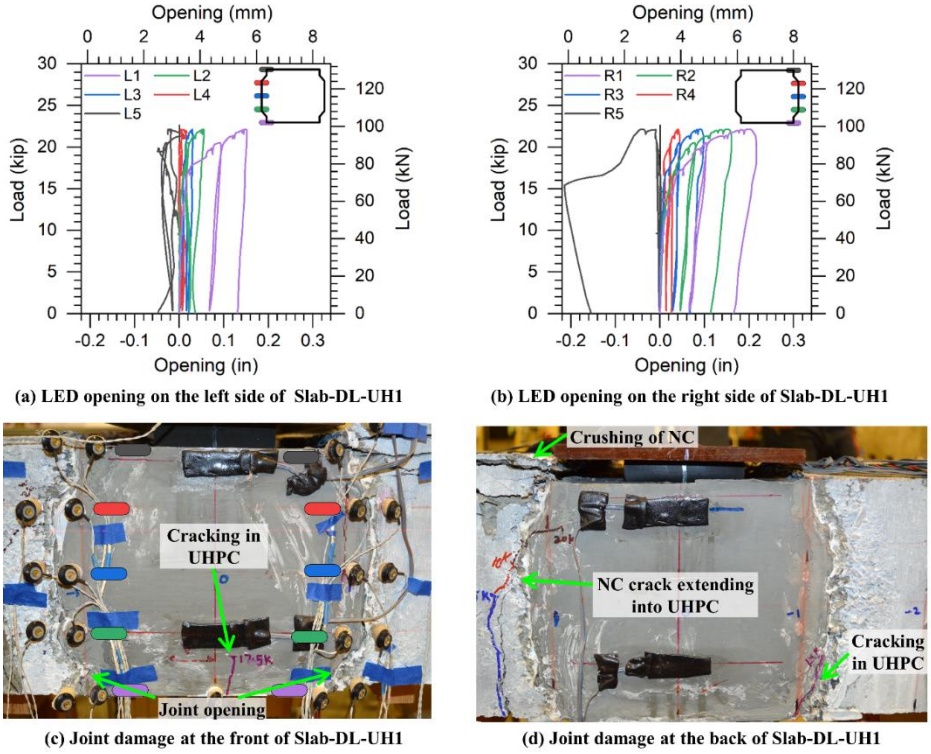

(a) LED opening on the left side of Slab-DL-UH1

(b) LED opening on the right side of Slab-DL-UH1

(c) Joint damage at the front of Slab-DL-UH1

(d) Joint damage at the back of Slab-DL-UH1

Figure 66. Measured LED joint opening and joint cracking of specimen Slab-DL-UH1

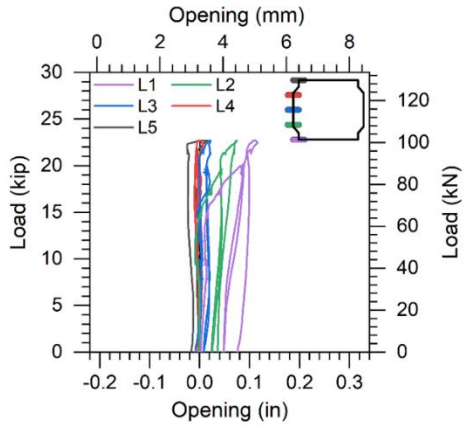

(a) LED opening on the left side of Slab-DL-UH2

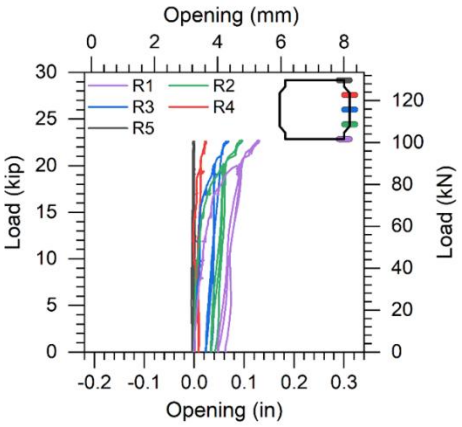

(b) LED opening on the right side of Slab-DL-UH2

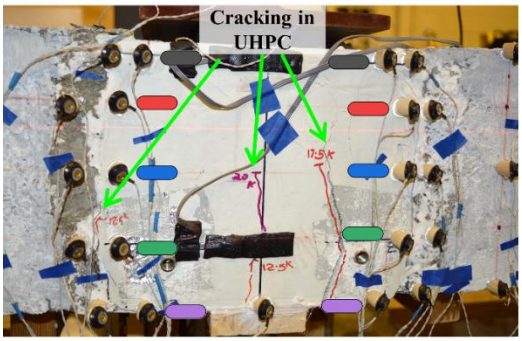

(c) Joint damage at the front of Slab-DL-UH2

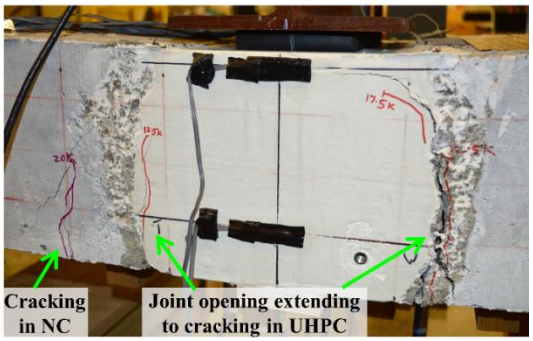

(d) Joint damage at the back of Slab-DL-UH2

Figure 67. LED joint opening and joint cracking of specimen Slab-SL-UH2

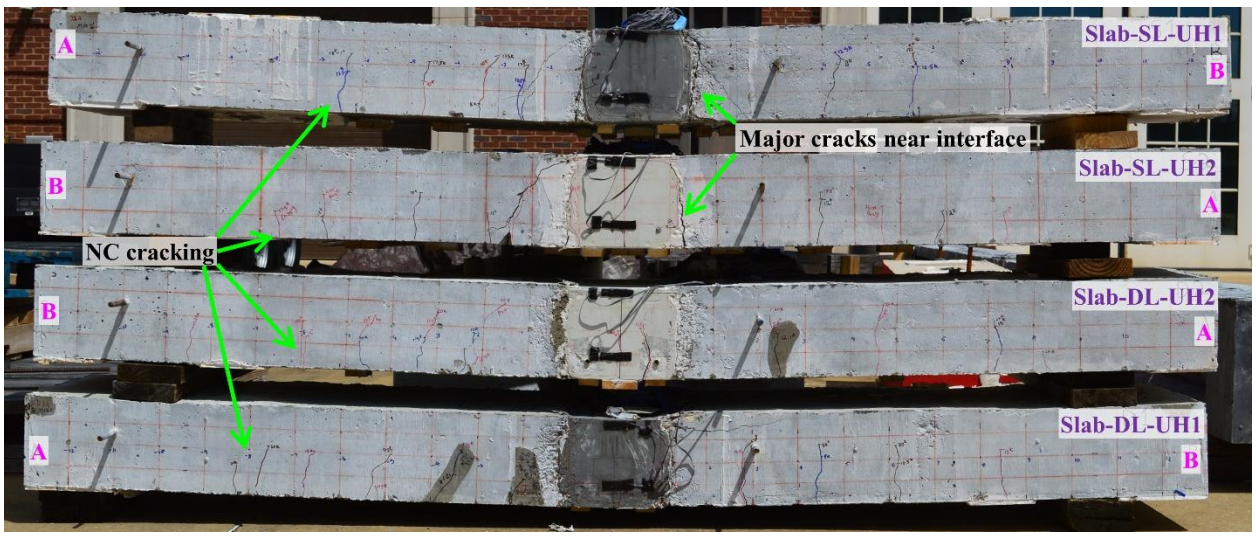

Figure 68. The observed crack patterns in all the slab specimens after Test S4

4.6 Observations and Results from the Double-tee Specimen Tests

The double-tee specimens were directly supported on the concrete floor of the Large Scale Structures Laboratory at the University of Alabama. All four specimens were subjected to the same testing protocol and had the same instrumentation setup. The tests D1, D2, D3, D4, and D5 started after the UHPC and NC materials achieved the desired compressive strength, and all the tests were completed within a 30 day period.

4.6.1 Test D1 – fatigue, 1,000,000 cycles

A total of 1,000,000 load-controlled cycles were applied to the double-tee specimens at a load of 21.3 kips (94.75 kN) and a frequency of 2 cycles per second. Similar to the testing of the slab specimens, the D1 test was periodically paused to allow the D2 tests to be conducted and to inspect the specimens for crack formation. No cracks were observed in any of the specimens during test D1. The same data reduction program used for the slab specimens was employed for the double-tee specimens to manage data file sizes. Despite the peak sinusoidal load increasing from 6.04 kips (26.87 kN) in test S1 to 21.3 kips in test D1, the load valley was maintained at 0.50 kips (2.22 kN). This lower load level was used solely to ensure continuous contact between the UHPC block, neoprene pad, and specimen, thereby preventing any shifting of these components or the actuator during testing. This section presents the variation in response, as captured by the instrumentation, between the peak load of 21.3 kips (94.75 kN) and the valley load of 0.50 kips (2.22 kN). The data acquisition system recording the data from specimen DTee-DL-UH1 experienced a malfunction in its hardware during cycle number 937,751. The problem occurred overnight, and testing could not be paused until after the last cycle of D1 was applied. Due to this issue, the responses from test D1 in specimen DTee-DL-UH1 are only shown from cycles 1 to 937,750.

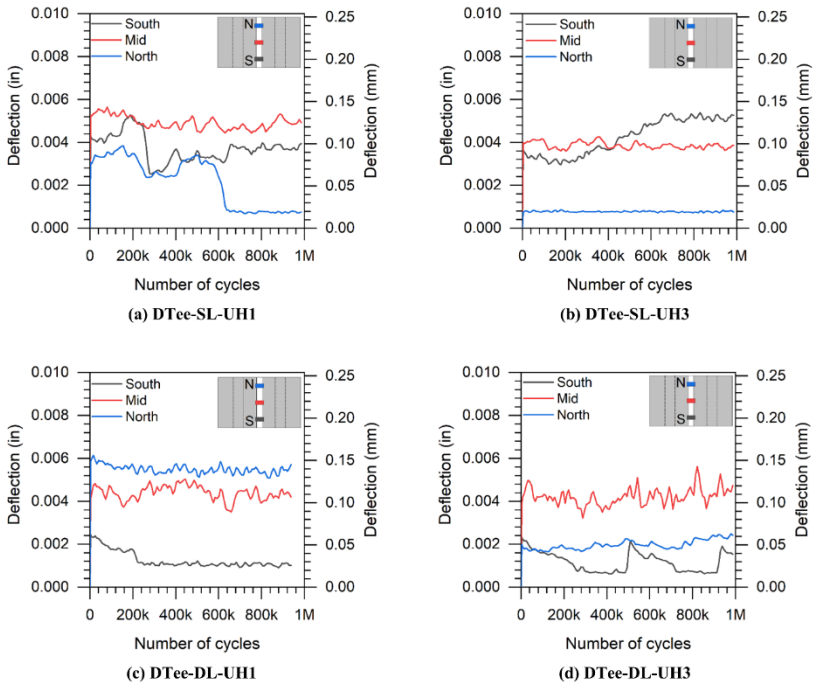

Figure 69. Measured deflections in double-tee specimens during tests D1

The deflections recorded by the string potentiometers during tests D1 are shown in Figure 69. In all specimens, the difference in deflection was less than 0.007 in. (0.18 mm). Figure 70 depicts the

location of all strain gauges in the double-tee specimens, along with the legend for Figure 71 and Figure 72, which show the difference in strain gauge responses in the DTee-SL and DTee-DL specimens, respectively. The captured strains in the double-tee specimens were significantly lower when compared to the slab specimens. All the strain gauges indicate that the specimens behaved elastically at all times during tests D1, with strains lower than 50 microstrain, which corresponds to approximately 2.5% of the yield strain of steel reinforcement. Similarly to the slab specimens, it was determined that fatigue loading did not result in a significant change in the strain recorded by the strain gauges.

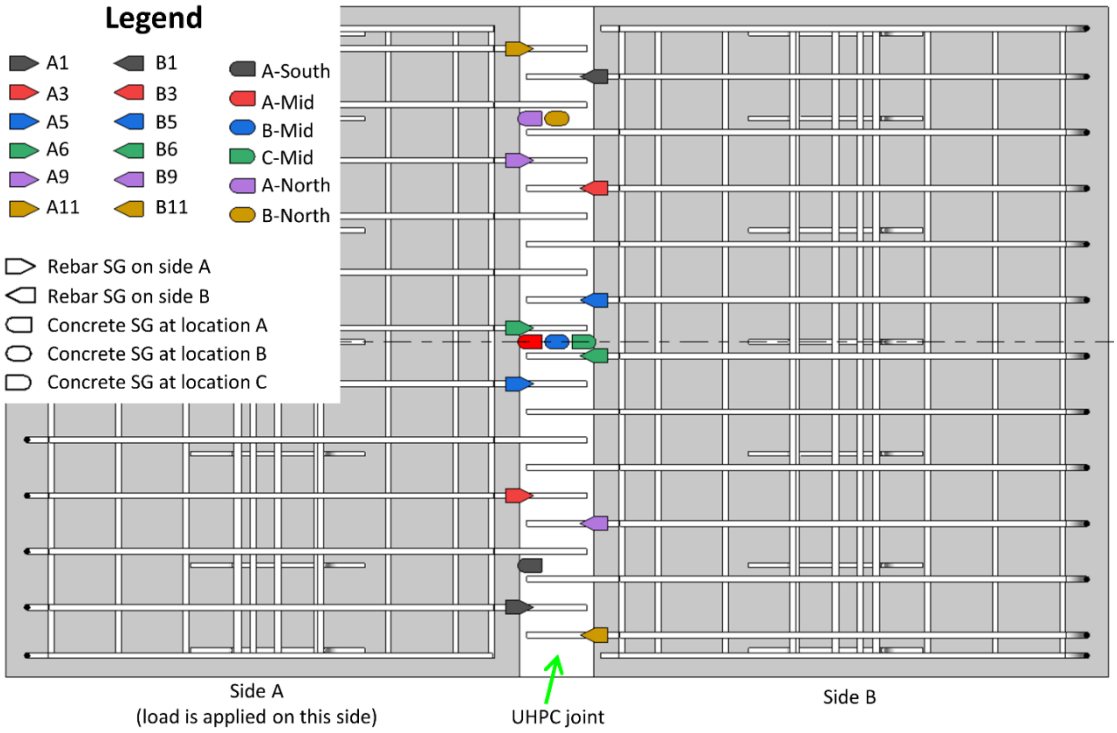

Figure 70. Schematic of strain gauges in double-tee specimens

Figure 73 shows the difference in the joint interface opening measured by LVDTs. In the figure legend, the letter A refers to side A of the specimens, and the letter B refers to side B. The letter S stands for LVDTs on the South side of the specimen, M stands for middle, and N stands for North. The difference in joint opening was observed to be less than 0.003 in. (0.08 mm) in the specimen DTee-DL-UH3 and less than 0.0008 in. (0.02 mm) in the other double-tee specimens.

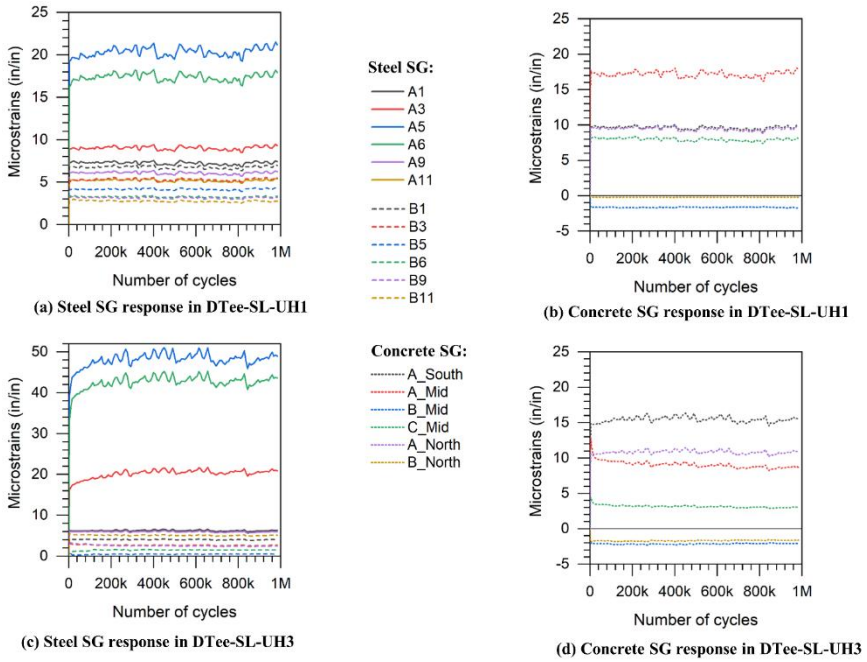

Figure 71. Strain gauge responses in DTee-SL specimens during tests D1

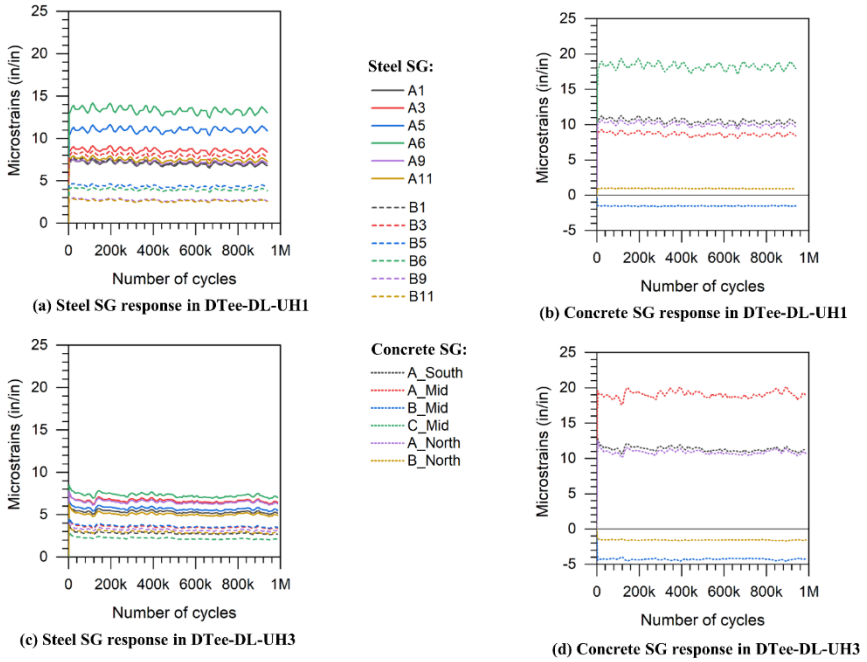

Figure 72. Measured strain gauge responses in DTee-DL specimens during tests D1

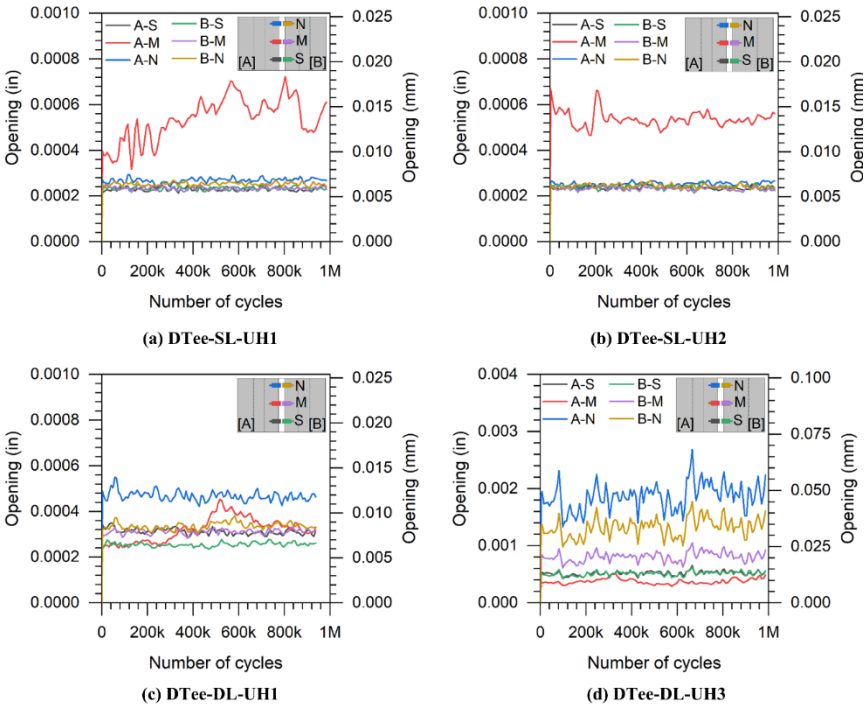

Figure 73. Measured interface opening using LVDT during tests D1

4.6.2 Test D2 – Stiffness Measurement Test

The stiffness measurement tests for the double-tee specimens, or tests D2, were conducted before, during, and after tests D1. Each double-tee specimen had their system stiffness evaluated by a test D2 before their respective test D1 started at 500,000 cycles of test D1, and after test D1 was completed at 1,000,000 cycles. This section presents this information by showing selected instruments placed on the specimens. The first one is the string potentiometer measuring the deflection at the center of the specimen (see Figure 42). The second instrument, rebar strain gauge A6, is the strain gauge placed on the rebar that is closest to the applied load. The gauge was applied close to the joint interface (see Figure 41). Finally, the last instrument selected to measure the change in stiffness is the LVDT at the middle of the specimen, on the side of the applied load (see Figure 42). The voltage supplier connected to the data acquisition system recording specimen DTee-DL-UH3 experienced a partial malfunction, and it was later determined that the only usable data was a partial response of the selected string potentiometer during the first applied D2 test.

The change in stiffness of the selected string potentiometer, steel strain gauge, and LVDT is shown in Figure 74, Figure 75, and Figure 76, respectively. It was observed that the DTee-SL specimens experienced higher deflections, strains, and joint opening values when compared to the DTee-DL specimens. However, the rebar strains indicate that the specimens are far from experiencing any plasticity in the steel, as the strains did not exceed 100 microstrains.

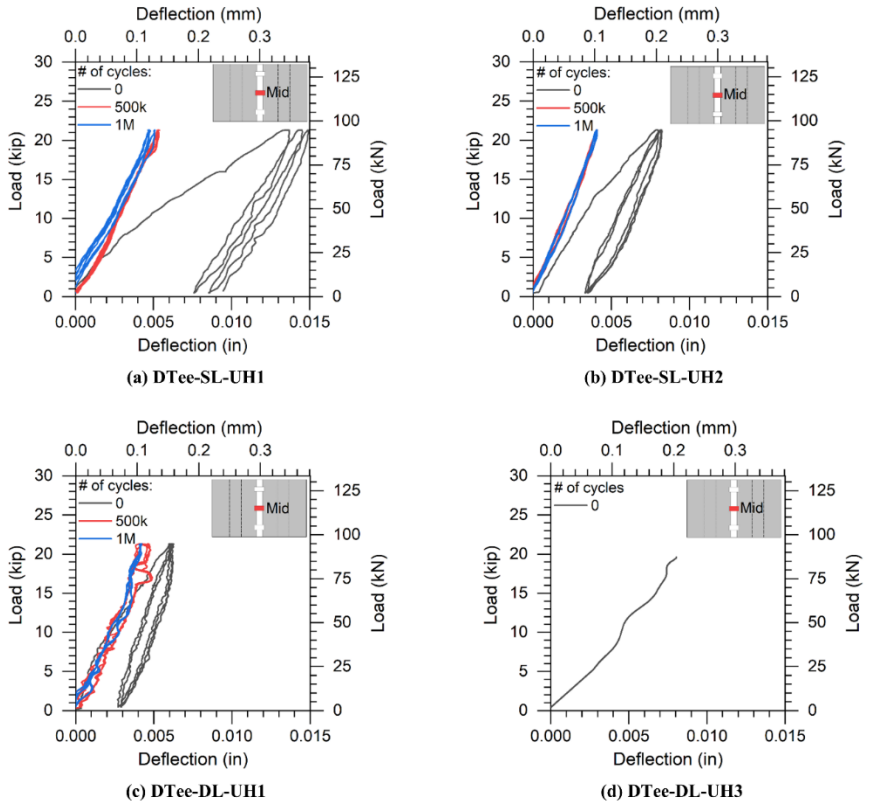

Figure 74. Selected string potentiometer response during tests D2

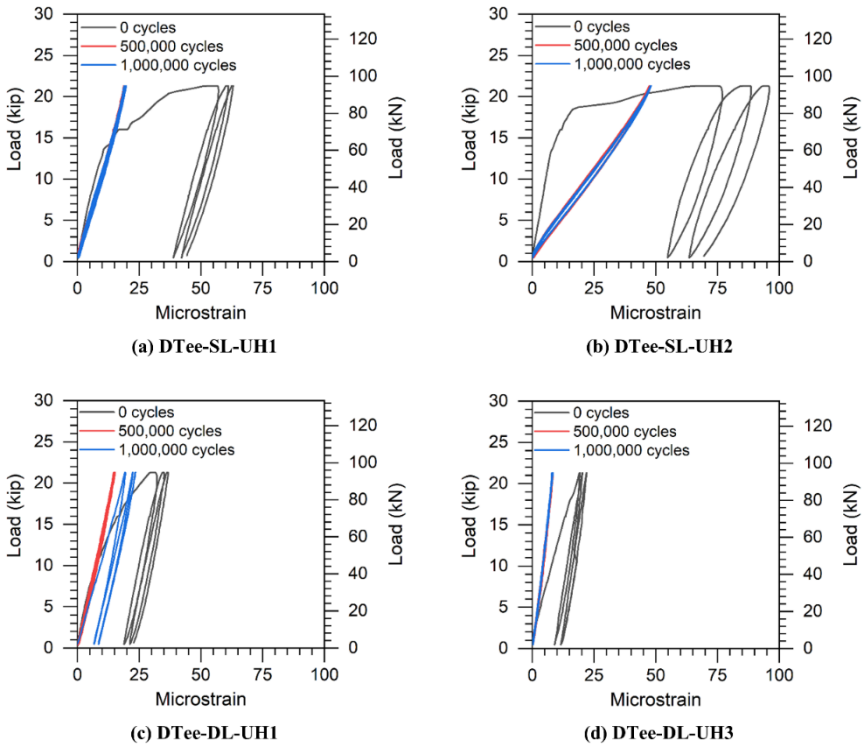

Figure 75. Measured response of steel strain gauge A6 during tests D2

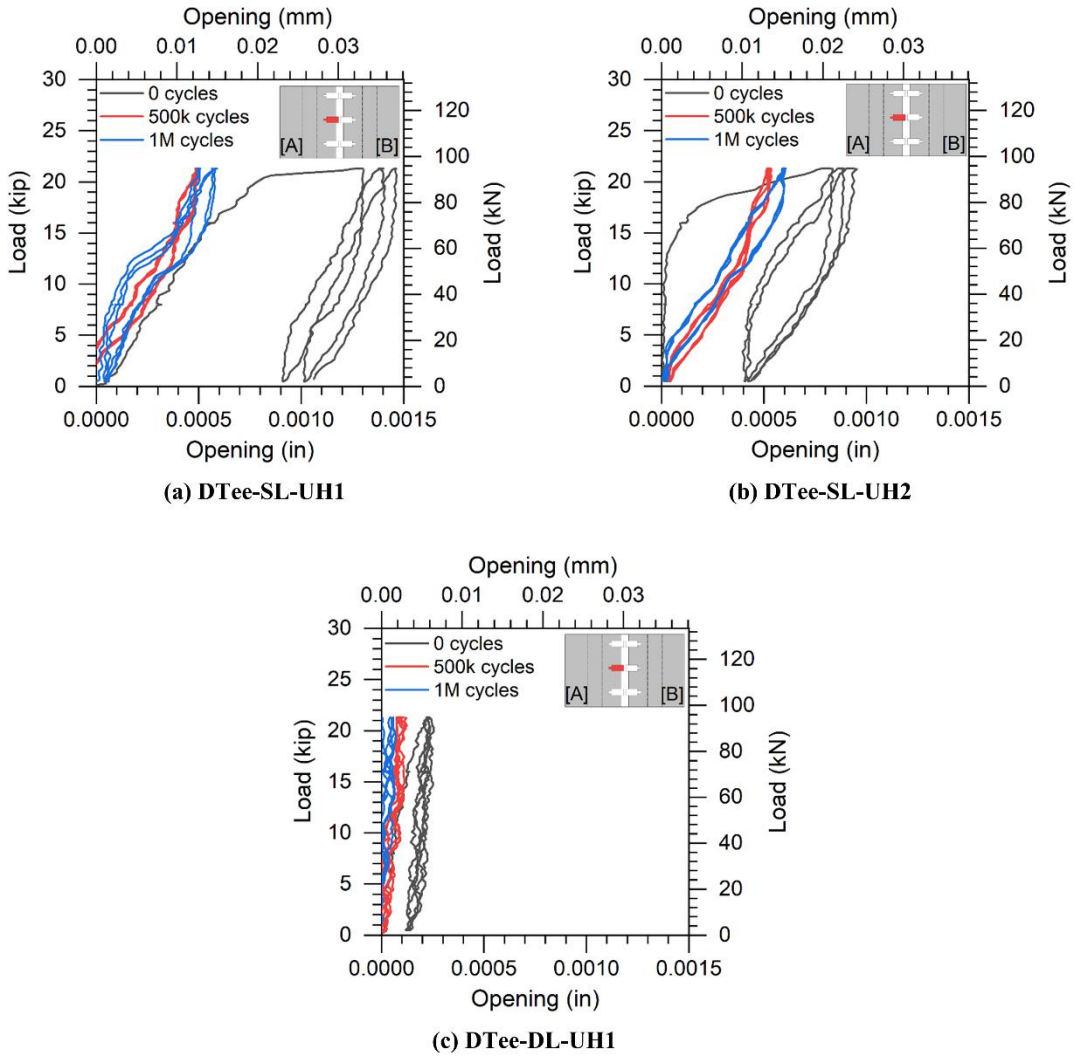

Figure 76. Response of selected LVDT during tests D2

4.6.3 Test D3 – Overload Test

The overload test D3 was executed after tests D1 and D2. A load of 28 kip (124.6 kN) was applied three times on the specimens using a ramp loading protocol. No cracking formation was observed during tests D3 in any of the four double-tee specimens. The same event that impaired the recording data from voltage-based instruments in specimen DTee-DL-UH3, as described in section 4.6.2, also affected the string potentiometer and LVDT data of that specimen during test D3. Due to this fact, the deflection read by string potentiometers and joint interface opening read by LVDTs for specimen DTee-DL-UH3 are not shown in this section.

The same string potentiometer, rebar strain gauge, and LVDT used to display the double-tee responses in tests D2 were also used to show the specimens' behavior during tests D3. These are the string potentiometer located at the center of the specimen, the steel strain gauge A6, and the horizontal LVDT at the center of the specimen measuring the interface opening on the side where load was applied. Figure 77 shows the response of the double-tee specimens during tests D3.

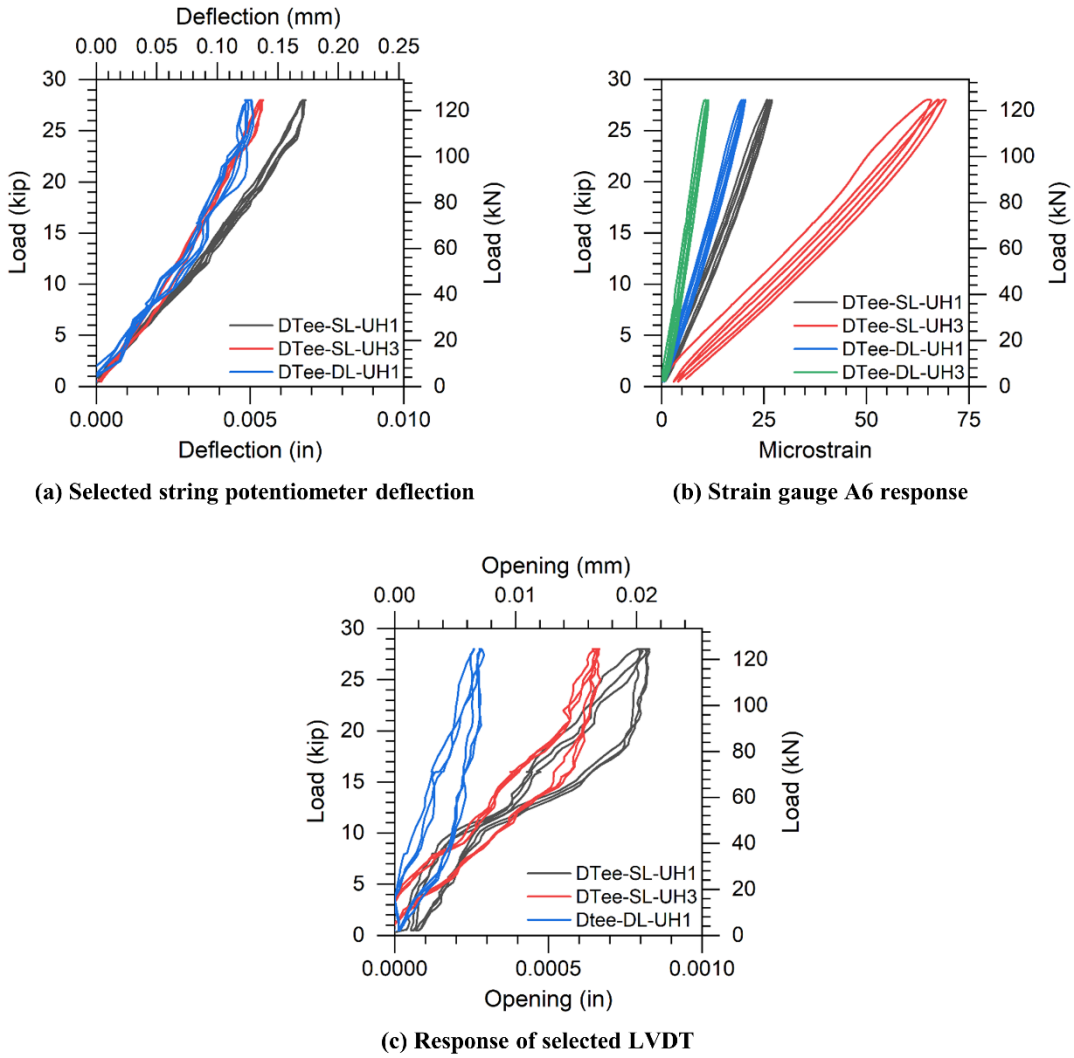

(a) Selected string potentiometer deflection

(b) Strain gauge A6 response

(c) Response of selected LVDT

Figure 77. Double-tee specimen responses during tests D3

4.6.4 Test D4 – Overload Cyclic Test

After tests D3 were completed, test D4 was performed on the double-tee specimens. Tests D4 had the same peak and valley loads as tests D3. A total of 1,500 sinusoidal cycles were applied on the specimens at a rate of two cycles per second. The results presented in this section followed the same format as the results from tests S1 and D1, which consisted of the difference in response captured at peak and valley loads applied on the specimens. The results from the string potentiometers, strain gauges in DTee-SL specimens, strain gauges in DTee-DL specimens, and LVDT joint openings are shown in Figure 78, Figure 79, Figure 80, and Figure 81, respectively. The location of the strain gauges, whose responses are shown in Figure 79 and Figure 80, is shown in Figure 70.

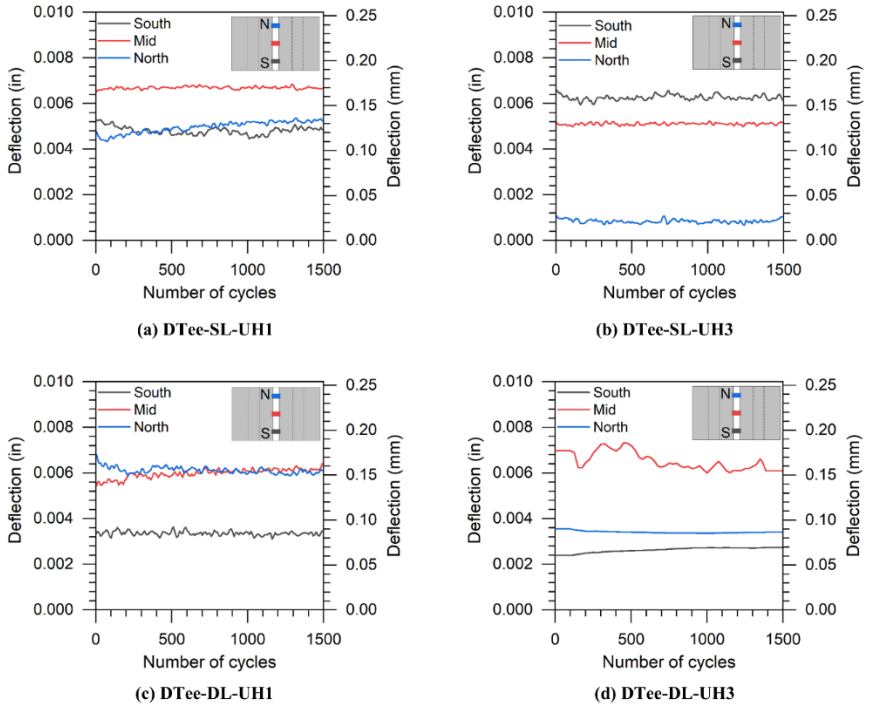

Figure 78. Measured String potentiometer deflections during tests D4

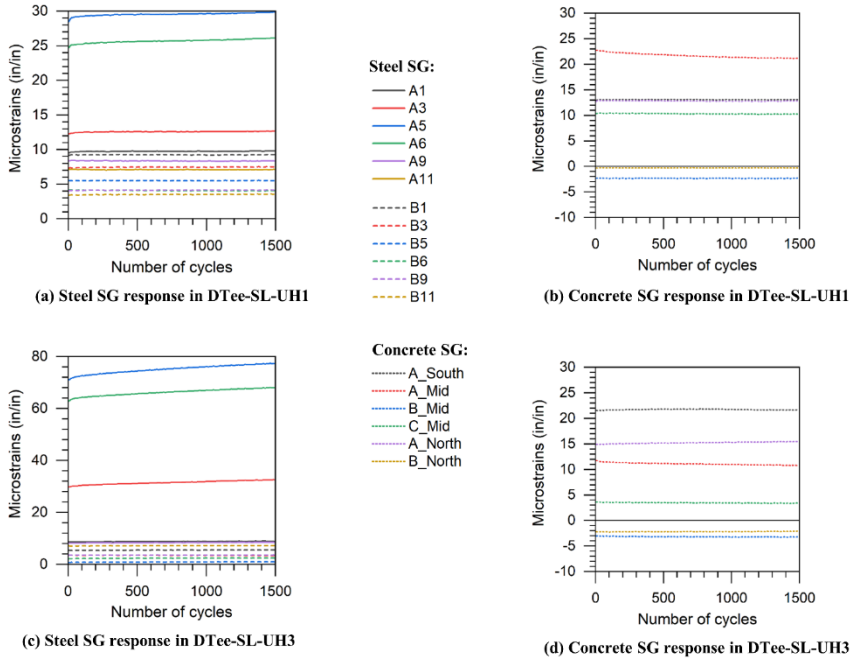

Figure 79. Measured strain gauge responses in DTee-SL specimens during tests D4

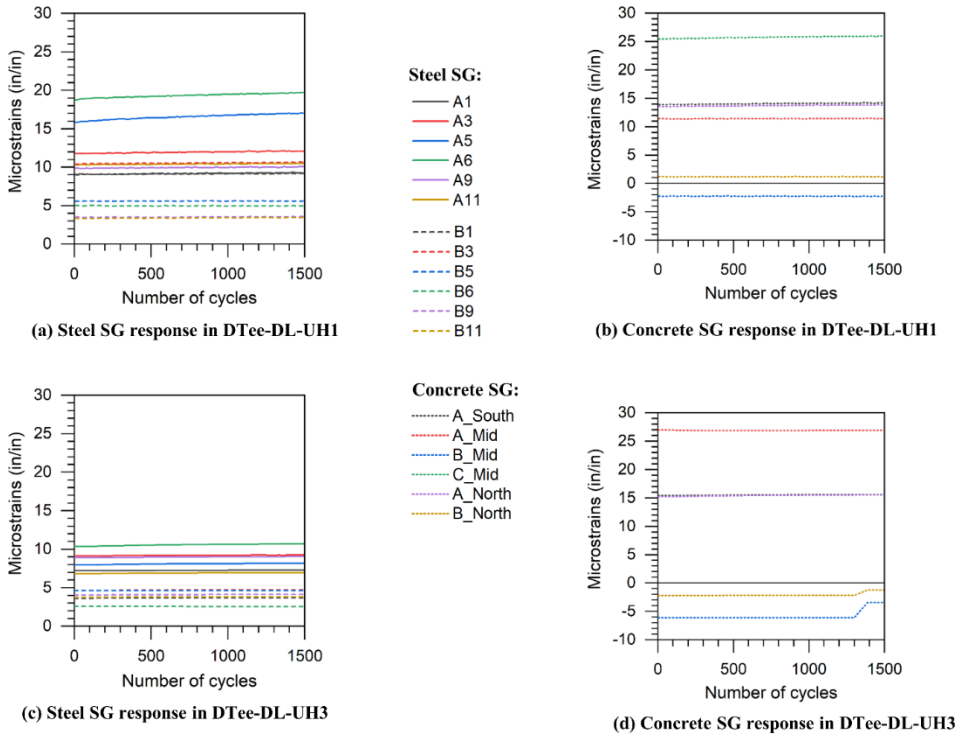

Figure 80. Measured strain gauge responses in DTee-DL specimens during tests D4

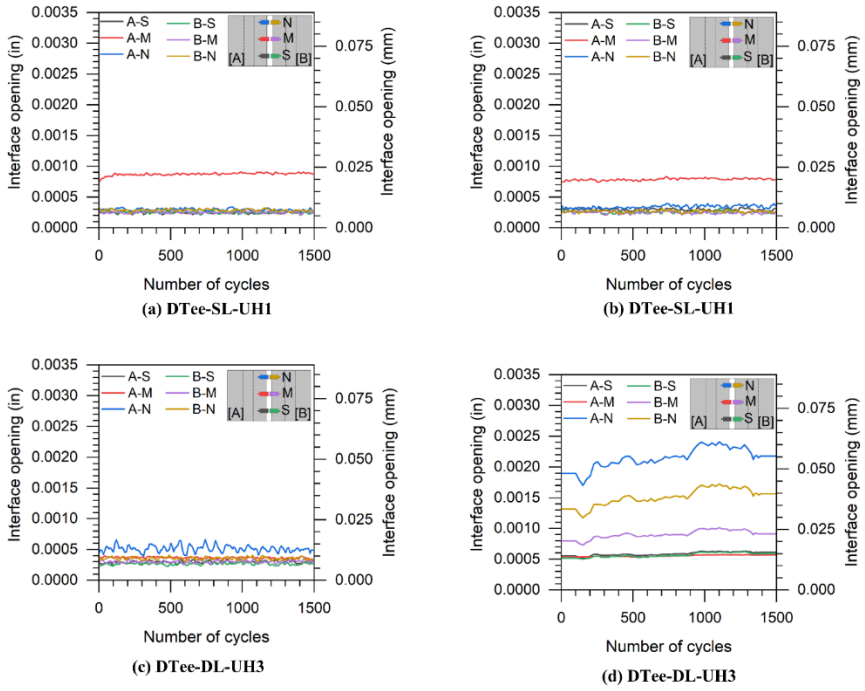

Figure 81. Measured joint opening responses using LVDTs during tests D4

4.6.5 Test D5 – Final Overload Test

The final overload test, or test D5, was performed on the double-tee specimens after tests D1, D2, D3, and D4 were completed. The location of the applied load remained the same in tests D5 as it was in the other tests. Differently from the other tests, which used a hydraulic actuator to apply loading, tests D5 used a manual hydraulic jack to apply loading on the double-tees. As described in section 4.3, the loading protocol for this test type consisted of three consecutive cycles of 48 kip (213.5 kN), and one cycle with a peak load of 64 kip (284.7 kN).

No cracking was visually detected in the UHPC at any point. Cracking in the NC was first observed at 48 kip (213.5 kN) for specimen DTee-SL-UH1, 35 kip (155.7 kN) for DTee-DL-UH1, and 48 kip (213.5 kN) for DTee-DL-UH3. Cracking extended and new cracks appeared in those three specimens as load increased or a new load cycle was applied. The observed cracks in the specimens DTee-SL-UH1, DTee-DL-UH1, and DTee-DL-UH3 are shown in Figure 86. No cracking was detected in specimen DTee-SL-UH3 during test D5. The measured deflections, strains in DTee-SL specimens, strains in DTee-DL specimens, and LVDT joint openings are shown in Figure 82, Figure 83, Figure 84, and Figure 85, respectively. The location of the strain gauges in test specimens used in test D5 are shown in Figure 70.

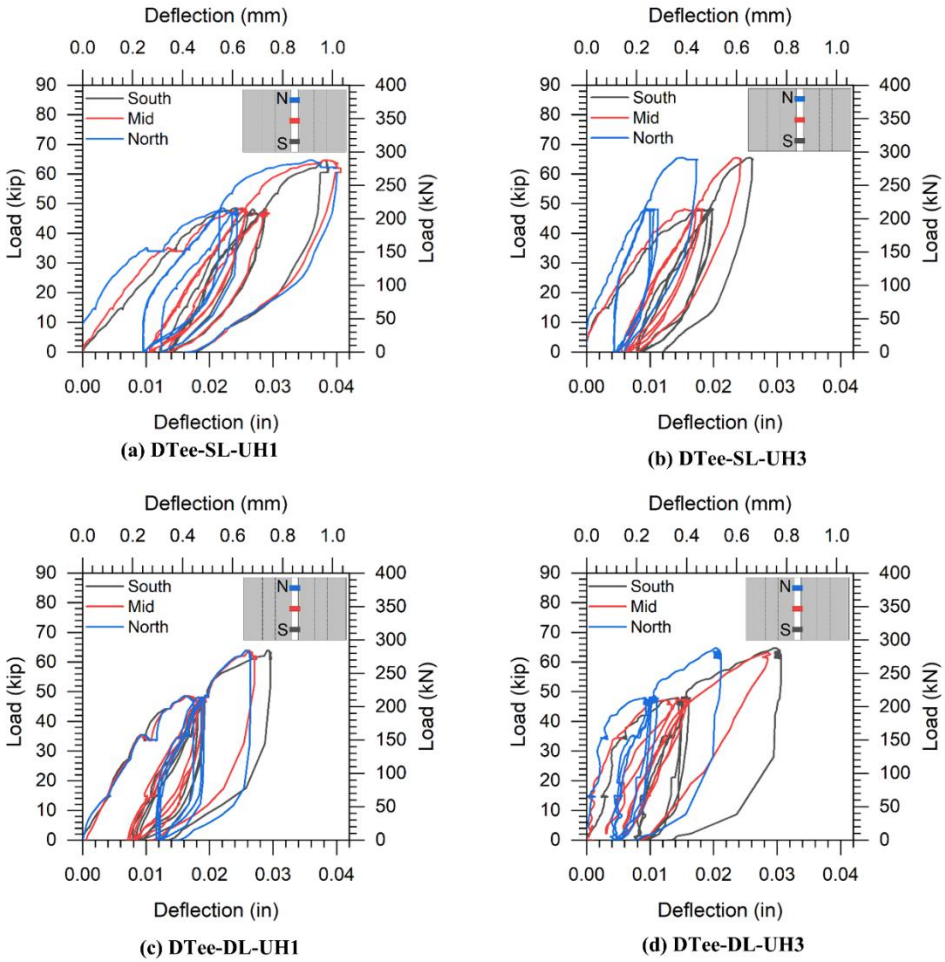

Figure 82. Measured deflection response of double-tee specimens during Test D5

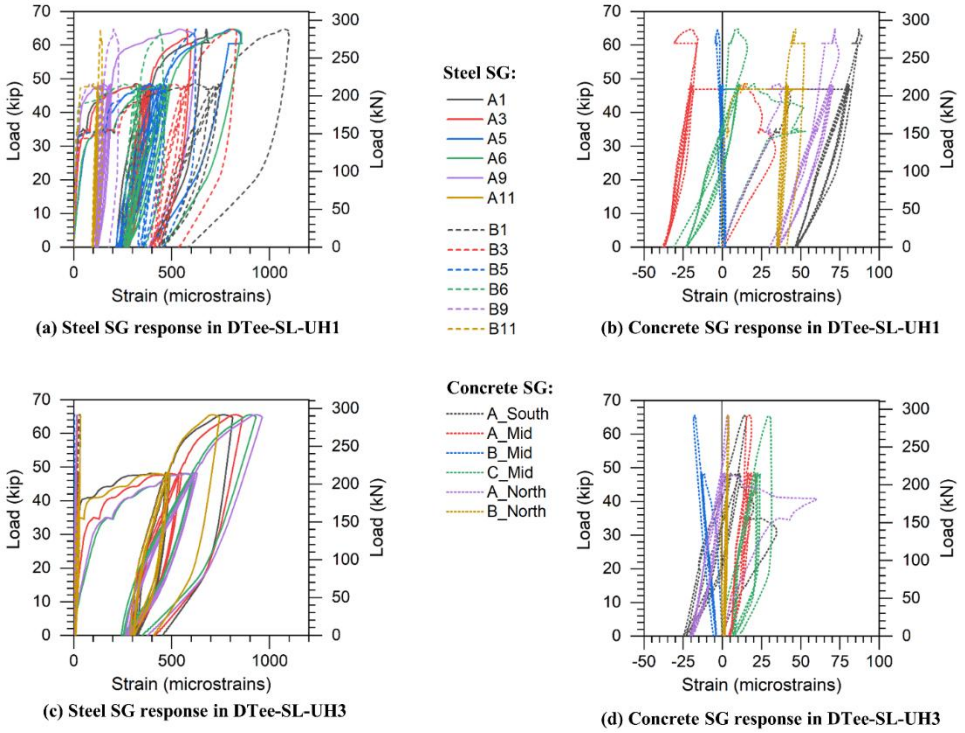

Figure 83. Measured strain gauge responses for specimens DTee-SL during tests D5

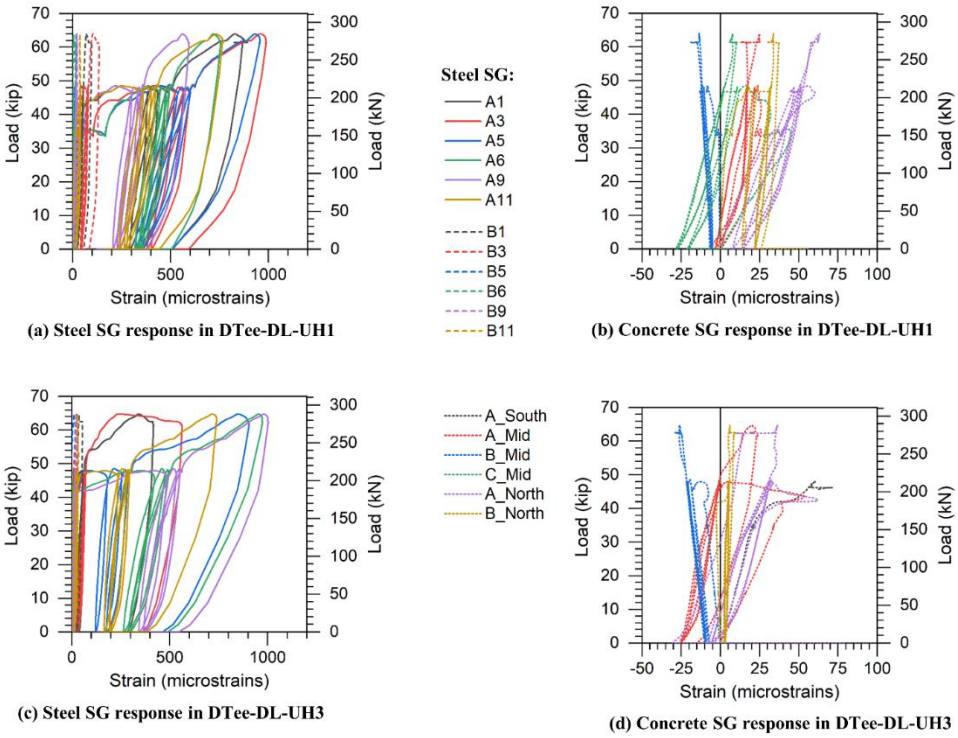

Figure 84. Measured Strain gauge responses for specimens DTee-DL during tests D5

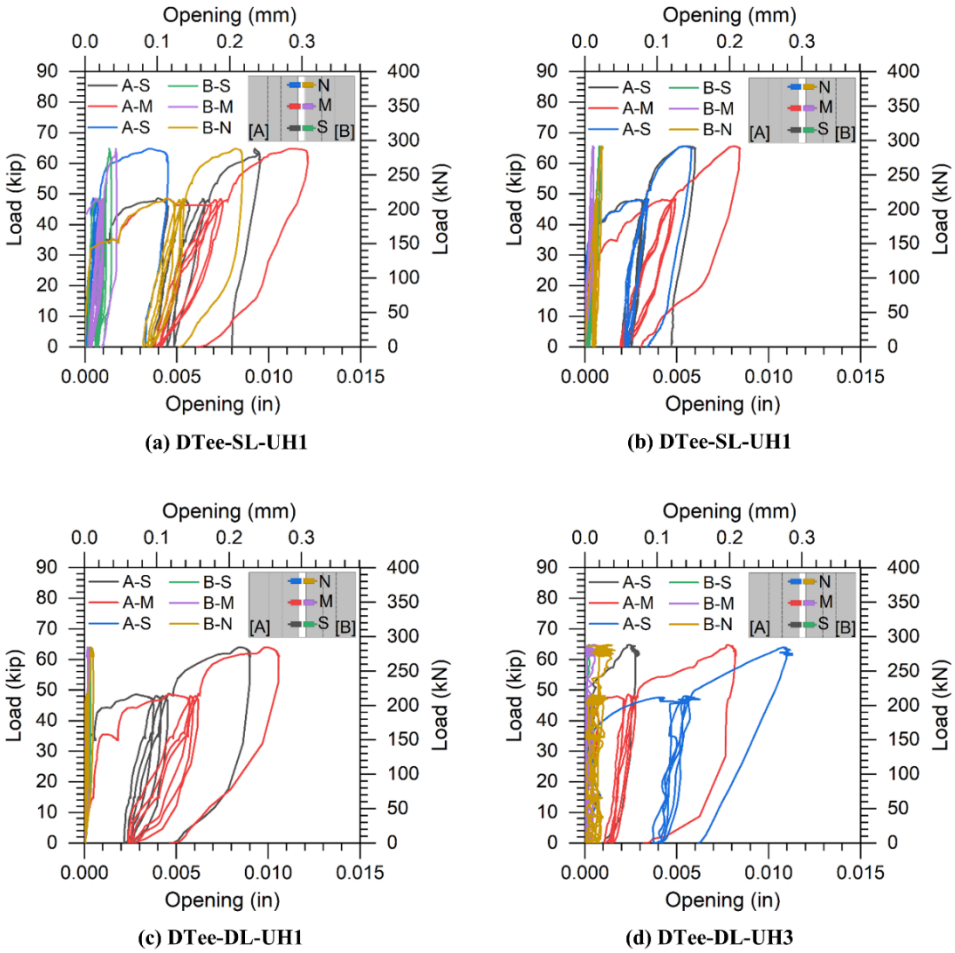

Figure 85. Measured joint interface opening in double-tee specimens with LVDT during tests D5

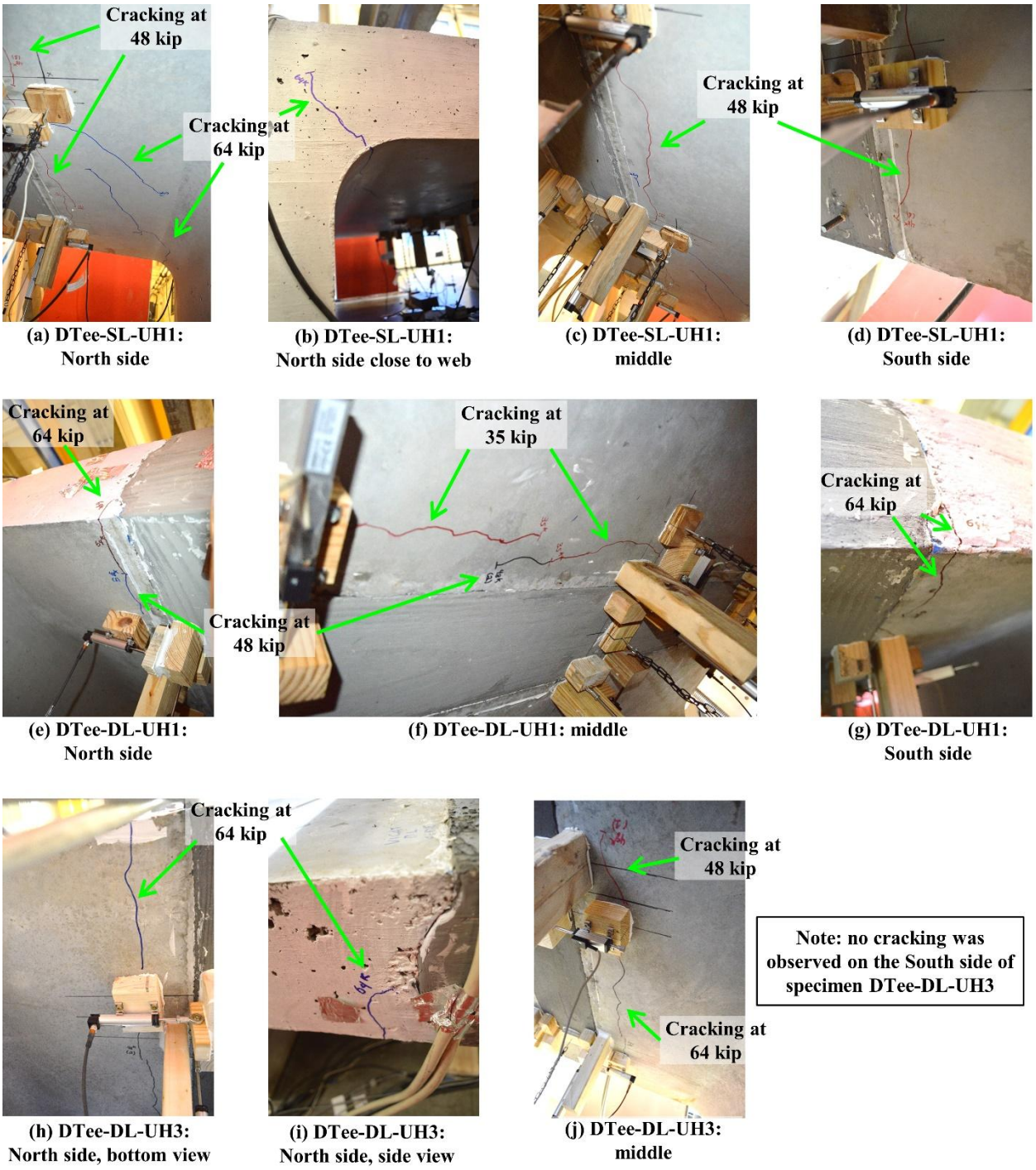

Figure 86. Cracking observed in specimens DTee-SL-UH1, DTee-DL-UH1, and DTee-DL-UH3 during tests D5.

5 FINITE ELEMENT MODELING

For this study, the software ATENA (version 5) was used to develop models and conduct all finite element analyses (FEA). The analysis focused on three primary models: slab, double-tee, and bridge models. The slab models included two reinforcement configurations: one layer of reinforcement, representing the Slab-SL specimens, and two layers of reinforcement, representing the Slab-DL specimens, in the UHPC joint.

For the double-tee models, three reinforcement configurations were analyzed: single-layer reinforcement (representing DTee-SL specimens), double-layer reinforcement (representing DTee-DL specimens), and a single-layer configuration representing the reinforcement used in a bridge in Mobile County, which utilized #6 headed rebars. This latter configuration will be referred to as DTee-Headed for simplicity. A bridge model was also developed, matching the concrete geometry of the bridge in Mobile, AL. However, this model used a single bottom layer of #5 rebars crossing the UHPC-NC interface, instead of the #6 headed bars used in the actual bridge. The modeled reinforcement was non-skewed, and the total bridge length was set at 60 feet (18,288 mm). The objective of the FEA in this investigation was to simulate realistic bridge loading and conditions similar to those present in the constructed bridge in Mobile, AL.

5.1 Structure geometry, reinforcement, boundary conditions, and loading

5.1.1 Slab and double-tee models

The geometry and reinforcement of the slab and double-tee models were replicated according to the as-built details of the specimens tested in the laboratory. Since the software does not accommodate curved shapes, the curves in the double-tee specimens were approximated using a combination of several straight lines. The specimens were simply supported, and a constant displacement was applied at the loading location. Figure 87 shows the geometry, reinforcement, boundary conditions, and applied loading location of the modeled slab and double-tee specimens.

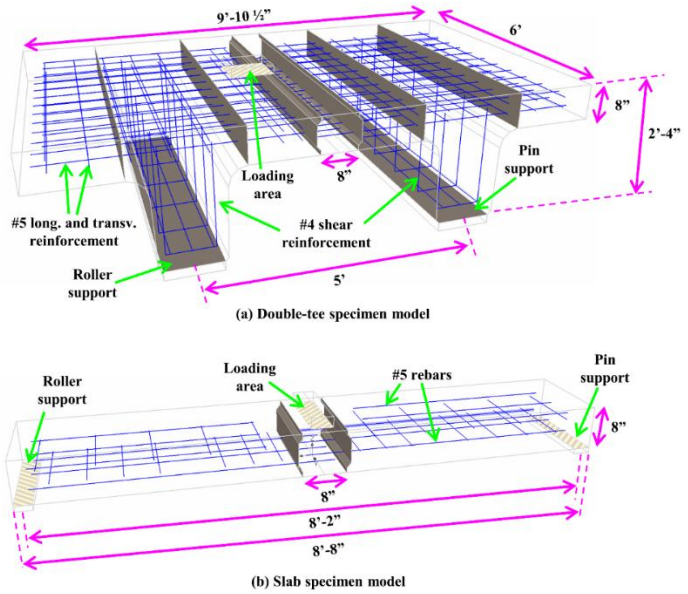

Figure 87. Geometry, reinforcement, boundary conditions, and applied loading of slab and double-tee models

5.1.2 Bridge model

The dimensions of the modeled bridge followed those of the bridge built in Mobile County, AL. The bridge was simply supported with supports below each end of the double-tee webs. The length of the supports was based on the ones used for the actual bridge construction and was taken as 1ft. 3.5 in. (393.7 mm). The reinforcement of the modeled bridge followed the same format as the double-tee specimens with a single reinforcement layer: #5 straight rebars at 6 in. (152.4 mm) on center.

The reinforcement of the modeled bridges was identical to the one in the actual bridge, with modifications in the joint region to accommodate the reinforcement configuration of the three models. The first and second models, with a single and double layer of #5 rebars, followed the same pattern as the double-tee models. The third modeled reinforcement configuration was obtained from the constructed bridge, in which a single layer of #6 headed bars was used. Since the models in this study utilized a perfect connection between concrete and rebars and all the rebars are truss elements, which have no 3D volume, the studs at the ends of #6 rebars were not modeled. Figure 88 shows the geometry, reinforcement, boundary conditions, and applied loading location of the modeled bridge. The loading areas simulate the area of contact of a truck, and the left-most plane of the figure represents an axisymmetric plane used in the model to simulate a bridge with eight webs and two double tee beams.

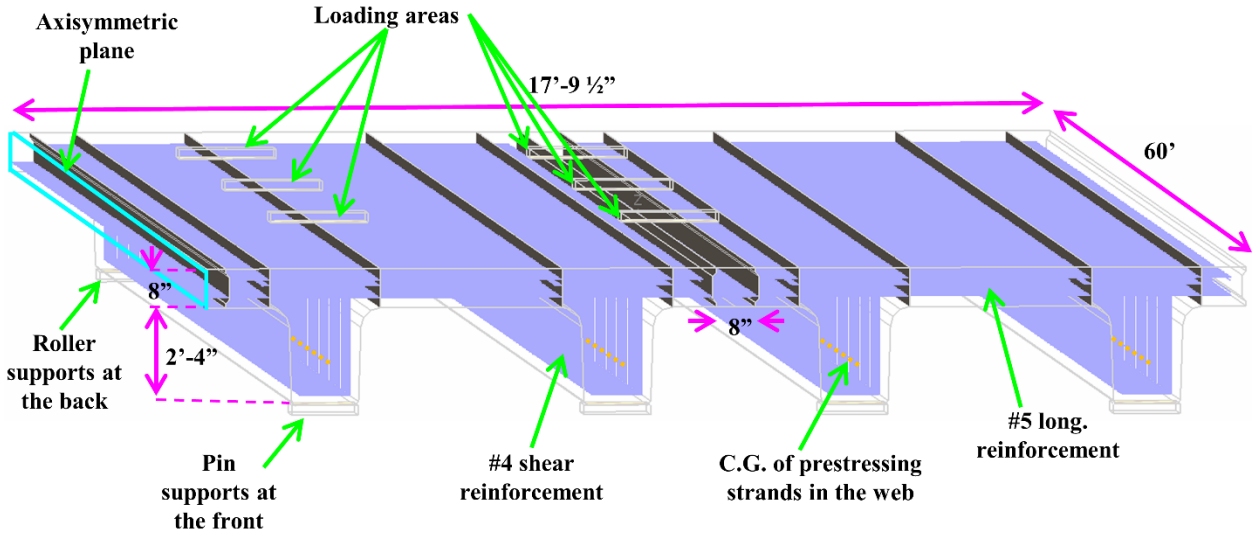

Figure 88. Geometry, reinforcement, boundary conditions, and applied loading of bridge model.

5.2 Calibration of FEA models

The calibration of FEA models includes the material properties used in the models, interaction properties between materials, element type, and element size. This information was the same for the slab and double-tee models but different for the bridge model.

5.2.1 Slab and double-tee models

Non-linear material properties were used for the NC and UHPC components modeled in the slab and double-tee specimens. The material type used in ATENA for these components was the "CC3NonLinCementitious2". The compressive strengths of the cementitious materials, the elastic modulus of UHPC, and the Poisson's ratio of UHPC were obtained from tested cylinders at the time

of tests S4 and D5. The elastic modulus and modulus of rupture of NC were obtained from the American Concrete Institute's (ACI's) Building Code Requirements for Structural Concrete (ACI 318) and Commentary (ACI 318R)[86]. The Poisson's ratio of NC was taken as 0.18 based on UHPC's measured Poisson's ratio of 0.20. The peak tensile stress of UHPC was obtained from tested direct tension specimen results. Table 15 summarizes the concrete material parameters used for the slab and double-tee specimens. The stress-strain behavior of the used rebars was obtained from experimental tensile testing.

Table 15. Material parameters used for slab and double-tee specimens

FEA material	Compressive strength ksi (MPa)	Tensile strength ksi (MPa)	Elastic modulus ksi (MPa)	Poisson's ratio
Slab NC	7.17 (49.4)	0.63 (4.34)	4,820 (33,233)	0.18
Double-tee NC	9.83 (67.8)	0.74 (5.10)	5,650 (38,955)	0.18
UHPC	20 (137.9)	1.51 (10.41)	7,000 (48,263)	0.20

Linear tetra elements, named "CCIsoTetra" by ATENA, were used for all concrete elements due to the non-rectangular shape of the UHPC joint. Rebars were modeled as truss elements, and a perfect bond was assumed between steel reinforcement and concrete. The contact between NC and UHPC was modeled as a 3D interface material, categorized as "CC3DInterface" in the software. The input values used in the interface model are shown in Table 16. The tangential stiffness, K_{tt}, was used as the software's default value. AASHTO LRFD Bridge Design Specifications[11] recommends cohesion and friction values for NC to NC interactions. The cohesion and friction values used in this study were obtained from the AASTHO Specifications[11] and slightly increased to accommodate the interaction properties between the power-washed NC surface and UHPC.

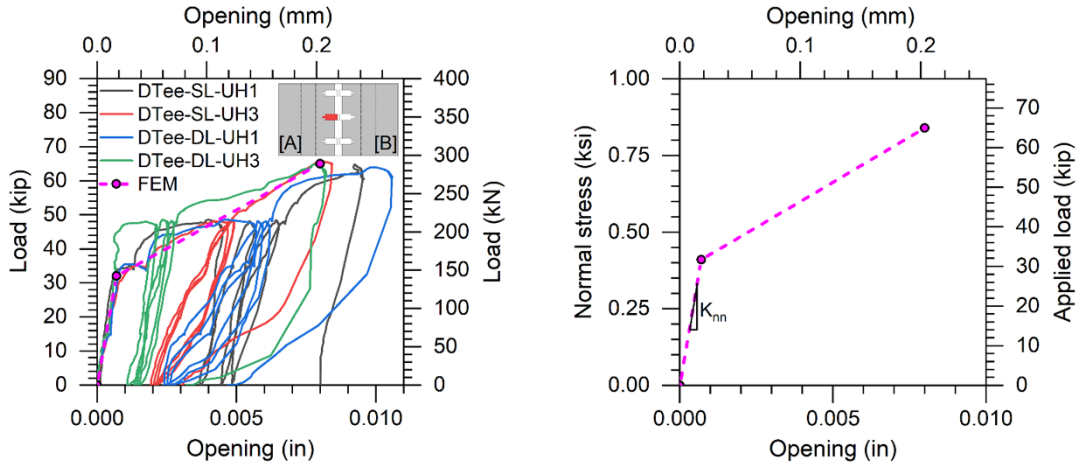

(a) Load vs. joint opening

(b) Bilinear behavior of normal stiffness in FEA

Figure 89. Normal stiffness behavior used in FEA.

The normal stiffness, K_{nn}, was obtained from the experimental results of tests D5. A bilinear behavior was assumed based on the experimental load-opening behavior captured by the load cell and the LVDT closest to the applied load at the center of the double-tee specimens (Figure 89 (a)). A structural analysis calculation was performed in which the top flange of the double-tee specimen was assumed to be a beam simply supported on the webs. The calculated moment resultant from the structural analysis combined with the load from the first FEM data point in Figure 89(a) (32 kip or 142.3 kN) resulted in a stress at the interface location of 0.41 ksi (2.83 MPa). This resultant stress

was used as the tensile strength, f_t, of the interface. The tensile strength was then divided by the assumed opening (7×10^{-4} in or 1.78×10^{-2} mm) at that load, which generated a K_{nn} of 586 kip/in^3 (1.59×10^8 kN/m^3). Figure 89(b) shows the bilinear normal stiffness behavior used in the interface behavior, and Table 16 lists all the parameters used for the interface behavior between NC and UHPC used in the slab and double-tee specimens.

Table 16. Parameters used for the interface behavior between NC and UHPC

Normal stiffness, K_{nn} kip/in^3 (kN/m^3)	Tangential sfinness, K_{tt} kip/in^3 (kN/m^3)	Tensile strength, f_t ksi (MPa)	Cohesion, C ksi (MPa)	Friction coefficient
586 (1.59×10^8)	7.37×10^5 (2.00×10^{11})	0.41 (2.83)	0.60 (4.14)	0.90

After the calibration of materials and interface properties, a mesh sensitivity study was performed on the modeled Slab-SL specimen. Several models representing the Slab-SL specimens with different mesh sizes were created, and their load-deflection responses were evaluated. Figure 90 depicts the mesh configurations evaluated for each model. Figure 91 shows the response of each model, and Table 17 summarizes their mesh sizes, peak load, load difference from previous mesh configuration, and computational time to run the model. As the element size in Table 17 increases, the load difference relative to the preceding mesh configuration keeps on decreasing until mesh configuration F. The change in element size from mesh configurations F to G resulted in a positive load difference, which was attributed to an artificial over stiffness of the system due to the small element sizes. This fact, combined with the large computational time required to run mesh configuration G, led to mesh configuration F being used for the slab model and for the double-tee model at the top flange close to the joint location. In order to save computational time, elements in the double-tee model in the web and the flange (away from the joint location) were scaled to 3 in. (76.2mm). Figure 92 shows the mesh configurations used in the slab and double-tee specimens.

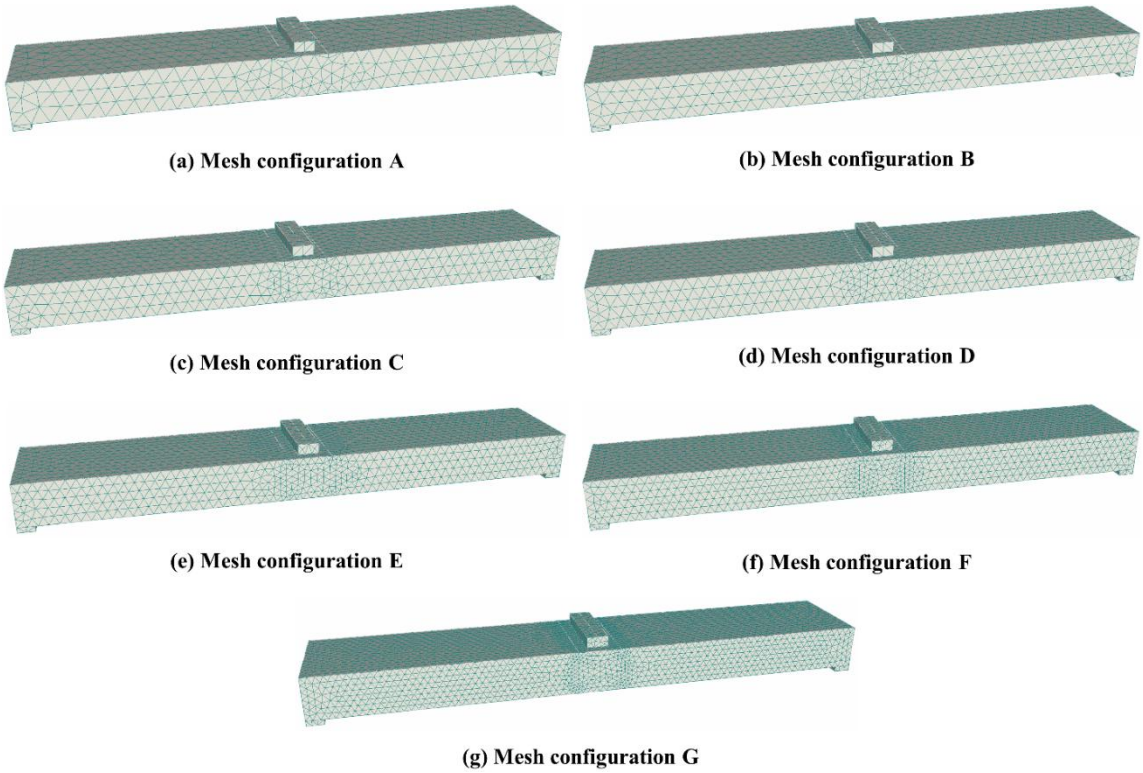

Figure 90. Mesh study performed on Slab-SL specimens

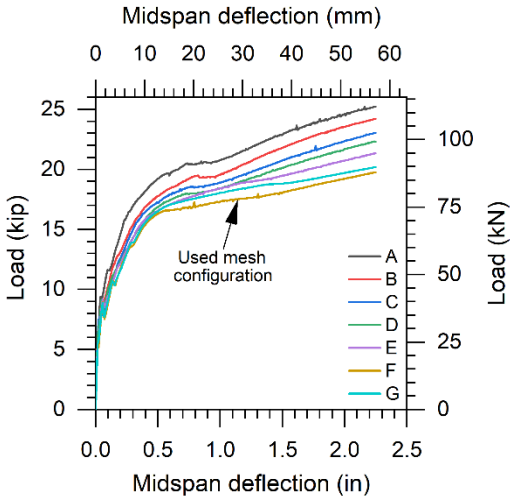

Figure 91. Response of each mesh configuration for slab mesh study

Table 17. Mesh study performed on Slab-SL specimens

Mesh configuration	Element size at interface in. (mm)	Element size elsewhere in. (mm)	Peak load kip (kN)	Load difference from previous mesh configuration kip (kN)	Computational time to run model (h:min)
A	2.50 (63.5)	3.00 (76.2)	25.23 (112.23)	0	07:04
B	2.00 (50.8)	2.50 (63.5)	24.23 (107.78)	-1.00 (-4.45)	10:41
C	1.75 (44.5)	2.25 (57.2)	23.06 (102.58)	-1.17 (-5.20)	13:28
D	1.50 (38.1)	2.00 (50.8)	22.34 (99.37)	-0.72 (-3.20)	15:51
E	1.25 (31.8)	1.75 (44.5)	21.35 (94.97)	-0.99 (-4.40)	28:07
F	1.00 (25.4)	1.50 (38.1)	19.75 (87.85)	-1.60 (-7.12)	46:14
G	0.75 (19.1)	1.25 (31.8)	20.20 (89.85)	+0.45 (+2.00)	63:46

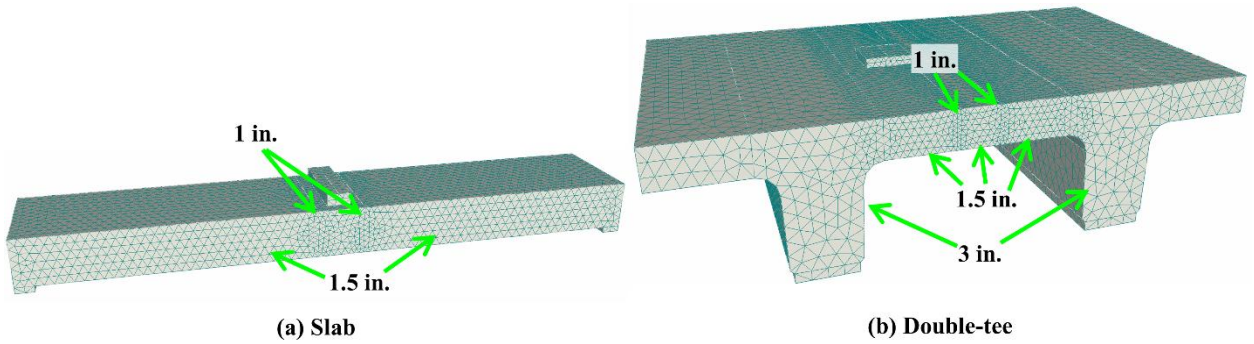

Figure 92. Mesh configuration used in slab and double-tee specimens

5.2.2 Bridge Model

Based on the AASHTO standard truck wheel load configuration, it was determined that the bridge materials would stay in the elastic region at all times. Therefore, all the elements in the bridge models were created with elastic materials of the types “CC3DElastIsotropic” for NC and UHPC, and “CCReinforcement” for rebars and prestressing strands. The elastic moduli of NC, UHPC, and rebar were obtained from the material characterization performed in this study, and the elastic modulus of the used prestressing strands was obtained from the PCI Handbook[77]. The elastic

modulus used for each material is shown in Table 18. The same element type and NC-UHPC interface behavior properties used in the slab and double-tee models were used in the bridge models. In order to reduce processing time with the computational power available to process the bridge models, a mesh study was conducted using the DTee-SL model. A coarser mesh was introduced, and the results are presented in Section 5.3.3.

Table 18. Elastic modulus of materials used in the bridge model

NC	UHPC	Rebar	Prestressing strands
5,650 ksi	7,000 ksi	24,830 ksi	28,500 ksi

5.3 Finite Element Analysis Results

5.3.1 Comparison of Experimental and FEA results

The location of the applied load and supports in the FEA models followed the same pattern as the ones in the slab and double-tee specimens tested in the laboratory. The loads were applied on each specimen model using an external steel block perfectly bonded to the specimens. A constant downward displacement was applied on the block, which increasingly loaded the specimen as the block displaced. The results of the FEA obtained from the models simulating the specimens Slab-SL, Slab-DL, DTee-SL, and DTee-DL are shown in Figure 93(a), Figure 93(b), Figure 93(c), and Figure 93(d), respectively.

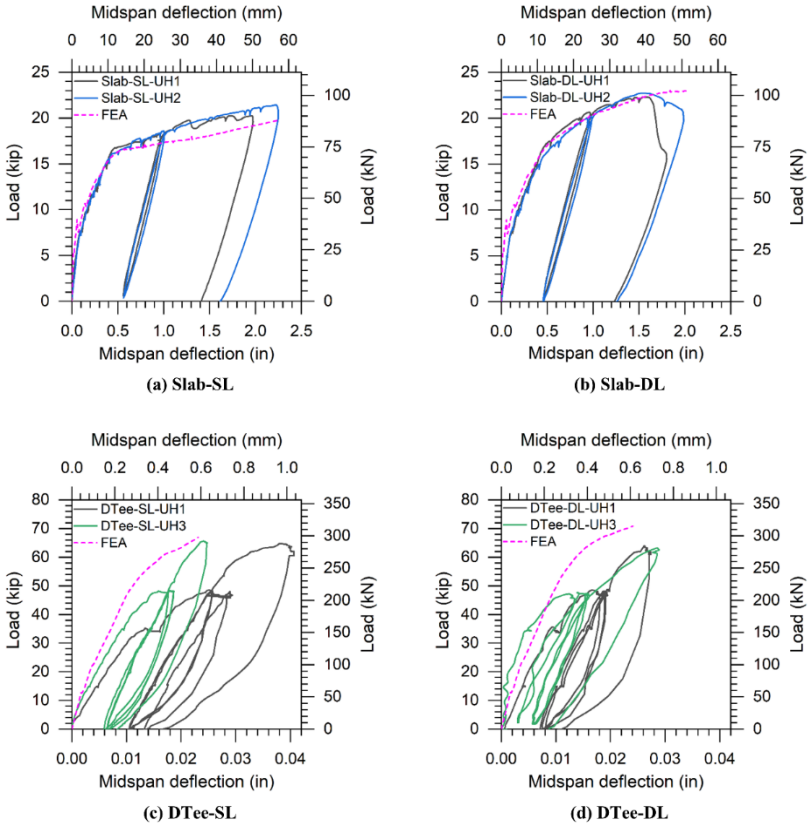

Figure 93. Comparison of FEA results from slab and double-tee models with measured response

Monitoring points were added in the model at the same locations where strain gauges were applied in the tested specimens. The monitoring points recorded strains in the steel reinforcement and UHPC. The strain gauges selected to compare the FEA to the actual strain gauge responses are the ones placed in the UHPC at the center of the specimen and on the rebar closest to where the cyclic load was applied. The strain gauge responses from the FEA and experimental testing for specimens Slab-SL, Slab-DL, DTee-SL, and DTee-DL are shown in Figure 94, Figure 95, Figure 96, and Figure 97, respectively. The exact location of the strain gauges in the slab and double-tee specimens is shown in Figure 48 and Figure 70, respectively.

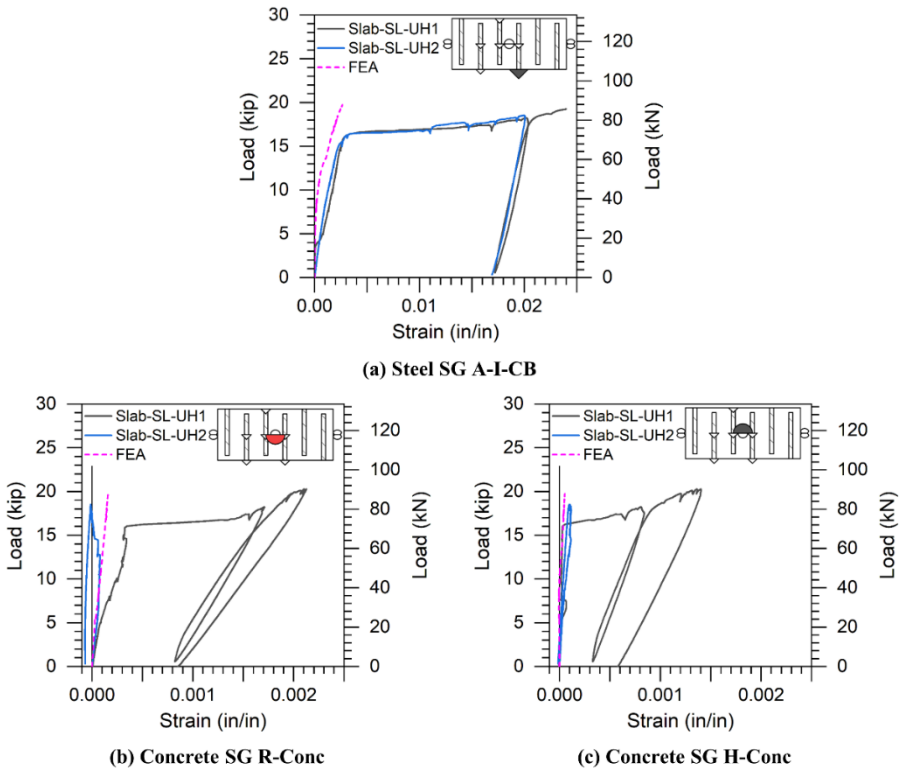

Figure 94. FEA and experimental strain gauge responses in Slab-SL specimens

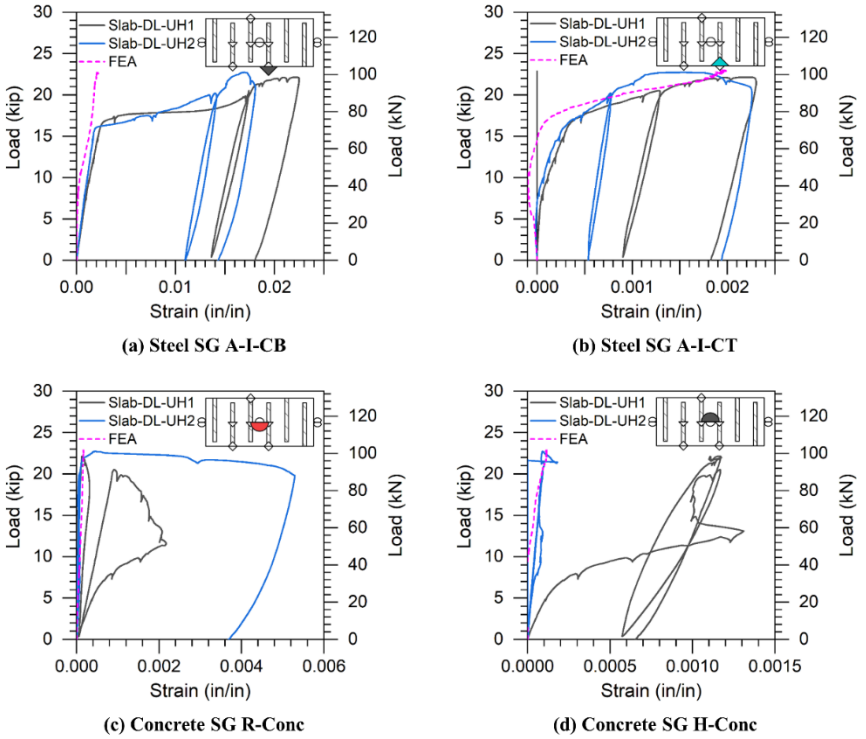

Figure 95. FEA and experimental strain gauge responses in Slab-DL specimens

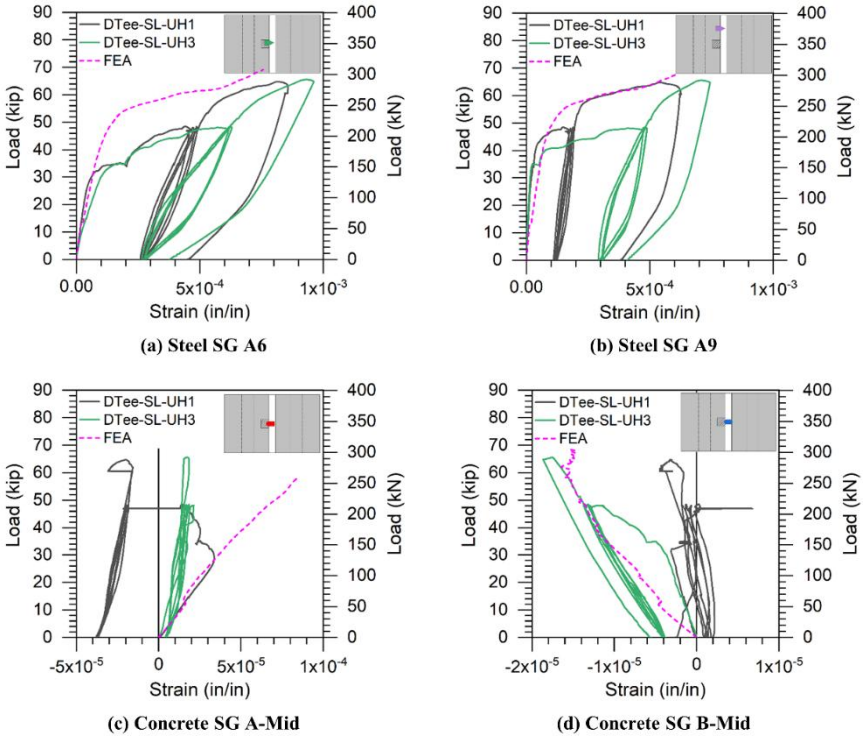

Figure 96. FEA and experimental strain gauge responses in DTee-SL specimens

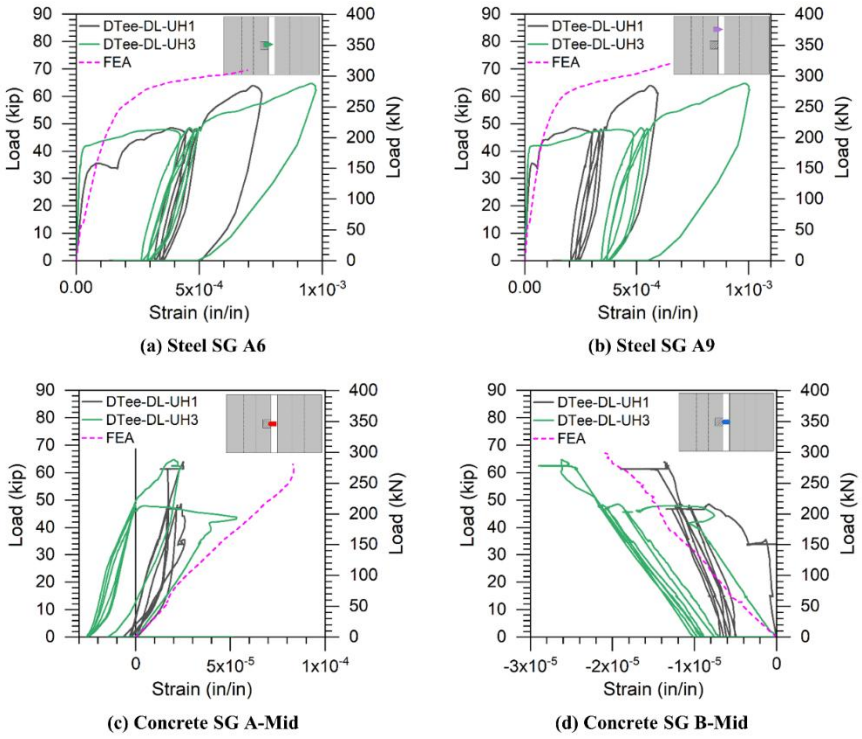

Figure 97. FEA and experimental strain gauge responses in DTee-DL specimens

A study was performed with the intent to evaluate the load distribution in the double-tee specimens across their joint length in the longitudinal direction of the joint. The responses of the concrete strain gauges A-South, A-Mid, and A-North were obtained from the experimental and modeled double-tee specimens and subsequently compared. The precise location of these concrete strain gauges placed in the UHPC joint is depicted in Figure 70. Figure 98 and Figure 99 show the responses of the selected strain gauges for DTee-SL and DTee-DL specimens, respectively. As expected and seen in Figure 98(c) and Figure 99(c), the FEA model, which is free from any imperfection in the system, shows that strain gauge A-Mid experienced slightly higher strains compared to strain gauges A-South and A-North due to its location being the closest to the applied load. Based on the observed experimental responses of the strain gauges, it was determined that the loading was satisfactorily distributed across the joint length. This can be observed based on the experimental strain gauges' behavior until approximately 35 kip (155.7 kN), at which point some of the strain gauges experienced some degree of plasticity or the specimens experienced some degree of internal cracking. For reference, some key load values were added to the figures:

- 16 kip (71.2 kN): half of the design truck load given by AASHTO[11];
- 21.3 kip (94.7 kN): half of the design truck load given by AASHTO[11] multiplied by the dynamic load allowance factor of 1.33;
- 28 kip (124.6 kN): half of the design truck load given by AASHTO[11] multiplied by the dynamic load allowance factor of 1.75;
- 42.6 kip (189.5 kN): two times half of the design truck load given by AASHTO[11] multiplied by the dynamic load allowance factor of 1.33;
- 64 kip (284.7 kN): four times the design truck load given by AASHTO[11] and maximum applied load to double-tee specimens during tests D5.

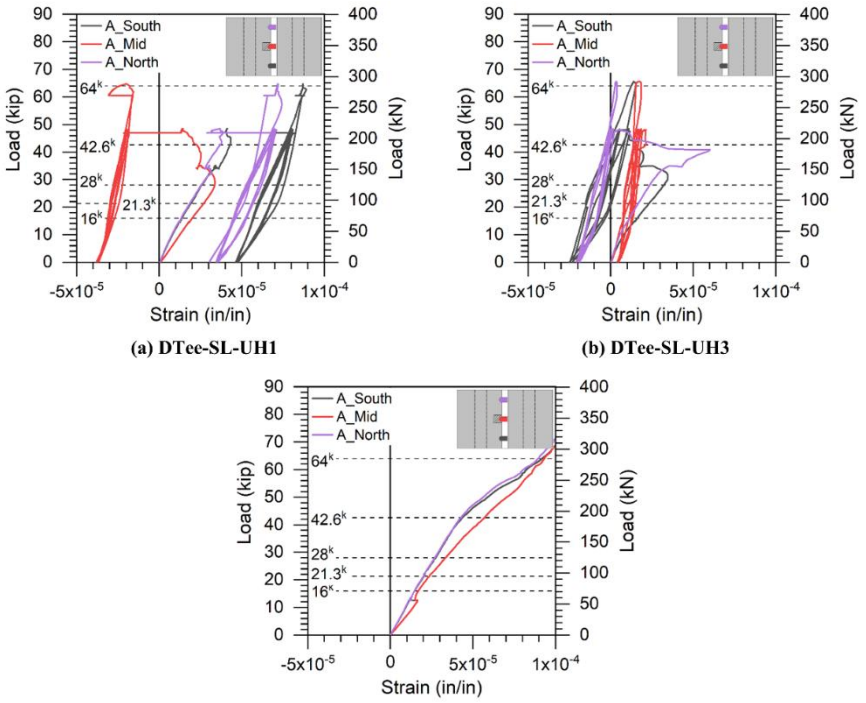

Figure 98. Strain gauge responses in DTee-SL specimens for load distribution study

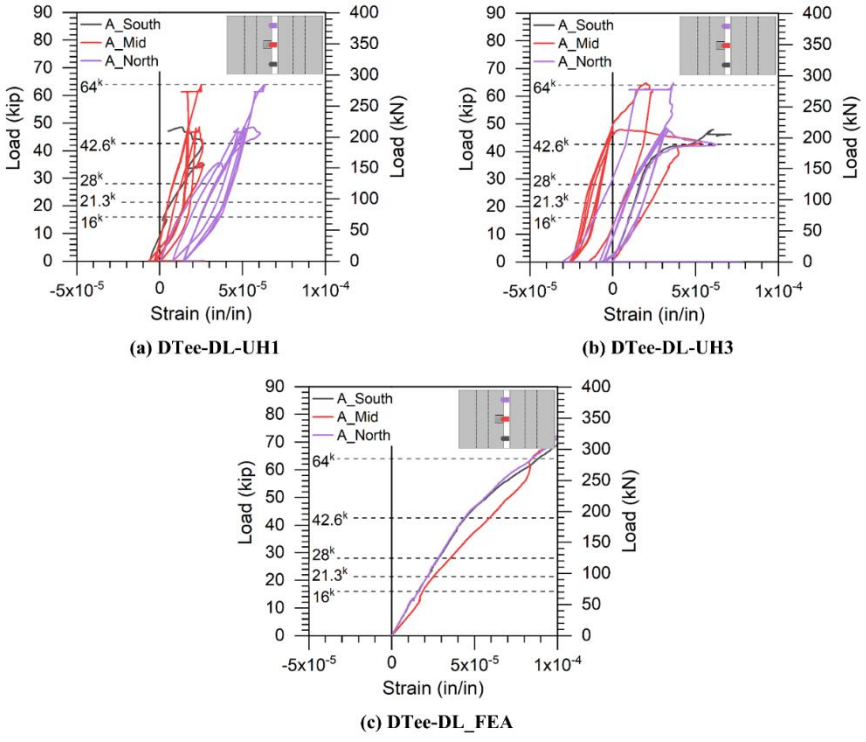

Figure 99. Strain gauge responses in DTee-DL specimens for load distribution study

5.3.2 Comparison of DTee-SL and DTee-DL FEA models to DTee-Headed FEA model

Selected monitoring points simulating experimental instrumentation were selected to compare the performance of the DTee-SL, DTee-DL, and DTee-Headed FEA models. The instruments were the string potentiometer measuring the midspan deflection, the LVDT measuring the horizontal interface joint opening closest to the applied load, steel strain gauge A6, and concrete strain gauge B-Mid. The responses of the tested specimens and FEA models are shown in Figure 100.

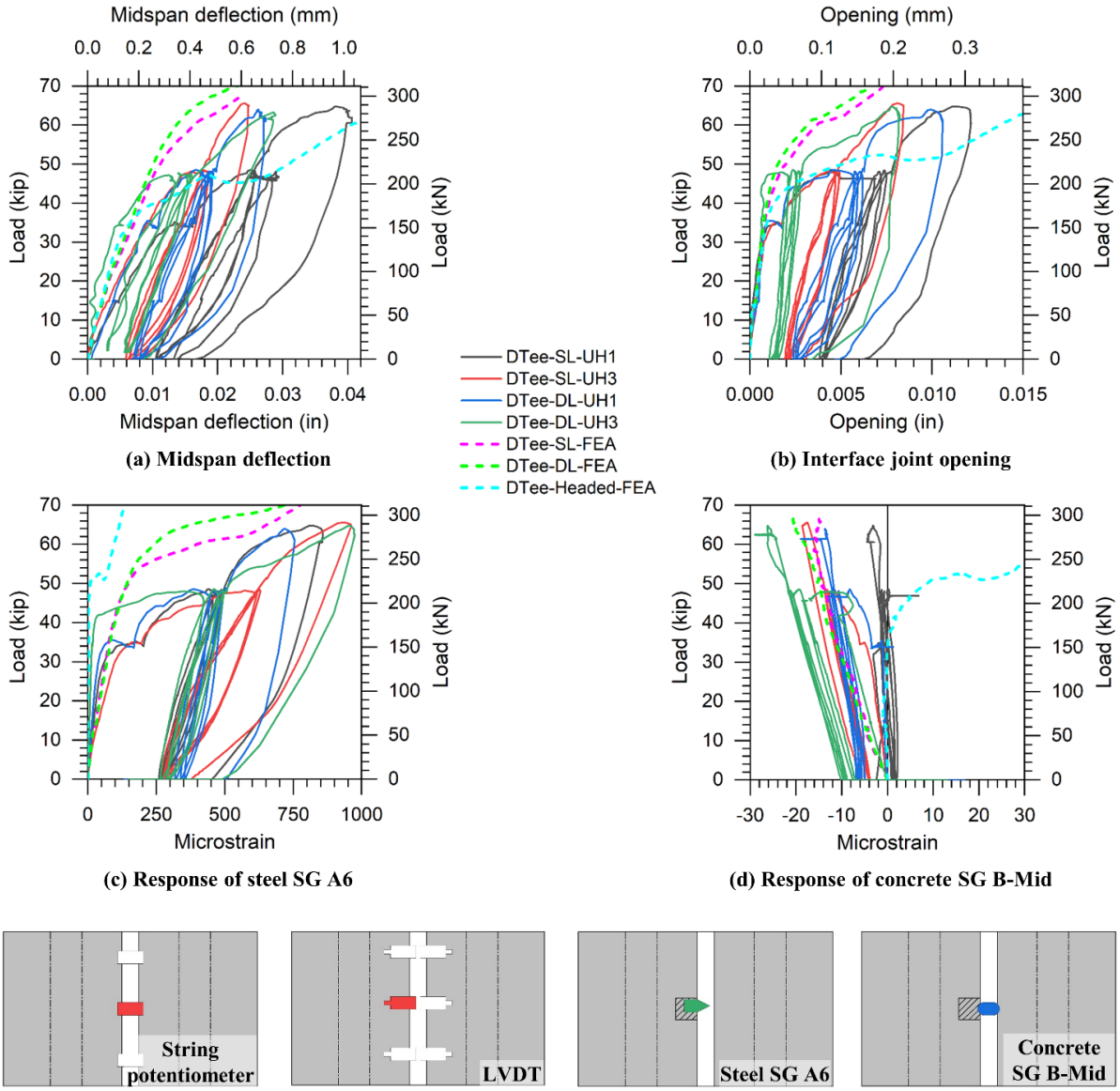

Figure 100. Comparison of DTee-SL and DTee-DL FEA models to DTee-Headed FEA model

It was observed that, among all three FEA models, the DTee-Headed one was the least stiff based on the midspan deflection and interface joint opening response. It was concluded that this is because of the heights of the reinforcement layers in the 8-in. (203-mm) high joint, which are 2 1/16 in. (52 mm) in the DTee-SL model and 3 3/4 in. (95 mm) in the DTee-Headed model. The higher reinforcement location in the DTee-Headed model (1/4 in. or 6 mm below the joint centroid) explains

the lower strain response in Figure 100(c) compared to the other models. Moreover, since the location of the rebar layer in the DTee-Headed is close to the centroid of the joint, the concrete and rebar strain responses (Figure 100(c) and Figure 100(d), respectively) are close to zero until the neutral axis depth is decreased enough to generate significant strains at that location.

5.3.3 Bridge model

Based on the results from the DTee-SL model (Figure 93(a)), a mesh sensitivity study was conducted in order to obtain a coarser mesh to be used in the bridge model that would reliably represent their FEA results without compromising the quality of the results. A coarser mesh was then introduced in the DTee-SL model, in which the element sizes were 2.5 in. (63.5 mm) at the NC-UHPC interface and 3 in. (76.2 mm) elsewhere. Having an element size of 3 in. (76.2 mm) allows the top flange of the bridge to have three mesh elements over its depth. With the modification from the original mesh configuration to the new mesh sizes, the FEA load-deflection response also changed. In order to artificially bring the new load-deflection response as close as possible to the original one, the K_{nn} value of the new model was reduced to $0.7 \times K_{nn}$. The new mesh configuration used in this study along with the load-deflection results of each model are shown in Figure 101.

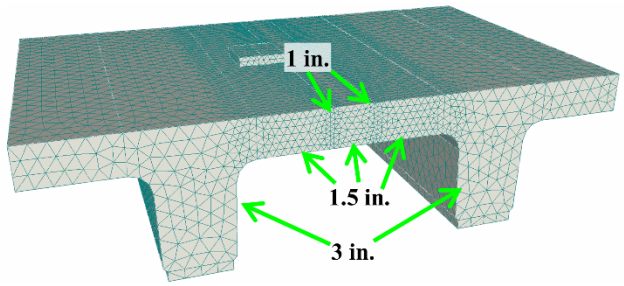

(a) Original meshing

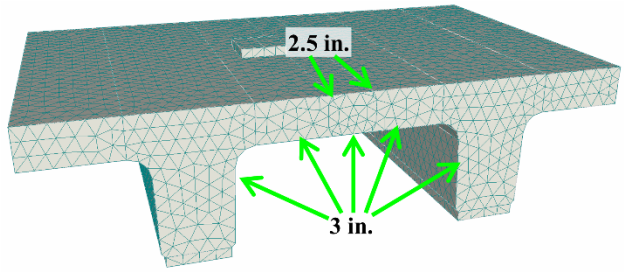

(b) Meshing used for bridge model

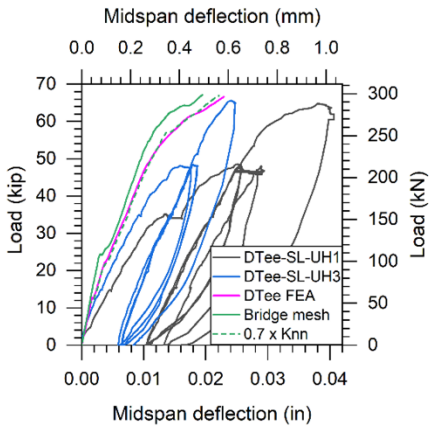

From the graph legend:

- **DTee FEA** = FEA response from original DTee-SL model
- **Bridge mesh** = FEA response from DTee-SL model with meshing used in figure (b)
- **0.7 x Knn** = FEA response from DTee-SL model with meshing used in figure (b) and Knn reduced to 70% of its original value

(c) Bridge mesh study results

Figure 101. Mesh study developed for bridge models

Before the load was applied on the bridge model, a prestressing load of 901.8 kip (4,011 kN) was applied in the web using one strand representing all 0.6-in. (15.24 mm) diameter strands embedded in the web. The single prestressing strand was modeled at the center of gravity of the combined strands in a beam web. A load of 16 kip (71.2 kN) was applied on each of the six loaded areas shown in Figure 88, following the AASHTO standard truck wheel loading protocol. Figure 102 shows the results obtained by the applied load on the bridge model. The joint opening shown in Figure 102(b) represents the opening of the interface between UHPC and NC closest to the centroid of the applied load on the deck of the modeled bridge. The rebar strain shown in Figure 102(c) represents the strain at a #5 reinforcement bar at midspan close to the joint interface, and the UHPC strain in the figure

shows the strain of the UHPC at a height of 3.875 in. (98.4 mm) from the bottom surface of the bridge flange. It was observed that the maximum midspan deflection observed in Figure 102 was 0.65 in. (16.5 mm), which represents a span (L) ratio of only L/1,108. Moreover, it was concluded that the observed strains of rebar and UHPC at midspan, along with the obtained joint opening are very small.

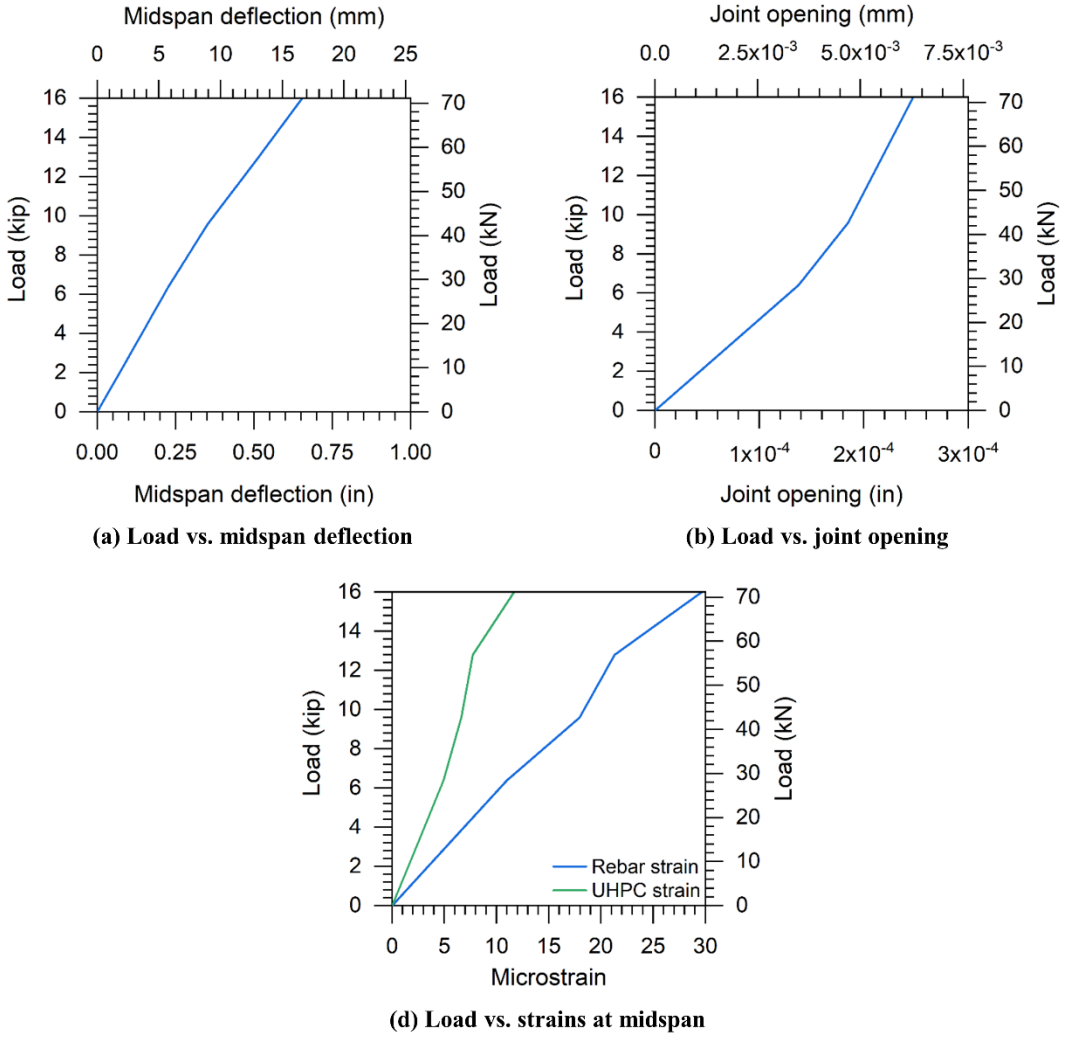

(a) Load vs. midspan deflection

(b) Load vs. joint opening

(d) Load vs. strains at midspan

Figure 102. Bridge FEA model results under single wheel load.

6 SUMMARY, CONCLUSIONS AND RECOMMENDATIONS

This study investigates the use of Ultra-High Performance Concrete (UHPC) in bridge deck connections, particularly focusing on the application of these materials in Northeast Extreme Tee (NEXT-D) beams for bridges. This research is highly relevant to the evolving trends in bridge construction, such as Accelerated Bridge Construction (ABC), which aims to reduce construction times and enhance the durability and longevity of bridge systems by using prefabricated bridge elements and systems (PBES). Traditional methods of cast-in-place concrete, which have been widely used in Alabama for short-span bridges, require significant construction time and labor. Although effective, these methods are less efficient than prefabrication methods, such as the use of precast beams and deck panels, which offer time and cost savings. In this context, UHPC emerges as a promising alternative material due to its superior mechanical properties, including high compressive strength, tensile capacity, durability, and enhanced bonding characteristics with reinforcement and normal concrete (NC). These properties make UHPC an ideal candidate for use in bridge deck joints, where the ability to resist cracking and withstand long-term loading is critical.

As part of this study, material characterization of three commercially available UHPC formulations was completed. These UHPC formulations included premixed cementitious materials, water, admixtures, and steel fibers, and were selected based on their availability and performance potential for bridge applications. The UHPC mixes were characterized through a series of tests that evaluated their compressive strength, elastic modulus, tensile behavior, and shrinkage properties. The compressive strength tests followed ASTM standards and were conducted on 3x6-inch UHPC cylinders to assess strength development over time, while tensile behavior was evaluated using both direct tension (DT) tests and four-point bending (4PB) tests. Shrinkage behavior was measured using shrinkage beams and strain gauges embedded in the UHPC joints and cylinders. The bond strength between UHPC and normal concrete was also assessed using pullout tests on composite specimens. The results indicated that all three UHPC mixes exhibited excellent compressive and tensile strength characteristics, with the ability to maintain these properties even under conditions of shrinkage and repeated loading. The compressive strengths of UHPCs varied anywhere from 16.2 ksi to 22 ksi, while the elastic modulus varied between 6000 ksi to 7500 ksi; The bond strength between UHPC and NC was found to be significantly higher than that of conventional materials, reinforcing UHPC's suitability for use in bridge deck joints.

This study included an experimental testing program using both slab and double-tee specimens. The slab specimens were designed to simulate the flange regions of NEXT-D beams, while the double-tee specimens were full-scale representations of NEXT-D beams used in real bridge projects. The primary objective of these tests was to evaluate the structural behavior of UHPC joint connections under various loading conditions, including static and fatigue loads. The tests were conducted in two phases: Phase I involved testing four slab specimens with different UHPC mixes and joint reinforcement layouts (single layer versus double layer), and Phase II involved testing four double-tee specimens to simulate the full-scale behavior of NEXT-D beams. In all specimens tested during this project, the joint reinforcement consisted of straight bars extending from the deck region, without the use of any headed reinforcement. The specimens were instrumented with strain gauges, load cells, and displacement sensors to monitor key performance metrics, such as joint opening, deflection, and strain under load. The load protocols for the slab specimens included fatigue tests with up to one million cycles, followed by stiffness measurement tests, overload tests, and ultimate failure tests. For the double-tee specimens, the testing protocols were similar, with the addition of cyclic overload tests to simulate long-term service conditions in bridges.

The results from the slab and double-tee tests demonstrated that UHPC joints provide excellent structural performance under both static and fatigue loading conditions. In the fatigue tests, the specimens withstood up to one million cycles without significant degradation in stiffness or strength, and minimal cracking was observed in the joints. The stiffness measurement tests showed that the UHPC joints retained their stiffness even after repeated loading, indicating their potential for long-term durability in bridge applications. The overload and failure tests confirmed that the UHPC joints were capable of withstanding high loads, with failure occurring primarily in the surrounding normal concrete rather than at the UHPC joint interface. These findings suggest that UHPC joints have the potential to improve the longevity and performance of bridge deck connections, particularly in ABC applications where rapid construction and long-term reliability are essential.

Finite element models (FEM) for the slab and double-tee specimens were development using the software ATENA (version 5) and were used to simulate the structural behavior of the UHPC joint connections under the same loading conditions as the experimental tests. The FEM models were calibrated based on the experimental data, and the results were compared to validate the accuracy of the simulations. The finite element analysis (FEA) results showed good agreement with the experimental data, particularly in terms of deflection, strain, and joint opening behavior. The models were then used to perform parametric studies to investigate the effects of different UHPC formulations, reinforcement layouts, and joint geometries on the structural performance of the connections. The FEA results confirmed the experimental findings, showing that UHPC joints provide excellent performance in terms of stiffness, strength, and fatigue resistance, even under the high demands of bridge loading conditions.

6.1 Conclusions

The research presented in this report leads to several key conclusions:

UHPC Properties: The material characterization tests confirmed that all three UHPC formulations used in the study exhibit high compressive and tensile strength, as well as excellent bonding characteristics with normal concrete. This makes UHPC a suitable material for use in bridge deck joints, particularly in areas subject to high traffic loads and environmental stressors.

Joint Performance: The UHPC joints in the slab and double-tee specimens demonstrated good performance under static and fatigue loading conditions. The joints were able to resist significant loads, maintain stiffness, and exhibit minimal cracking even after one million fatigue cycles. These findings suggest that UHPC joints are highly durable and capable of withstanding long-term service conditions in bridge applications. The 8-in. (203 mm) UHPC joint width and 6-in. (152-mm) rebar spacing used in this study were sufficient to allow the #5 straight bars to fully develop and yield during the slab failure test. This observed result, combined with past studies led to the conclusion that headed rebars are not necessary using the suggested joint width, joint spacing, and rebar size. The presence of two layers or single layer also didn't affect the overall performance of the joint under fatigue loading. The joint surface preparation applied to the NC at the joint interface is considerably beneficial to the performance of the joint by increasing the bond between UHPC and NC.

Fatigue Resistance: Fatigue testing of slab and double-tee specimens yielded satisfactory results. No cracking in the NC or UHPC was observed during this test type, and the materials behaved elastically. The UHPC joints in this study successfully resisted fatigue loading, showing no significant deterioration in performance after extended cycles. This highlights UHPC's potential to enhance the longevity of bridge deck connections.

Finite Element Analysis: The FEA models developed as part of this study closely matched the experimental results, validating the accuracy of the simulations. This suggests that FEA can be a valuable tool for predicting the behavior of UHPC joints in bridge applications, reducing the need for extensive physical testing. The FEA modeling approach and the interface parameters used in this study effectively captured the behavior of the slab and double-tee specimens simulating NEXT-D beams. The load applied on double-tee specimens was satisfactorily distributed across the UHPC joint length based on concrete strain gauge data. Based on FEA results, the DTee-Headed model was observed to be the least stiff when compared to the DTee-SL and DTee-DL models.

Construction Efficiency: The use of UHPC in bridge joints has the potential to reduce construction time and costs. The high strength of UHPC allows for shorter development lengths and simpler joint reinforcement layouts, making the construction process more efficient while maintaining the structural integrity of the joint.

6.2 Recommendations

Based on the findings of this research, the following recommendations are proposed:

- Given the promising results from the experimental testing and FEA modeling, it is recommended that ALDOT consider incorporating UHPC joints in future bridge designs, particularly for projects involving ABC. There is no need for using headed reinforcement in 8 in. wide joints with UHPC. Straight #5 rebar from the deck extending into the joint should be able to develop sufficiently with in the 8 in. wide joint. The use of UHPC can significantly improve the durability and longevity of bridge structures, reducing long-term maintenance and repair costs.
- Although the experimental tests provided valuable insights into the short-term performance of UHPC joints, long-term monitoring of these joints in real-world bridge applications is recommended. This will provide a better understanding of how UHPC performs over time under varying environmental and loading conditions.
- To facilitate the adoption of UHPC in bridge projects, it is recommended that standardized design guidelines and construction specifications be developed. These guidelines should cover material selection, joint design, construction procedures, and quality control measures to ensure consistent and reliable performance of UHPC joints across different projects.
- While UHPC offers significant performance benefits, its higher initial cost compared to traditional materials could be a barrier to widespread adoption. A detailed cost-benefit analysis should be conducted to quantify the long-term savings in maintenance and repair costs, which could offset the higher initial investment in UHPC.

7 REFERENCES

1. Culmo, Michael P. *Accelerated Bridge Construction - Experience in Design, Fabrication and Erection of Prefabricated Bridge Elements and Systems*. (2011). Report No. FHWA-HIF-12-013.
2. Precast/Prestressed Concrete Institute. "History of Significant Changes made to the PCI Northeast NEXT Beam Typical Guide Details since March 2015." 2021, https://www.pci.org/PCINE/Technical_Resources/Bridge_Resources/Northeast_Extreme_Tee_NEXT_Beam/PCINE/Technical_Resources/Bridge_Resources/NEXT_Beam.aspx.
3. Precast/Prestressed Concrete Institute. "Northeast Extreme Tee (NEXT) Beam." https://www.pci.org/PCINE/Technical_Resources/Bridge_Resources/Northeast_Extreme_Tee_NEXT_Beam/PCINE/Technical_Resources/Bridge_Resources/NEXT_Beam.aspx.
4. Precast/Prestressed Concrete Institute Northeast. *Northeastern Extreme Tee (NEXT) Beam Guide Details*. (2021). Report No. PCINER-12-NEXT.
5. Ronanki, V. S., S. Aaleti, and D. B. Valentim. "Experimental investigation of bond behavior of mild steel reinforcement in UHPC." *Engineering Structures*, vol. 176 (2018): pp. 707-18. https://doi.org/10.1016/j.engstruct.2018.09.031.
6. ASTM C1856/C1856M-17. "Standard Practice for Fabricating and Testing Specimens of Ultra-High Performance Concrete." West Conshohocken, PA: ASTM International, 2017.
7. Benjamin, A. Graybeal, and Baby Florent. "Development of Direct Tension Test Method for Ultra-High- Performance Fiber-Reinforced Concrete." *ACI Materials Journal*, vol. 110, no. 2. https://doi.org/10.14359/51685532.
8. ASTM C1609/C1609M - 19a. "Standard Test Method for Flexural Performance of Fiber-Reinforced Concrete (Using Beam With Third-Point Loading)." West Conshohocken, PA: ASTM International, 2019.
9. ASTM C157/157M - 17. "Standard Test Method for Length Chance of Hardened Hydraulic-Cement Mortar and Concrete." West Conshohocken, PA: ASTM International, 2017.
10. ASTM C39/C39M - 21. "Standard Test Method for Compressive Strength of Cylindrical Concrete Specimens." West Conshohocken, PA: ASTM International, 2021.
11. ASTM C469/C469M - 22. "Standar Test Method for Static Modulus of Elasticity and Poisson's Ratio of Concrete in Compression." West Conshohocken, PA: ASTM International, 2022.
12. ASTM E965 - 15 (Reapproved 2019). "Standard Test Method for Measuring Pavement Macrotexture Depth Using a Volumetric Technique." West Conshohocken, PA: ASTM International, 2019.
13. ASTM A370 - 22. "Standard Test Methods and Definitions for Mechanical Testing of Steel Products." West Conshohocken, PA: ASTM International, 2022.
14. ASTM C31/C31M - 22. "Standard Practice for Making and Curing Concrete Test Specimens in the Field." West Conshohocken, PA: ASTM International, 2022.
15. American Association of State Highway and Transportation Officials. *AASHTO LRFD Bridge Design Speficications*. 9th ed. Washington, DC: American Association of State Highway and Transportation Officials, 2020.
16. Wille, Kay, Sherif El-Tawil, and Antoine E Naaman. "Properties of strain hardening ultra high performance fiber reinforced concrete (UHP-FRC) under direct tensile loading." *Cement and Concrete Composites*, vol. 48 (2014): pp. 53-66.
17. Baby, Florent, Benjamin Graybeal, Pierre Marchand, and François Toutlemonde. "UHPFRC tensile behavior characterization: inverse analysis of four-point bending test results."

Materials and Structures, vol. 46, no. 8 (2012): pp. 1337-54. https://doi.org/10.1617/s11527-012-9977-0.

18. Qian, Shunzhi, and Victor C Li. "Simplified inverse method for determining the tensile properties of strain hardening cementitious composites (SHCC)." *Journal of Advanced Concrete Technology*, vol. 6, no. 2 (2008): pp. 353-63.
19. Rigaud, S, G Chanvillard, and J Chen. "Characterization of bending and tensile behavior of ultra-high performance concrete containing glass fibers." In *High Performance Fiber Reinforced Cement Composites 6*, 373-80: Springer, 2012.
20. ACI Committee 318. *Building Code Requirements for Structural Concrete: (ACI 318-14); and Commentary (ACI 318R-14)*. Famington Hills, MI: American Concrete Institute, 2014.
21. Precast/Prestressed Concrete Institute. *PCI Design Handbook*. 7th ed. Chicago, IL: Precast/Prestressed Concrete Institute, 2010.
22. B. A. Graybeal, "Design and construction of field-cast UHPC Connections," Federal Highway Administration, FHWA-HRT-14-084, Oct. 2014.
23. Yuan, J., Graybeal, B., and Zmetra, K. (In press). Box Beam Bridges: Testing of Conventional Grout and Ultra-High Performance Concrete Connection Details, Report No. FHWA-HRT-17-093, Federal Highway Administration, Washington, DC.
24. S. Aaleti and S. Sritharan, "Design of Ultrahigh-Performance Concrete Waffle Deck for Accelerated Bridge Construction," *Transp. Res. Rec. J. Transp. Res. Board*, vol. 2406, pp. 12–22, 2014, doi: 10.3141/2406-02.